AD-A041 492 TRW INC CLEVELAND OHIO MATERIALS TECHNOLOGY F/G 13/8
AIR BONDED, FOD RESISTANT METAL MATRIX FAN BLADES.(U)
SEP 76 G S DOBLE, P MELNYK F33615-75-C-5222
UNCLASSIFIED ER-7850-2 AFML-TR-76-218 NL

1 OF 2
ADA
041492

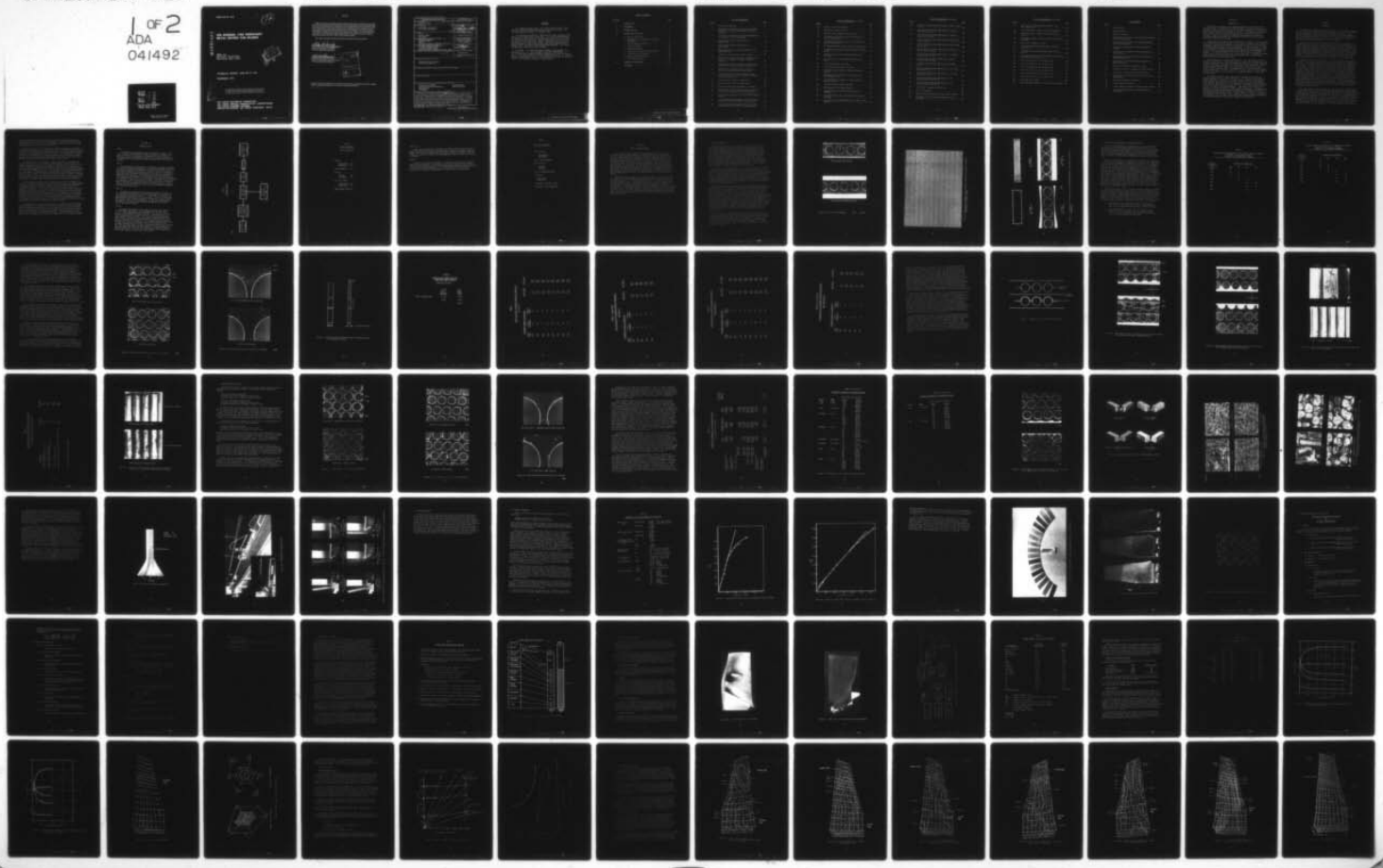

AFML-TR-76- 218

(12)

AIR BONDED, FOD RESISTANT METAL MATRIX FAN BLADES

TRW, Inc.
Materials Technology
Cleveland, Ohio 44117

TECHNICAL REPORT AFML-TR-76- 218

DECEMBER 1976

Approved for public release; distribution unlimited

AIR FORCE MATERIALS LABORATORY
AIR FORCE WRIGHT AERONAUTICAL LABORATORIES
AIR FORCE SYSTEMS COMAND
WRIGHT-PATTERSON AIR FORCE BASE,OHIO 45433

NOTICE

When Government drawings, specifications, or other data are used for any purpose other than in connection with a definitely related Government procurement operation, the United States Government thereby incurs no responsibility nor any obligation whatsoever; and the fact that the government may have formulated, furnished, or in any way supplied the said drawings, specifications, or other data, is not to be regarded by implication or otherwise as in any manner licensing the holder or any other person or corporation, or conveying any rights or permission to manufacture, use, or sell any patented invention that may in any way be related thereto.

This technical report has been reviewed and is approved for publication.

Philip A. Parmley

Philip A. Parmley, Aerospace Engineer
Advanced Development Division
Air Force Materials Laboratory

Wendall C. Bauman

Wendall C. Bauman, Col. USAF
Chief, Advanced Development Division
Air Force Materials Laboratory

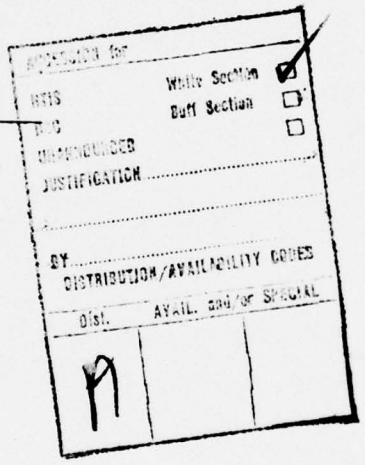

Copies of this report should not be returned unless return is required by security considerations, contractual obligations, or notice on a specific document.

AIR FORCE - 28 JUN 77 - 200

SECURITY CLASSIFICATION OF THIS PAGE (When Data Entered)

REPORT DOCUMENTATION PAGE

READ INSTRUCTIONS BEFORE COMPLETING FORM

1. REPORT NUMBER: AFML-TR-76-218	2. GOVT ACCESSION NO.
3. RECIPIENT'S CATALOG NUMBER	
4. TITLE (and Subtitle): AIR BONDED, FOD RESISTANT METAL MATRIX FAN BLADES.	5. TYPE OF REPORT & PERIOD COVERED: FINAL REPORT. 20 June 1975 to 30 July 1976
6. PERFORMING ORG. REPORT NUMBER: ER-7850-2	
7. AUTHOR(s): GORDON S. DOBLE, PAUL MELNYK	8. CONTRACT OR GRANT NUMBER(s): F33615-75-C-5222
9. PERFORMING ORGANIZATION NAME AND ADDRESS: MATERIALS TECHNOLOGY EQUIPMENT GROUP, TRW INC., 23555 EUCLID AVENUE, CLEVELAND, OHIO 44117	10. PROGRAM ELEMENT, PROJECT, TASK AREA & WORK UNIT NUMBERS: PROJECT 7351-07-08, PE 6.2 102F
11. CONTROLLING OFFICE NAME AND ADDRESS: AIR FORCE MATERIALS LABORATORY/LC, AF WRIGHT AERONAUTICAL LAB, AIR FORCE SYSTEMS COMMAND, WRIGHT-PATTERSON AIR FORCE BASE, OHIO 45433	12. REPORT DATE: SEPTEMBER 1976
	13. NUMBER OF PAGES: 124
14. MONITORING AGENCY NAME & ADDRESS (if different from Controlling Office): 134 p.	15. SECURITY CLASS. (of this report): UNCLASSIFIED
	15a. DECLASSIFICATION/DOWNGRADING SCHEDULE

16. DISTRIBUTION STATEMENT (of this Report)

APPROVED FOR PUBLIC RELEASE:
DISTRIBUTION UNLIMITED

17. DISTRIBUTION STATEMENT (of the abstract entered in Block 20, if different from Report)

18. SUPPLEMENTARY NOTES

19. KEY WORDS (Continue on reverse side if necessary and identify by block number)

FABRICATION DEVELOPMENT
ADVANCED METAL MATRIX COMPOSITES
BORON-ALUMINUM
AIR BONDING
COST REDUCTION
ENGINE FAN BLADES

20. ABSTRACT (Continue on reverse side if necessary and identify by block number)

A low cost air bonding process ~~has been~~ was developed for the fabrication of boron-aluminum fan blades from monotapes. Boron-aluminum systems of 8 mil boron-1100, 1100/2024 hybrid, and 6061 aluminum were successfully air bonded with properties equivalent to higher cost vacuum bonded material. The 8 mil boron-1100 system was selected for property characterization because of high Charpy energy absorption, 46 foot-lbs in ±15° orientation. The mechanical properties were compared to design requirements analytically determined for an advanced first stage fan blade, the J-101.

DD FORM 1 JAN 73 1473 EDITION OF 1 NOV 65 IS OBSOLETE

Unclassified

SECURITY CLASSIFICATION OF THIS PAGE (When Data Entered)

405 613

FOREWORD

This Technical Report covers the work performed under Air Force Contract F-33615-75-C-5222 from 20 June 1975 to 30 July 1976. It was submitted by the authors in September 1976.

This contract with TRW Inc., 23555 Euclid Avenue, Cleveland, Ohio 44117, was initiated under Project 7351. It is being performed under the technical direction of Mr. William Schulz and Mr. Philip Parmley, Air Force Materials Laboratory, Advanced Development Division, Wright-Patterson Air Force Base, Ohio 45433. A portion of the contract is being performed by the Aircraft Engine Group of the General Electric Company under a subcontract TRW purchase order 88-35977. This report has been given TRW report number ER-7850-2.

At TRW Dr. G. S. Doble was Program Manager, working under the direction of Dr. I. J. Toth, Manager of Materials Development. Mr. P. Melnyk was the project engineer responsible for material fabrication. At General Electric the Program Manager was Mr. A. J. Albright. The GE project engineer was Mr. M. W. Stanley working under the direction of Mr. R. G. Stabrylla, Technical Program Manager.

TABLE OF CONTENTS

LIST OF ILLUSTRATIONS

LIST OF ILLUSTRATIONS (continued)

LIST OF ILLUSTRATIONS (continued)

LIST OF ILLUSTRATIONS (continued)

LIST OF TABLES

SECTION I

INTRODUCTION

Boron-aluminum composites are characterized by very high modulus and strength levels. Incorporation of boron-aluminum into the fan section of a gas turbine engine has the potential to make major improvements in the engine because of the large size and weight of the fan. Significant improvements in cost, weight, efficiency (fuel consumption) and life cycle costs can be realized. However, utilization of boron-aluminum composites requires low cost fabrication and improved FOD resistance while maintaining the design properties required for the blade.

Significant cost reduction may be achieved by air bonding. The advantages of air bonding are that the process is low in cost, requires minimal capital investment, employes existing hot die technology and facilities, offers ease of automation and produces properties equivalent to vacuum bonding. The key to the successful bonding of aluminum composites in air, as practiced by TRW, lies in the use of a surface treatment which removes oxide and roughens the surface. The surface preparation is used in both primary and secondary bonding but is particularly critical in the latter case. The prepared surface contains asperities which promote localized deformation and break up the oxide layer during the bonding process.

FOD resistance is a primary consideration in the fabrication of boron-aluminum for fan blades. While affected by filament, matrix composition, and filament orientation, the fabrication parameters have an overriding influence on the final impact resistance. The TRW rapid air bonding process is well suited to providing high impact resistance through the use of a wrought ductile energy absorbing matrix, the employment of a low fabrication temperature, and the use of a minimum cycle time. The versatility of rapid heating and cooling afforded by air bonding is an important element in maintaining FOD resistance.

The program objective was to develop and validate the low cost air bonding process for use in blade fabrication. The program investigated air bonding fabrication parameters for three different boron-aluminum systems which included the three aluminum alloys of major interest in composites; 1100, 6061 and 2024 aluminum. After parameters were established, properties of the three systems were determined for fiber orientations and panel thicknesses of interest for blade application. One system, 8 mil boron-1100 aluminum, was then selected for further property evaluation. Throughout the program the properties obtained were compared to the properties required in a representative advanced fan blade, the J101 stage 1 fan blade. To provide this comparison the General Electric Company, under a subcontract, performed an analytical study of steady state stress and transient impact responses of the J101 blade geometry using various composite constructions.

SECTION II

BACKGROUND

The TRW rapid air bonding process has evolved by modification of standard industry practices in fabrication of boron-aluminum. The driving forces have been cost reduction, process versatility and property improvement. The important elements of the process are not only the use of an air atmosphere but also the reduction of cycle time, the use of fully dense monotapes, monotape surface preparation, and hot insertion with rapid cooling. A brief review of the process development will be discussed here.

Fabrication of boron-aluminum complex shapes such as a fan blade can be accomplished using a partially densified monotape such as a plasma tape, some type of green tape which has a fugitive binder, or a fully dense monotape. Formerly, panel and blade fabrication was performed in vacuum using very long cycles. Typically, the panel or blade was started at room temperature, slowly raised to the bonding temperature, usually with provision for a lengthy outgassing cycle, and used a very long bonding cycle, one to four hours not being uncommon. The rational for such a cycle was the desire to minimize internal and external oxidation of the monotape, to completely bake out the vacuum system, and to volatilize all of the fugitive binder at a low temperature.

Gradually, at TRW and other sources, the vacuum cycle has been reduced. Insertion of the composite between hot dies and rapid cooling has reduced the dwell time. With reduced dwell time it has been found possible to reduce the bonding time. Instead of a vacuum chamber a simple bagging system has been used. Finally, the feasibility of a very short cycle and an air atmosphere was demonstrated. The effectiveness of air bonding may be readily explained, at least on a qualitative basis, by considering the oxidation of aluminum. Because of the high reactivity of aluminum and high thermodynamic stability of aluminum oxide, aluminum oxide will form at very low temperatures and low oxygen partial pressures. The pressures found in commercial vacuum systems used in composite fabrication, particularly during system bakedown or fugitive binder outgassing, plus the very long half day heating cycles result in an oxide layer which must be broken up during bonding. The key to successful bonding of aluminum is not to prevent oxidation but to minimize the thickness of the oxide layer and provide plastic deformation at the interface. Successful air bonding requires a very short cycle time, and the promotion of plastic deformation at the bond line.

While the program reported here was concerned with secondary fabrication in air, primary fabrication of boron-aluminum monotapes in air has been demonstrated by TRW on IR&D programs. Air bonding was used in roll diffusion bonding of monotapes under Air Force sponsorship.(1) More recently, the production of boron-aluminum monotape by step diffusion bonding in air has been reported.(2) When using an air atmosphere in the primary fabrication of monotapes, there are two potential problems that could occur; oxidation of the filament with subsequent loss of strength and oxidation of the matrix producing poor matrix-matrix or filament matrix strength. Under the heating and processing cycles used in the above programs and with the geometry of filament and matrix, there was no

loss of filament strength as measured by monotape, panel, and extracted filament tests. No significant contamination at the matrix-matrix or filament-matrix bond line was found by microprobe, scanning electron microscopy, metallography, and transverse tensile testing.

While the use of an air atmosphere is certainly practical for primary fabrication, the commercially available monotape or broadgood materials at the initiation of the program were all fabricated in vacuum. To make the present program s widely applicable as possible, as well as to isolate the variables in secondary air bonding, all starting monotapes were fabricated in vacuum. However, the air bonding process developed is applicable to any fully dense monotape starting material produced in either air or vacuum.

The TRW rapid air bonding process employs monotapes, fully dense and having a wrought matrix. A monotape is advantageous for fabrication of a complex blade shape because of the improved properties which result from the uniform filament distribution and alignment. The use of a wrought matrix, that is using monotapes diffusion bonded from foil starting material, provides three additional advantages. First, the monotapes are highly formable which is a requirement in the production of blades with a high degree of twist or section change. Second, the ductile matrix offers superior impact resistance. Finally, the use of foil provides very uniform thickness. The use of a fully dense starting material is of considerable benefit by eliminating debulking in the bonding of a blade which has taper and section thickness differences.

The fully dense monotape starting material has a smooth surface finish which, in certain alloy systems, may be difficult to bond. To promote bonding an inexpensive chemical surface treatment has been developed by TRW.[3] As previously stated, the tenacious oxide on the surface of aluminum is an impediment to bonding. The surface treatment both removes initial oxide and roughens the surface, promoting an intimate metal-to-metal interface. Both mechanical and chemical treatments have been investigated but the latter is most effective in providing an appropriate surface topography. The important features of this process are the improved bondability of difficult to bond systems, the ability to bond at low temperatures, and the employment of an air atmosphere. The process also may be used in primary fabrication to provide adjustment in interfacial filament-matrix bond strength.

The purpose of the program reported here is to demonstrate and validate that air bonding can be applied to a number of composite alloy systems and provide properties comparable to vacuum bonded material, but at much lower cost. The fabrication conditions and experimental design have been directed toward the requirements of advanced fan blades. Specimen geometry, fiber orientation, composite systems, FOD resistance, and fabrication cycles have been chosen with regard to the properties needed for a first stage fan blade.

SECTION III

PROGRAM OUTLINE

Task I

A schematic of the program outline is presented in Table 1. The first task was the fabrication and quality control of monotapes to be used in later tasks. Monotapes were fabricated by press diffusion bonding in vacuum using conditions selected from previous experience and were selected to provide maximum impact resistance rather than maximum strength.

Task II

The 2nd task was the optimization of secondary air bonding parameters. A series of monotape time-temperature exposures was conducted to evaluate the resistance to thermal interaction. The residual tensile strength was used as a measure of the degree of reaction. Four-ply unidirectional panels were then fabricated by air bonding and screened by interlaminar shear and tensile testing. The objective was to use time-temperature conditions which were adequate for a good matrix-matrix bond, as measured by interlaminar shear stress, while not providing filament-matrix interaction, as reflected in a drop in the tensile strength. Two matrix systems were pre-selected for this optimization task, 1100 aluminum and an 1100/2024 hybrid. The hybrid construction consisted of a monotape with a layer of 1100 on one side and 2024 on the other. One set of processing parameters was selected for each system.

Task III

The processing parameters were then used to produce test panels in ±15° orientation of each system. Properties measured in screening the two systems are summarized in Table 2. In addition, a third system was selected after screening the first two systems. The third system was a 6061 aluminum matrix selected because of its wide use in boron-aluminum applicatons. Because of the large amount of fabrication data on 6061 the conditions for primary and secondary fabrication were selected without optimization studies.

Task IV

The properties measured in the screening 3rd task were compared with the design requirements for an advanced fan blade, the stage 1 J-101. These requirements were established in an analytical finite element study conducted by General Electric. These analyses include four frequency and stress cases. The first two cases were frequency, nodal pattern, steady state stress and deflection determination of two material properties resulting from boron fiber orientation variations. The next two cases were evaluation of the vibratory stress and deflection distributions induced in the blade in the first flexural and first torsional frequency modes. The blade finite element analyses also included four transient impact cases for bird ingestion. Cases considered were starling, medium and large size bird strikes at 70% blade span during take-off conditions. The results of these analyses were to provide the blade impact response for variation in bird size.

TABLE 1

PROGRAM OUTLINE

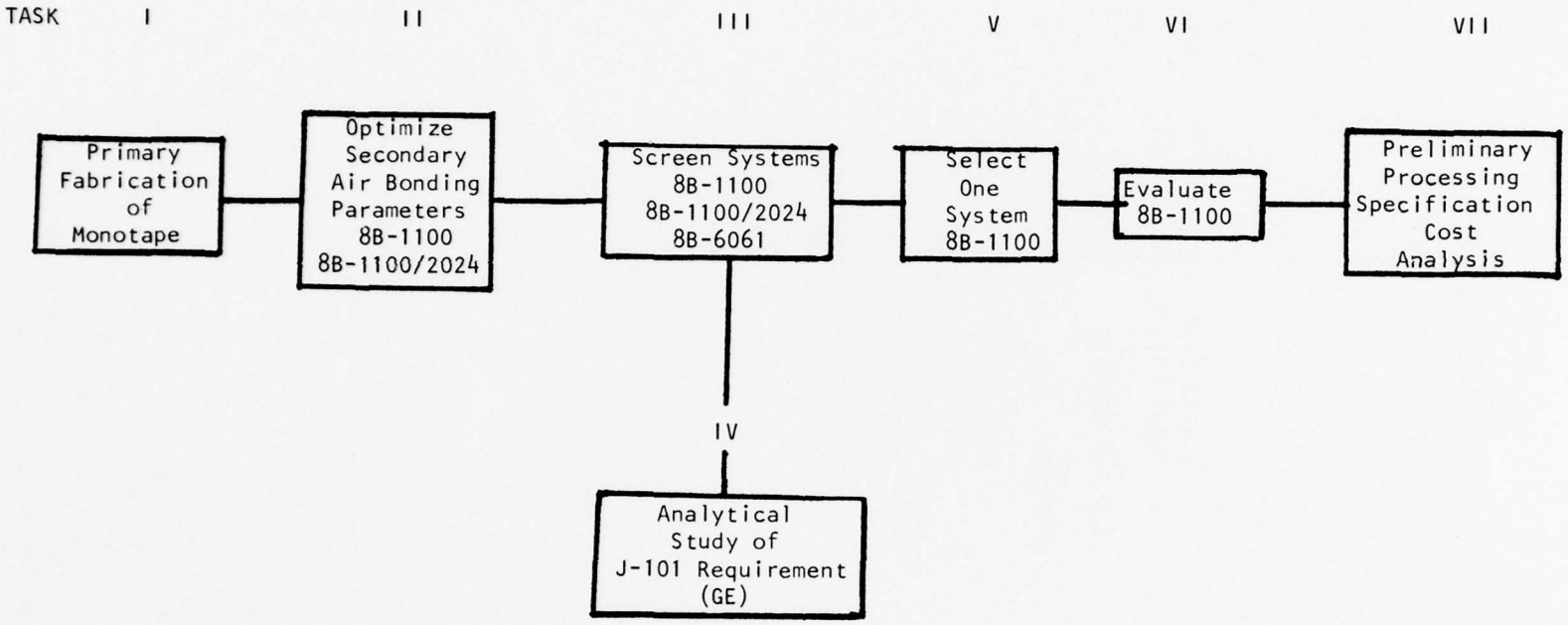

TABLE 2

SYSTEM SCREENING

Room Temperature

TENSILE		
	LONGITUDINAL	(2)
	TRANSVERSE	(2)
3 POINT BENDING		(2)
FATIGUE		
	FLEXURAL	(2)
	TORSIONAL	(2)
FULL SIZE CHARPY		
	LONGITUDINAL	(2)
	TRANSVERSE	(2)
INTERLAMINAR SHEAR		(2)

Task V & VI

Based upon a comparison of mechanical properties and analytical requirements, one system was selected for evaluation. Selection was based upon the highest FOD resistant material meeting projected blade requirements. The 1100 system was selected in Task VI and the properties listed in Table 3 determined in Task VII.

Task VII

Following the property evaluation, a preliminary material and processing specification was written. Included was raw material requirements, primary fabrication by diffusion bonding, and composite fabrication by secondary bonding of fully consolidated monotapes in air. A preliminary cost analysis was performed to illustrate the projected cost savings over vacuum bonding.

TABLE 3

MATERIAL EVALUATION

350°F TENSILE

- LONGITUDINAL
- TRANSVERSE

350°F 3 POINT BENDING

350°F FATIGUE

- FLEXURAL
- TORSIONAL

350°F INTERLAMINAR SHEAR

RT MODULUS

- LONGITUDINAL
- TRANSVERSE

UN-NOTCHED THIN PANEL CHARPY

RESISTANCE TO SALT CORROSION

SECTION IV

RESULTS AND DISCUSSION

This program on air bonding of boron-aluminum was performed with fully dense vacuum bonded monotapes as starting material. The monotapes were air bonded together using various parameters and the properties subsequently determined to be comparable to vacuum bonded material. Boron filament diameter was 8 mils selected for improved impact resistance.[4] The nominal volume fraction was 55 volume percent. The volume fraction was controlled by the filament spacing and monotape thickness which were held constant. No adjustment was made for variation in filament diameter which would change the volume fraction slightly. The monotape fabrication conditions were chosen from previous programs and no attempt was made to shorten the 15 minute consolidation time although this would certainly be possible based upon the results of monotape fabrication by roll diffusion bonding.[1]

Three major matrix systems were chosen for study. The first was 1100 aluminum which is acknowledged to provide the highest energy absorption of any composite matrix.[4] Because the 1100 system is a ductile but lower strength aluminum alloy, the 1100/2024 hybrid was selected for applications or locations where matrix enhancement might be required. The hybrid is constructed of a monotape with 1100 on one side and 2024 on the other. After screening of the 1100 and 1100/2024 systems, the 6061 matrix was selected as the third matrix. The 6061 alloy was included to demonstrate the air bonding process to a third system of commercial importance and because it was hoped that the alloy would provide the improved strength of the hybrid with better impact resistance.

A. PRIMARY FABRICATION

Boron-aluminum monotapes were produced by winding the fibers on a large diameter mandrel to provide the desired spacing and held together by an organic binder, polystyrene, which is subsequently removed by volatilization during the hot pressing cycle. The filaments are wound directly onto the mandrel and stripped off when dry, forming a filament mat. The collimated filament layers are then sandwiched between two matrix foil layers. The assembly is placed in a vacuum chamber which is inserted between hot dies with a clamping load to maintain filament alignment. A dynamic vacuum is maintained during pressing. The package has a low thermal mass and comes to temperature quickly, the exact time depending upon the number of monotapes being produced. The consolidation time was measured after the package was at temperature. After pressing the encapsulator is removed from the dies and air cooled.

All monotapes were made at 850°F, 15 minutes, 8 KSI which was selected on the basis of previous TRW experience. After property evaluation it was found that the primary fabrication temperature affects shear strength so runs made in later tasks used a 900°F primary fabrication temperature for the 1100 system. Typical monotapes are shown in Figure 1. Note that the1100 alloy is softer than the 2024 and extrudes further between the fiber. A metallographic sample from each run revealed full consolidation for all monotapes of 1100 and 100/2024. The 6061 alloy produced in a later task was not fully consolidated after primary fabrication at 850°F, but was fully dense after subsequent secondary fabrication.

As part of incoming material quality control, a monotape selected at random from each pressing run was characterized by visual inspection, longitudinal tensile tests, radiography, ultrasonic C-scan, thickness measurement, and optical microscopy. This quality control program was used to insure that the panels produced were of suitable quality. The visual inspection is a powerful tool in monotape manufacture because the thinness of the layer makes this a sensitive method for examining gross filament cracking, gaps, or lack of bonding, particularly at the corners. Radiography was used to observe filament breakage. A typical radiograph is shown enlarged in Figure 2. The excellent filament distribution, alignment and absence of filament breakup is apparent. Longitudinal monotape tensile tests were run on unidirectional monotape but showed considerable experimental scatter. Monotapes which provided low strength subsequently produced panels with high strength. Later monotapes made with 15° filament orientation were particularly difficult to test and results were not judged significant for quality control.

Ultrasonic C-scan and optical microscopy were used to determine if bonding was complete. Boron-aluminum requires sensitive inspection methods for bonding because full consolidation and density may be achieved without a complete metallurgical bond. Careful metallographic preparation was the best way to verify the presence of a metallurgical bond and freedom from oxide at the interface, both in monotapes and panels. The C-scans easily picked out monotapes which were not fully consolidated. An example is shown in Figure 3.

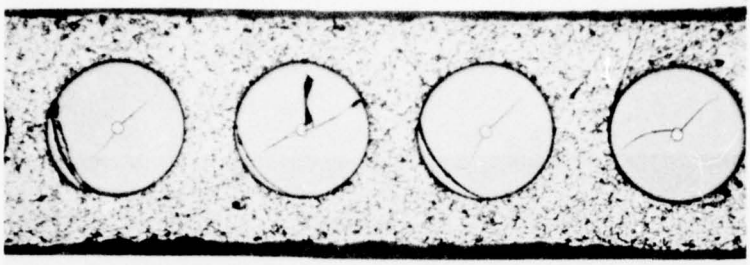

8 Mil Boron-1100 Aluminum

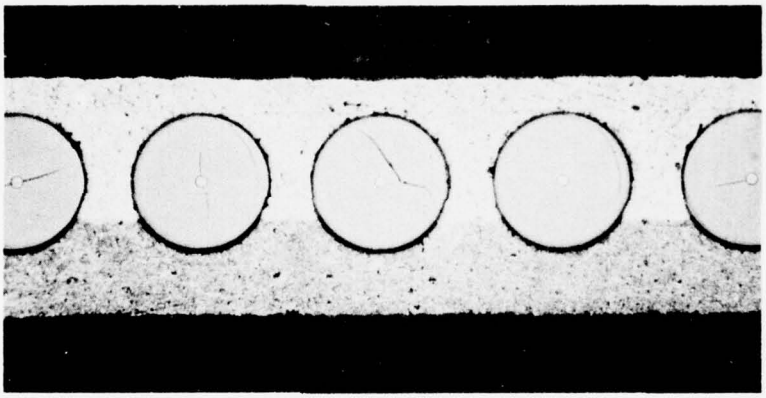

8 Mil Boron-1100/2024 Aluminum

Figure 1. As Fabricated Monotape 100X Etched

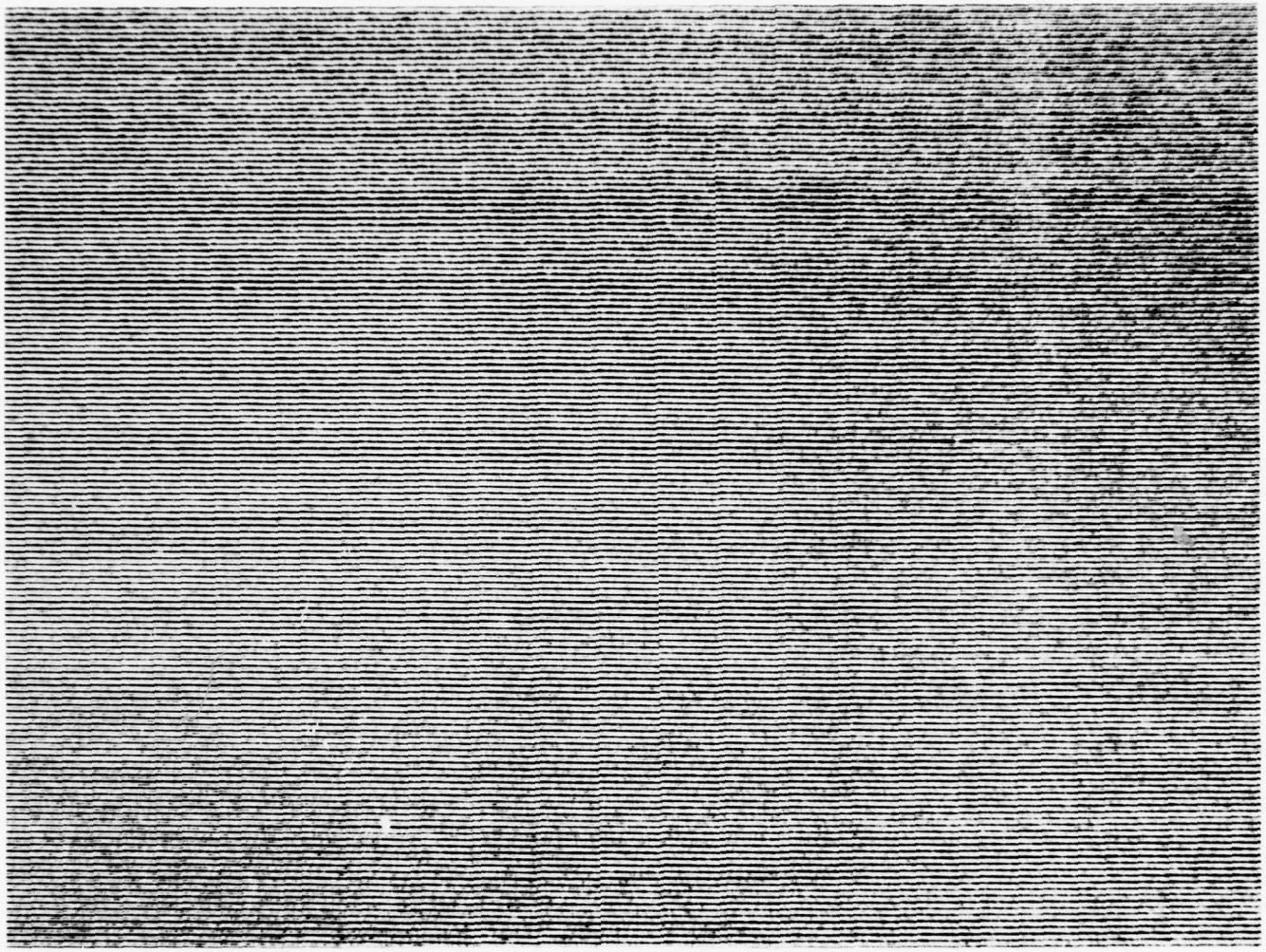

Figure 2. Radiograph of Monotape Illustrating Good Filament Distribution, Alignment and Absence of Filament Breaks.

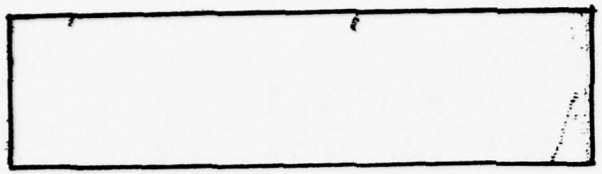

Run #43
8B - 1100 Al

Run #81
8B - 6061 Al

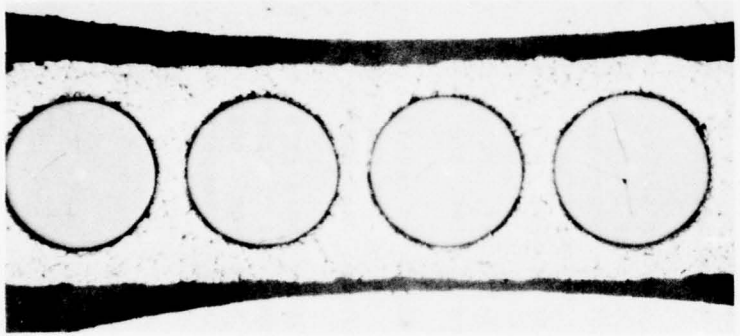

Run #43 100X
8B - 1100 Al

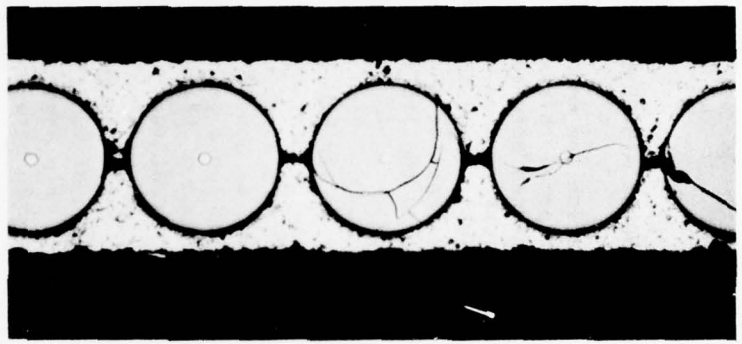

Run #81 100X
8B - 6061 Al

Figure 3. Correlation of Ultrasonic C Scan and Metallography in the Quality Control of Monotapes.

B. OPTIMIZATION OF SECONDARY AIR BONDING PARAMETERS

After primary fabrication the monotapes were surface treated and assembled into the desired panel thickness and configuration. The assembled monotapes were placed between hot flat dies in air and clamped until bonding temperature was reached. Steel plates were placed on the top and bottom of the assembly to prevent die sticking and distribute load. The bonding load was applied and the bonding time measured from this time. Only the 1100 and the 1100/2024 systems were studied at this time.

While the feasibility of air bonding has previously been established, the conditions for a balance of properties was not known. The ideal cycle is as low a bonding temperature as possible to improve impact properties with as short a bonding time as possible to reduce cost. If the bonding cycle is too long or at too high a temperature, the tensile and impact strength will decrease because of filament matrix interaction. If the bonding cycle is too short or at too low a temperature, the monotapes will not bond together. The tests used for the effectiveness of the secondary bonding cycle were tensile tests and interlaminar shear tests. In addition, the residual tensile strength of monotapes after thermal exposure was determined. Because of the thin panel sizes used in the program, 4 to 8 ply thickness, the relationship between bonding time and cycle time was very close. However, even very small fan blades have thicknesses of one inch and ply numbers up to 150 in the dovetail. Because of the finite heating times required for real blades, the cycle times in this program, and therefore the bonding times, were kept in the more realistic range of 15 minutes rather than a few minutes.

Monotapes were given a series of time-temperature exposures from 850°F 2 hours to 950°F 15 minutes using a total of 26 runs. The objective was to simulate potential secondary bonding cycle to establish conditions under which no significant filament-matrix reaction occurred to lower mechanical properties. Monotape tensile results are shown in Tables 4 and 5. The values are listed as a percentage of the as-fabricated tensile strength which ranged from 13-210 ksi. Values are the average of two tests. While the results show some scatter, the following conclusions can be drawn:

1) The 1100 matrix is relatively resistant to filament-matrix reaction. Using the requirement of 80% strength retention after exposure, degradation did not occur at 950°F/15 minutes.

2) The 1100/2024 hybrid is also relatively stable but does undergo some loss of strength. The low strength at 950°F is due to some liquid phase present in 2024 at this temperature, the solidus temperature being 935°F.

TABLE 4

RESIDUAL TENSILE STRENGTH OF 8 MIL BORON-1100/2024 ALUMINUM MONOTAPES AFTER THERMAL EXPOSURE (PERCENT OF AS-FABRICATED STRENGTH)

Exposure Temperature (°F)	Exposure Time (Minutes)			
	15	30	60	120
950	56			
925	84	77		
900	81	84		
875		79	91	
850			76	80
825			100	83
800			95	

TABLE 5

RESIDUAL TENSILE STRENGTH OF 8 MIL BORON/1100 ALUMINUM MONOTAPES AFTER THERMAL EXPOSURE (PERCENT OF AS-FABRICATED STRENGTH)

Exposure Temperature (°F)	Exposure Time (Minutes)			
	15	30	60	120
950	78			
925	69	86		
900	78	83		
875		95	94	
850			97	97
825			98	93
800			83	91

The efficiency of the rapid air bonding process was measured by tensile testing and shear testing of the matrix-matrix bond. Test panels were made of 4-ply unidirectionally reinforced 8 mil boron-1100 and 1100/2024 with all monotapes made under common processing conditions of 850°F, 15 minute, 8 KSI. These conditions were selected on the basis of impact resistance and were based on results obtained on another program. Except where noted, the monotapes were sized in thickness to provide a 55 volume percent reinforcement. After surface preparation, the monotapes were bonded together in air at temperatures of 825°F-925°F, times of 5-30 minutes, and pressures of 8-10 KSI. Typical microstructures are shown in Figures 4 and 5. No evidence of oxide or contamination is present at the air bonded interface.

The specimen used for determination of interlaminar shear strength was a double notch specimen and is illustrated in Figure 6. The specimen was selected specifically to force failure between monotape layers. As in all shear specimen configurations, the method has some limitations. It is known that the shear stress distribution is not uniform, rising sharply at the notches. The specimen also has a bending moment resulting from the nonlinear load application. Finally, there is at least some scatter due to machining and testing procedure. In the following tabular data presentation, for instance, the first and duplicate specimens were machined and tested in separate batches but the first specimen was always lower in strength.

The resulting data should be regarded on a comparative rather than on an absolute basis. Specimens with the distance between notches increased from 1/8" to 3/8" on panels of 5.6 boron-6061 aluminum provided from another program produced shear strength decreases of 100%. The selection of the 1/4" distance was conservative on this basis. A comparison between double notch shear results and short beam shear under three point loading is shown in Table 6. These data were obtained by shear testing an 8 ply double notch specimen and subsequently testing the two halves of the specimen so that the same specimen was tested by both procedures. Again the double notch shear specimen provides a lower, and, therefore, conservative shear strength.

Tensile and shear results are summarized in Table 7 for 8 mil boron-1100 aluminum. Uncorrected shear strength values ranged from 2-5.6 KSI with the higher values obtained at the higher bonding temperatures and times. Tensile strength values were from 170-210 KSI and showed no systematic variation with secondary bonding parameters. Shear and tensile results for the hybrid 8 mil boron-1100/2024 aluminum are shown in Table 8. Shear strength levels were higher than the 1100 aluminum matrix with a value of 6-9.3 KSI being obtained. The tensile strength was generally higher than the 1100 matrix specimens.

The shear strength values obtained were below the 9 KSI handbook value of the shear strength for annealed 1100 aluminum, even when corrected for specimen geometry. The reason for the lower strength was evident from observations of the fracture surface. The failure was between the filament and matrix indicating that this region is a weak link in shear. The failure

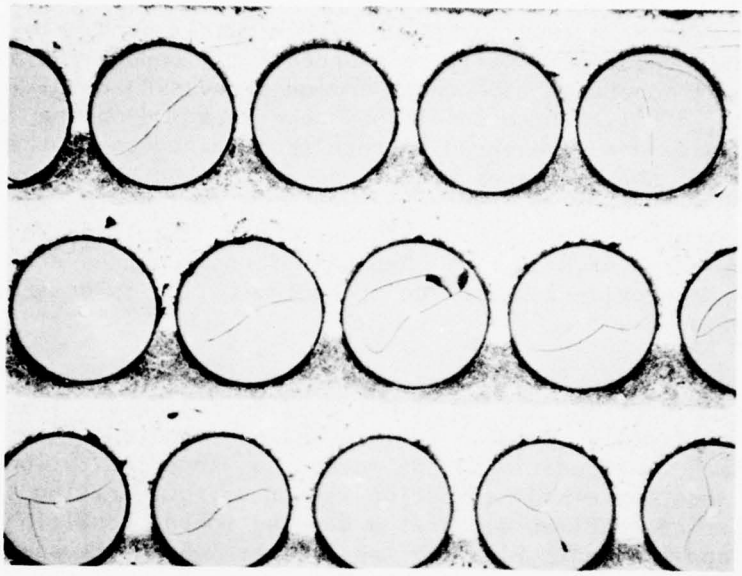

8 mil B-1000/2024 Hybrid Construction

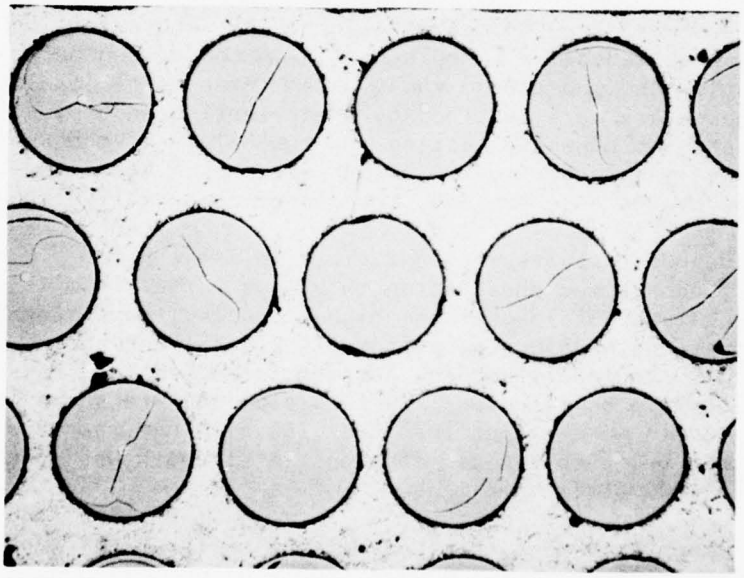

8 mil B-1100 Aluminum

Figure 4. Boron-Aluminum Panels Fabricated by Air Bonding 100X

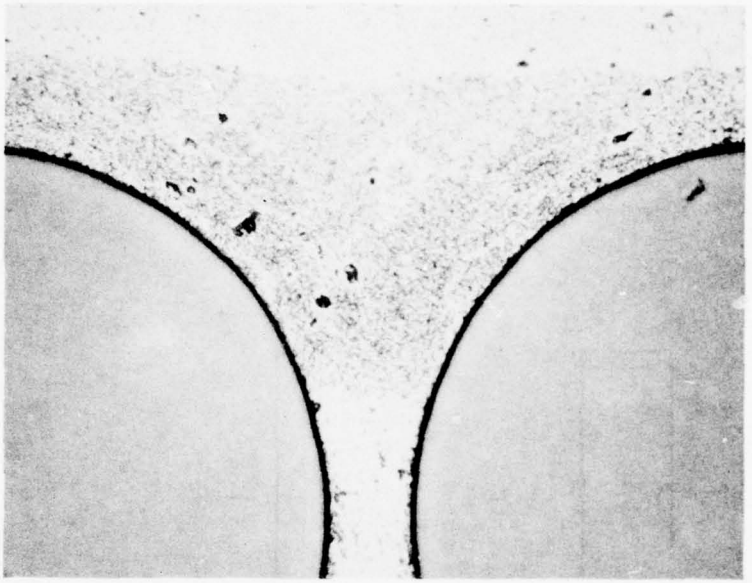

8 mil B-1100/2024 Hybrid Construction

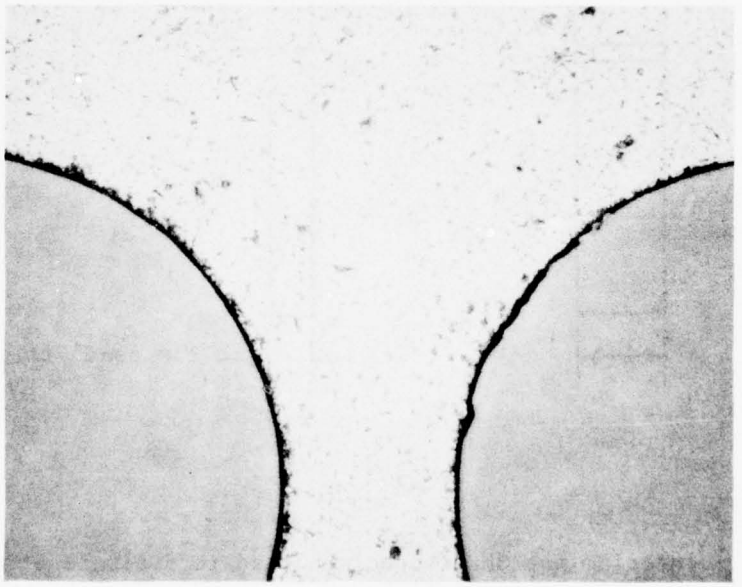

8 mil B-1100 Aluminum

Figure 5. Boron-aluminum Panels Fabricated by Air Bonding 500X

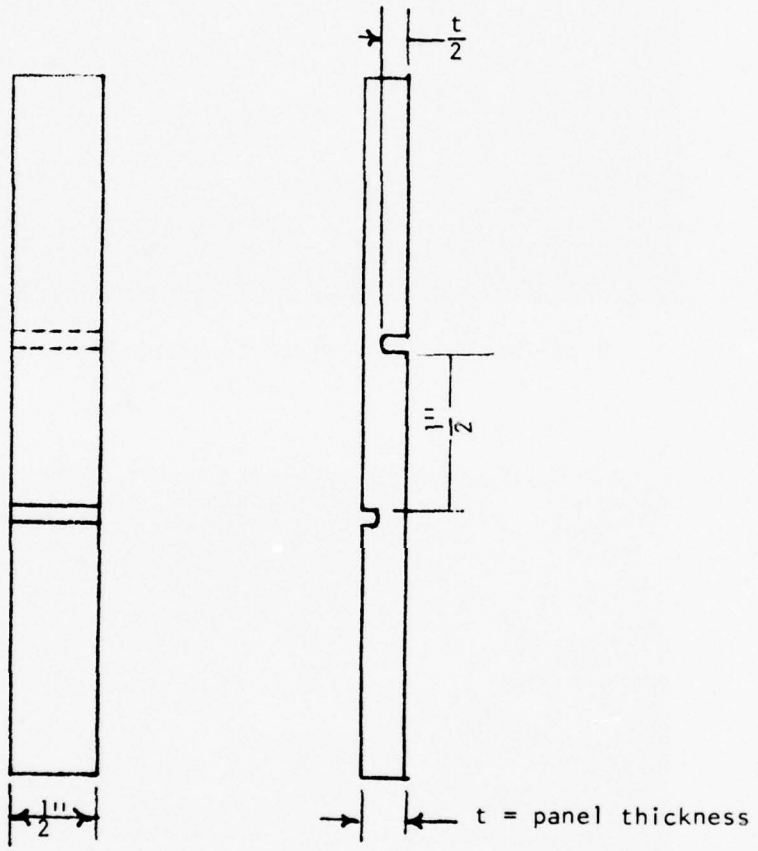

Figure 6. Interlaminar Shear Specimen Used to Evaluate Strength of Air Bonded Interface.

TABLE 6

COMPARISON OF DOUBLE NOTCH AND SHORT BEAM SHEAR STRENGTH

(8B-1100 Aluminum)

	Double Notch Specimen	Short Beam Shear
Shear Strength (KSI)	4,400	7,300
	3,750	7,300
		6,530

TABLE 7

OPTIMIZATION OF SECONDARY BONDING PARAMETERS

8B 1100 A1

SECONDARY BONDING PARAMETERS			ILSS (KSI)	UST (KSI)
Temp (°F)	Time (minutes)	Pressure (KSI)		
925	15	10	3.2	182
			5.6	172
925	15	8	4.0	180
			5.4	201
925	5	10	2.2	181
			2.2	180
900	30	10	1.9	172
			2.6	173
900	15	10	1.7	184
			2.4	211
875	30	8	1.6	182
			1.6	173
875	15	10	2.1	186
			2.3	175
875	15	8	0.7	179
			1.3	174

TABLE 7 (continued)

OPTIMIZATION OF SECONDARY BONDING PARAMETERS

8B-1100 A1

SECONDARY BONDING PARAMETERS			ILSS (KSI)	UTS (KSI)
Temp (°F)	Time (minutes)	Pressure (KSI)		
850	30	8	2.0	192
			2.0	191
850	15	10	2.3	159
			2.3	174
850	15	8	1.7	183
			2.1	178
825	30	10	2.2	193
			2.6	178
825	15	10	1.8	200
			1.6	170

TABLE 8

OPTIMIZATION OF SECONDARY BONDING PARAMETERS

8B-1100/2024 A1

SECONDARY BONDING PARAMETERS			ILSS (KSI)	UTS (KSI)
Temp (°F)	Time (minutes)	Pressure (KSI)		
925	15	10	>6.5	182
			9.3	242
925	15	8	7.6	210
			7.3	244
925	5	10	6.4	>208
			7.8	>213
900	30	10	6.5	199
			8.7	242
900	15	10	7.8	243
			8.3	216
875	30	8	6.9	210
			8.0	216
875	15	10	5.8	210
			7.1	177
875	15	8	6.3	213
			6.7	202

TABLE 8 (continued)

OPTIMIZATION OF SECONDARY BONDING PARAMETERS

8B-1100/2024 A1

SECONDARY BONDING PARAMETERS			ILSS (KSI)	UTS (KSI)
Temp (°F)	Time (minutes)	Pressure (KSI)		
850	30	8	3.1 1.5	213 195
850	15	10	5.8 5.6	211 223
850	15	8	6.9 7.4	198 211
825	30	10	2.7 2.2	210 216
825	15	10	3.5 3.3	222 210

surface is schematically illustrated in Figure 7. All monotapes were made in vacuum, while the panels were made in air. The dotted failure path is between the vacuum bonded filament-matrix and then through the thin bridge of vacuum bonded matrix rather than the matrix-matrix air bonded interface. Figures 8 and 9 illustrate the shear failures obtained from the two systems. In both cases the failure is in the filament-1100 aluminum interface. It is apparent that the primary fabrication conditions employed did not produce a strong filament-matrix bond between the boron and the 1100 aluminum. Scanning electron micrographs of the boron-1100 aluminum system shown in Figure 10 reveal the clean filaments after shear failure and the ductile failure of the matrix in between filaments. The lack of adhesion between filament and matrix was also noted during tensile testing of 8 mil boron-1100 aluminum by the presence of extensive filament pullout. The lower strength of the 1100 matrix composite compared to the hybrid 1100/2024 composite is due to the filament pullout which produces a composite strength close to the filament bundle strength.

Because the interface between filament and matrix appeared to be limiting the shear strength, several methods of improving the bond were examined. A primary surface preparation was included in one case prior to monotape consolidation. A second set of monotapes was made at 1000°F. For comparison, an eight-ply specimen was also fabricated. Test results are shown in Table 9 for panels made at 875°F, 15 minutes, 10 KSI. The improvement in strength in all cases is apparent and the 7-8.5 KSI obtained with the 1000°F monotape is particularly encouraging compared to the 9 KSI shear strength of the matrix. Failure was still at the filament-matrix interface but the improved adhesion of matrix to filament is shown in Figure 11. The tensile strength of the panels is reduced on this series of experiments because the volume fraction was reduced to 40 volume percent. Primary fabrication at 1000°F produced further drop in tensile strength of approximately 10 percent.

To further evaluate the effect of primary surface preparation and primary fabrication temperature, monotapes were prepared of 8 B-1100 aluminum using primary fabrication temperature of 900°-950°F with and without primary surface preparation. The monotapes were air bonded into panels at 925°F. Shear strength of these panels was very low with failure taking place at the matrix-matrix interface. A duplicate set of panels was made with similar results. Analysis of the fracture characteristics indicates that these panels were on the thin side of the dimensional tolerance and the thin cover skin did not provide sufficient material for bonding. This effect has been more fully documented in vacuum bonding on another program and is not a result of air bonding.

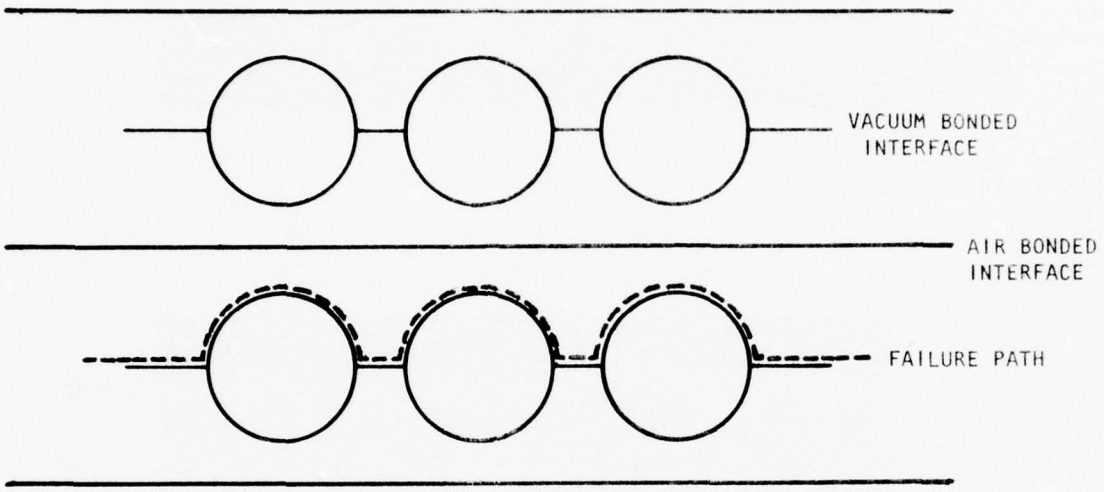

Figure 7. Schematic of Failure Path in Shear Testing

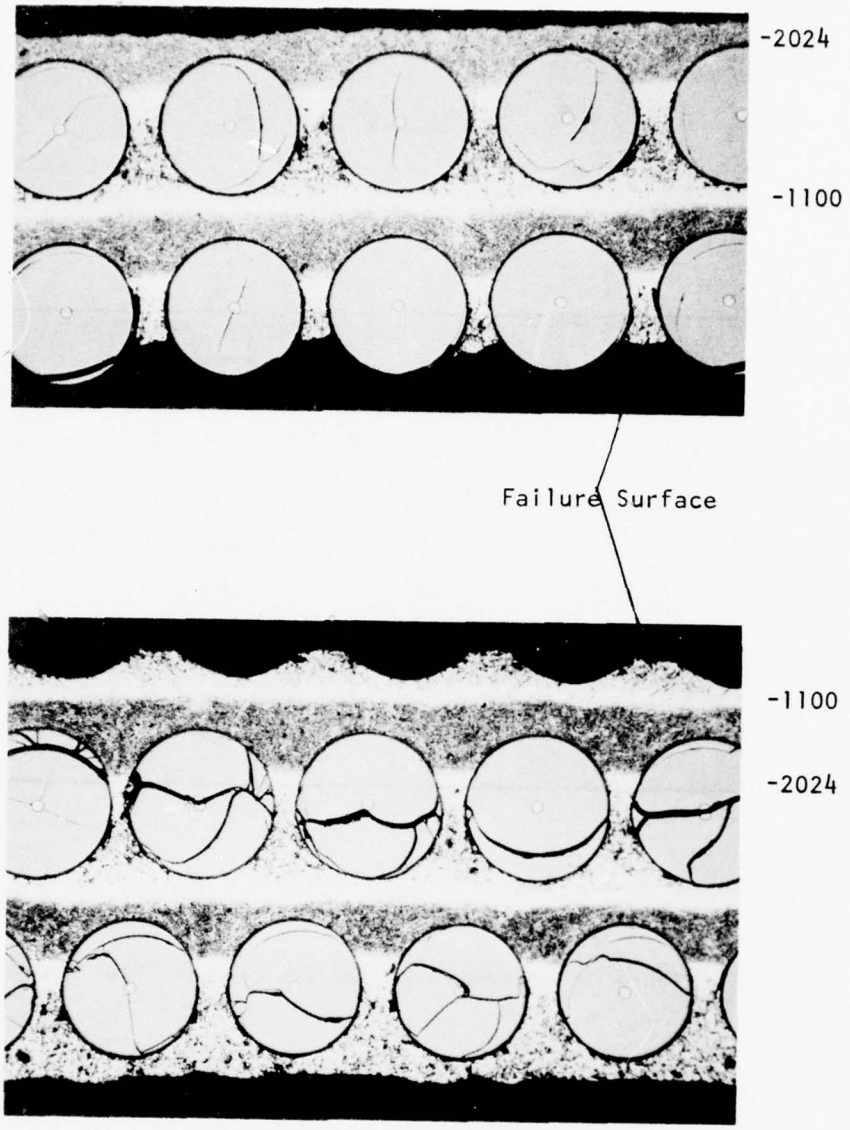

Figure 8. Metallographic Section Transverse to Shear Failure Surface of Air Bonded 8 Mil Boron-1100/2024 Aluminum.

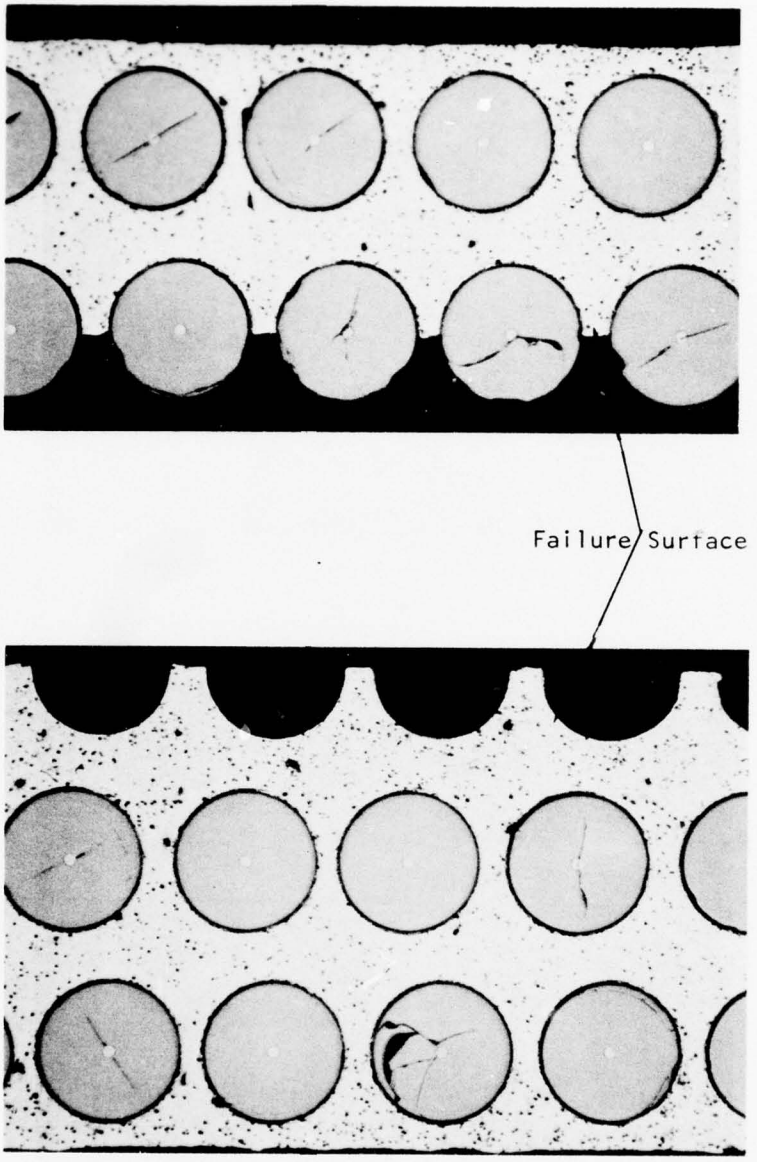

Figure 9. Metallographic Section Transverse to Shear Failure Surface of Air Bonded 8 Mil Boron-1100 Aluminum.

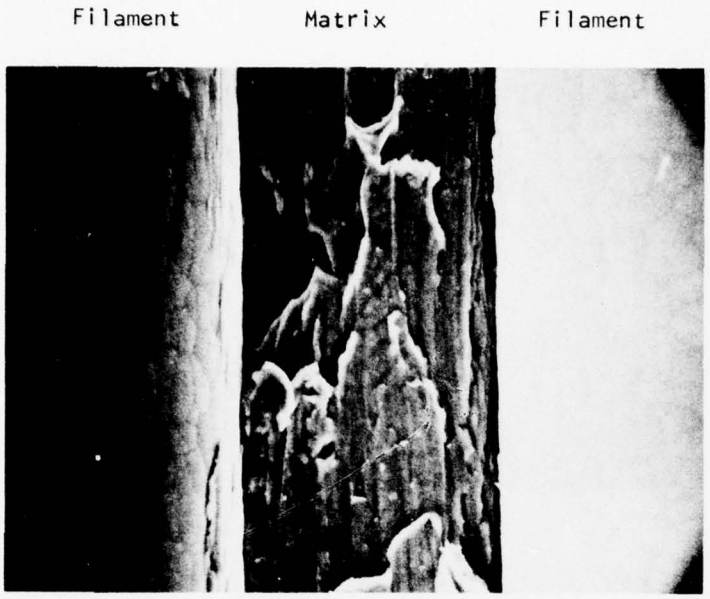

Figure 10. Shear Failure at Filament-Matrix Interface of 8 Mil Boron-1100 Aluminum Air Bonded Panel.

TABLE 9

OPTIMIZATION OF SECONDARY BONDING PARAMETERS

All at 875°F 15 Min. 10 KSI Secondary
(8 mil Boron-1100 Aluminum)

Condition	ILSS (KSI)	UTS (KSI)
Standard Fabrication	2.1	186
Primary 850°/15 min/8 ksi/4 ply	2.3	175
Primary Surface Preparation	5.2	151*
Primary 850°/15 min/8 ksi/4 ply	4.5	148*
8 ply	4.4	154*
Primary 850°/15 min/8 ksi	3.7	158*
Monotapes Fabricated at 1000°F/15 min/8 ksi/4 ply	7.0	137*
	8.5	141*

* = 40 volume percent reinforcement

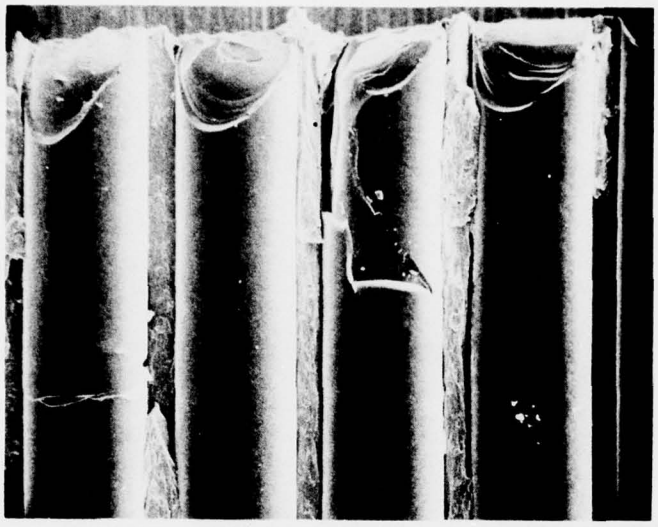

5.6 KSI Shear Strength

850°F Monotape Air Bonded at 875°

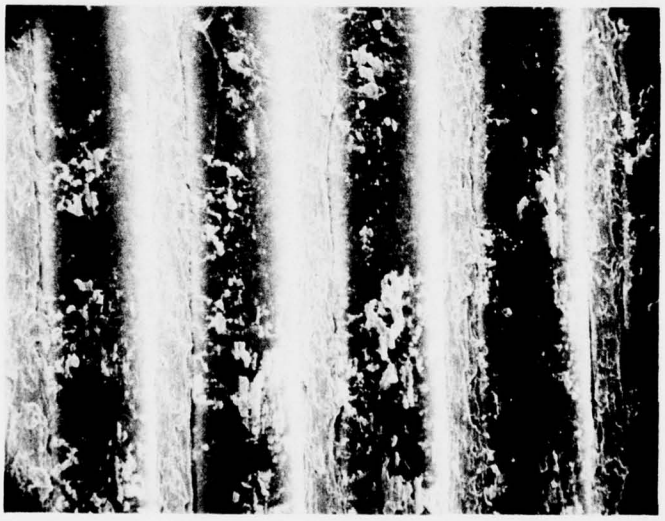

7.0 KSI Shear Strength

1000°F Monotape Air Bonded at 875°F

Figure 11. Scanning Electron Micrograph of Shear Surface Illustrating Correlation of Filament-Matrix Bond With Shear Strength.

C. SCREEN CANDIDATE MATERIAL

The results of secondary bonding were reviewed and the following systems and conditions selected for screening. No primary surface treatment was employed.

8 mil boron-1100 aluminum ±15°
monotapes fabricated at 900°F 15 minutes 8 KSI
secondary bond in air at 925°F 15 minutes 10 KSI

8 mil boron-1100/2024 aluminum ±15°
monotapes fabricated at 850°F 15 minutes 8 KSI
secondary bonding in air at 910°F 15 minutes 10 KSI

The preliminary J-101 stress analysis indicated a maximum requirement of 5-6 KSI shear stress under steady state conditions. The conditions selected for secondary bonding were, in general, the highest times and temperatures used in order to achieve this shear strength. The 910°F temperature picked for the hybrid was chosen so as to be 25°F below the solidus of 2024 aluminum. The primary fabrication temperature of the 1100 aluminum was increased from 850°F to 900°F to insure adequate consolidation and improve the filament-matrix bond.

A third system was also selected which was the 8 mil boron-6061 aluminum which employed the following fabrication parameters:

8 mil boron-6061 aluminum ±15°
monotapes fabricated at 850°F 15 minutes 8 KSI
secondary bonding in air at 900°F 15 minutes 10 KSI

Monotapes were not completely consolidated after primary fabrication but the panel was fully consolidated after secondary fabrication. The 8 mil boron-6061 system was included in the program because it is a widely used system with impact properties reported from moderate to good. It was also considered beneficial to demonstrate the applicability of air bonding to a third alloy matrix.

A brief study was also made of a modified hybrid construction. The composite consisted of a monotape of 2024 aluminum sized just thick enough to cover the filaments. When assembled into panels, layers of 1100 aluminum were added in between the monotape as shown in Figure 12. The purpose was to improve the shear strength of the composite by surrounding the filament with 2024 while providing layers of 1100 to add impact resistance. A single Charpy panel was made of this material at 910°F/15 minutes /10 KSI.

Panels from all four systems were fabricated by air bonding using a ±15° filament orientation and an 8 ply thickness for test panels and a 0.41 inch thickness for the Charpy panels. The thicknesses of 1100 and 2024 in the hybrid construction were adjusted to provide an equal thickness of each material. Representative microstructures are shown in Figures 12 and 13. The clean bond line for the 6061 and modified hybrid constructions is shown in Figure 14.

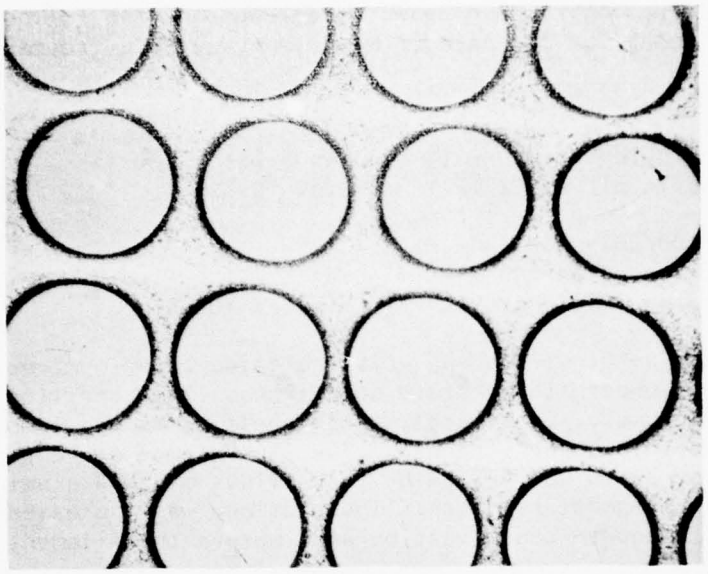

8 Mil Boron - 1100/2024 Aluminum (Modified Hybrid)

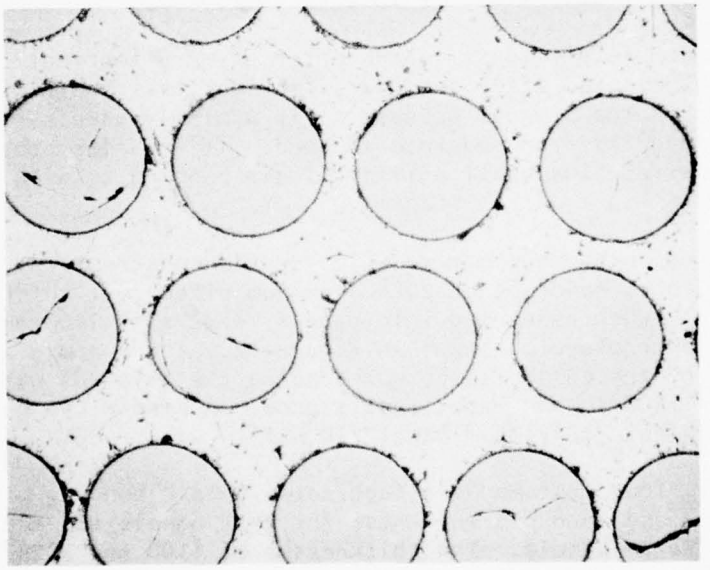

8 Mil Boron - 6061 Aluminum

Figure 12. Microstructures of ±15° Air Bonded Panels.

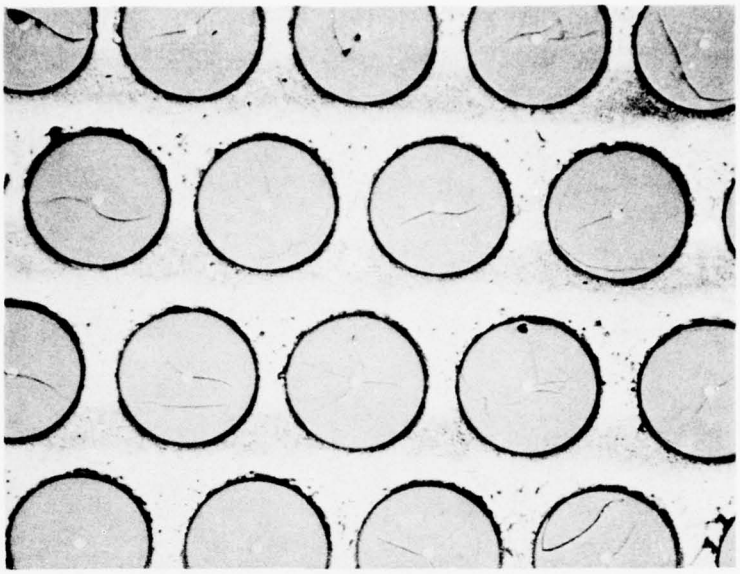

8 Mil Boron-1100/2024 Aluminum 100X

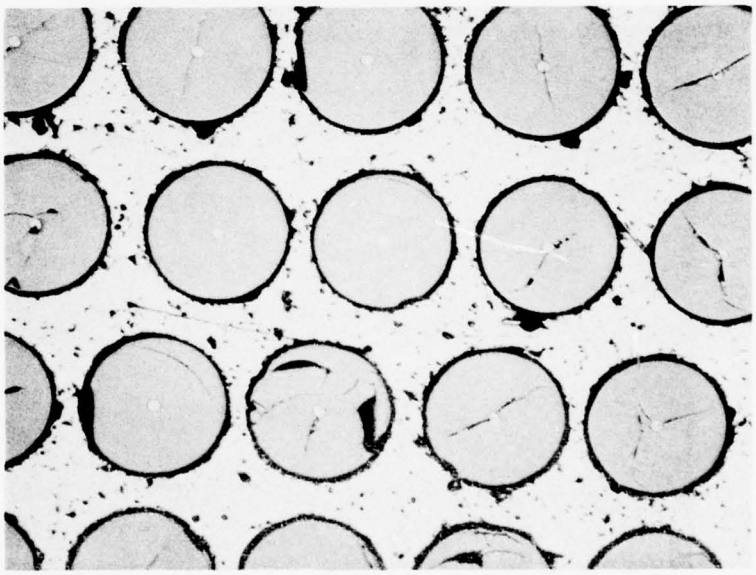

8 MIL Boron-1100 Aluminum 100X

Figure 13. Microstructure of ±15° Air Bonded Panels.

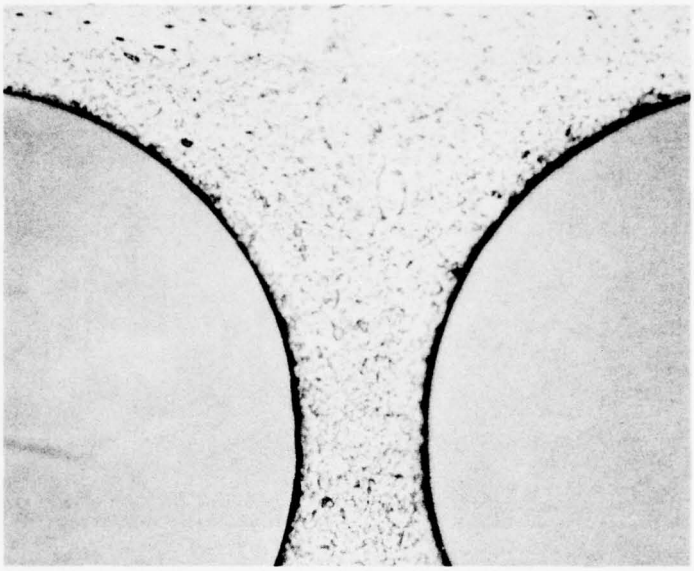

±15° 8 Mil Boron - 1100/2024 Aluminum (Modified Hybrid)

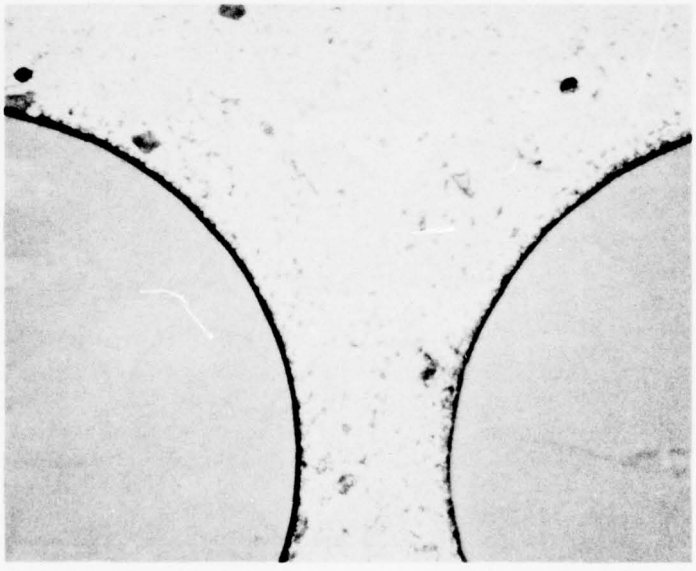

±15° 8 Mil Boron - 6061 Aluminum

Figure 14. Boron-Aluminum Panels Fabricated by Air Bonding.

500X

Properties of the systems are summarized in Table 10. Tensile strength was determined from 1/4 inch wide longitudinal and 1/2 inch wide transverse specimens with aluminum tabs adhesively bonded at the grips. Both longitudinal and transverse tensile strength are highest in 6061, then the 1100/2024 hydrid, and the 1100 matrix. Tensile failure was planar in the 6061 fractures, while considerable filament pullout occurred in the 1100 matrix. The 1100/2024 hybrid showed some pullout.

Shear strength measured by the double notch specimen was in the same range for the $\pm 15^{\circ}$ filament orientation as in the previous unidirectional panels. Fractographic observation also agreed with previous data in showing a filament/matrix failure for the 1100 and 1100/2024 hybrid. The 6061 gave a high shear strength and the fracture, shown in Figure 15, did not generally include filament/matrix failure. The three point bending test gave higher shear values than the notched specimens for all systems but the 6061. Three point bend testing was used as an alternate method of measuring interlaminar shear strength. Specimen size was 1/2 inch x 0.080 inch thickness with spans of 0.350 inch and 0.510 inch used on different ends of the same specimen. Shear failure was judged by either a significant deflection in the load-crosshead curve, observation of specimen shear failure, or an audible failure without observing flexural failure. The shear strength of 1100 and 6061 was measured using a deviation from linearity that was very difficult to accurately measure. The 1100/2024 hybrid exhibited a sharp inflection with shear failure. The load continued to increase in all systems and the maximum point is taken as the maximum flexure strength. This value is consistently higher than the tensile strength although showing some scatter.

Fatigue specimens were sectioned to 1 inch x 4 inches x 0.080 inch with a reduced section 5/8 inch wide between circular notches 5/32 inch in radius. The end of the cantilever specimen was clamped and the free end excited acoustically. Surface strain was monitored with strain gages. Fatigue test results are listed in Table 10. The specimens were run 5×10^6 cycles at one stress level and the stress increased for another 5×10^6 cycles until failure occurred. While the data show some scatter, failure in flexural fatigue correlated with the tensile strength, the 1100/2024 hybrid and 6061 having the highest flexural fatigue strength and the 1100 lower flexural fatigue strength. The 6061 provided the highest torsional fatigue strength while the 1100/2024 hybrid and the 1100 had lower torsional fatigue strength. Torsional fatigue strength appears to correlate with interlaminar shear strength.

Results of impact testing standard 0.394 inch Charpy specimens are summarized in Table 10 and fractured Charpy specimens are shown in Figure 16. The 1100 specimen which absorbed 47 ft-lb of energy exhibits gross specimen deformation as well as filament pullout. The modified 1100/2024 hybrid was the poorest of the group and was dropped from study at this point. The 6061 and 1100/2024 hybrid have slight indications of filament pullout. Scanning electron micrograph of the fractures are shown in Figures 17 and 18. The filament pullout of the 1100 is again obvious. The 1100/2024 illustrates an interesting mixed behavior in Figure 18 where pullout of the 1100 occurs on one half of the filament, the top of the micrograph, while the 2024 has adhered very strongly other half.

TABLE 10

MECHANICAL PROPERTIES OF CANDIDATE SYSTEMS

(All ±15°F 8 Mil Boron)

	1100	1100/2024 Hybrid	6061	1100/2024 Modified Hybrid
Longitudinal Tensile	111,800	151,300	179,200	
Strength (psi)	116,800	158,600	151,800	
Transverse Tensile	9,700	15,400	17,200	
Strength (psi)	10,800	12,900	22,800	
3 Point Bend (psi)				
Shear Stress				
.510" span	-	9,470	13,600	
	-	8,906	12,900	
Shear Stress	7,500	10,125	10,300	
.350" span	7,500	9,562	11,900	
Maximum Flexure Stress	141,000	165,000	209,300	
.510" span	156,000	174,515	186,100	
Maximum Flexure Stress	136,200	136,200	178,900	
.350" span	136,200	95,200	146,300	
Interlaminar Shear	5,620	6,738	14,000	
Strength (psi)	5,407	7,390	> 5,100	
Charpy Impact Energy (ft-lb)				
Longitudinal	47, 45	11.5, 12.5	10, 9.5	7, 7.5
Transverse	5.5, 7	3.5, 4	3.5, 3.5	1, 1.5

TABLE 10 (continued)

MECHANICAL PROPERTIES OF CANDIDATE SYSTEMS

Matrix	Mode	Room Temperature Fatigue Stress	Cycles*
1100	1 Flex	45.3	437,000
1100	1 Flex	45.3	Runout
		51.6	Runout
		55.4	1,386,253
1100	1 Torsional	20	Runout
		25	Runout
		30	1,903,200
1100/2024	1 Flex	45	Runout
		50	Runout
		55	Runout
		60.2	Runout
		65.2	Runout
		70.3	Runout
		75.3	Runout
		78.3	600,000
1100/2024	1 Flex	45	Runout
		50	Runout
		55	Runout
		60	Runout
		65	Runout
		70	Runout
		75	1,200,000
1100/2024	1 Torsional	20	Runout
		25	6×10^6 (failed)
1100/2024	1 Torsional	20	Runout
		25	Runout
		29.5	3.9×10^6
6061	1 Flex	45	Runout
		50	Runout
		55	Runout
		60	Runout
		65	Runout
		70	192,223
6061	1 Flex	45	Runout
		49.9	Runout
		54.7	Runout
		59.6	Runout
		64.4	Runout
		69.3	Runout
		74.2	5×10^6

Runout = 5×10^6 cycles. All stresses are single amplitude.

TABLE 10 (continued)

MECHANICAL PROPERTIES OF CANDIDATE SYSTEMS

Matrix	Mode	Room Temperature Fatigue Stress	Cycles
6061	1 Torsional	20	Runout
		25	Runout
		30	Runout
		35	Runout
		40	Runout
		45	Runout
		50	Runout
		55	5×10^6
6061	1 Torsional	20	Runout
		25	Runout
		30	Runout
		35	Runout
		40	Runout
		45	1,064,000

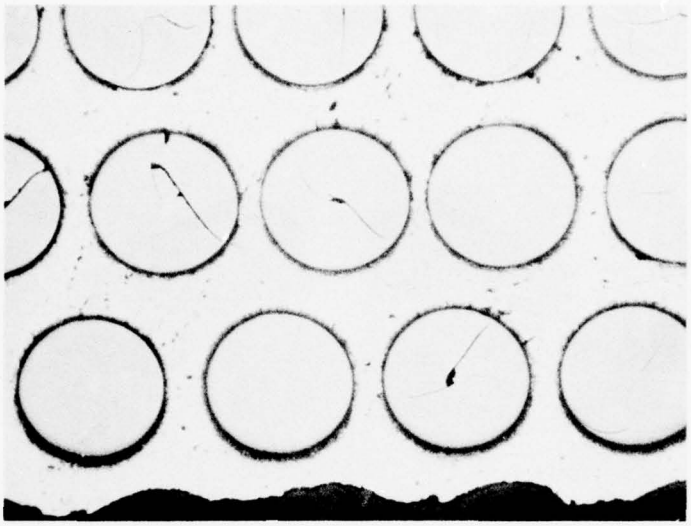

100X

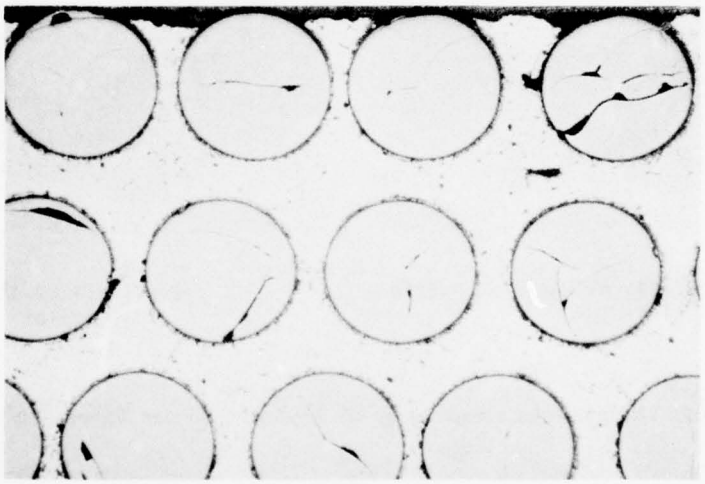

100X

Figure 15. Metallographic Section Transverse to Shear Failure Surface of Air Bonded ±15° 8 Mil Boron - 6061 Aluminum.

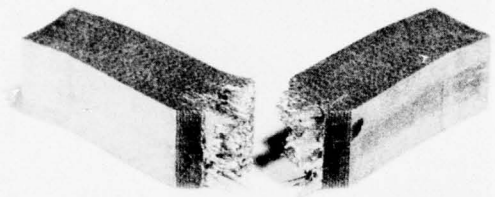

8 Mil B - 1100 Al
47 ft-lbs

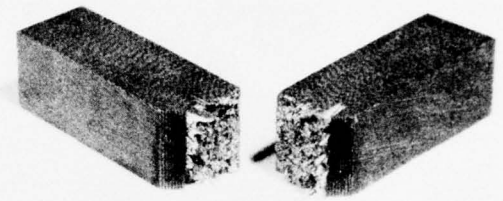

8 Mil B - 1100/2024
11.5 ft-lbs

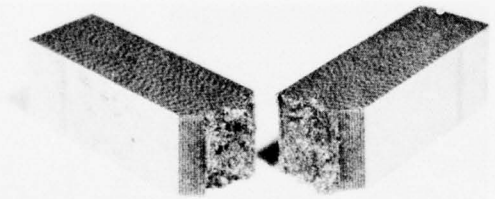

8 Mil B - 1100/2024 Al Modified Hybrid
7 ft-lbs

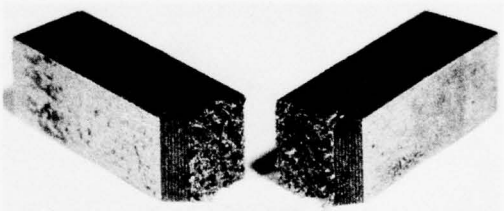

8 Mil B - 6061 Al
10 ft-lbs

Figure 16. Charpy Impact Specimens of ±15° Air Bonded Composite Systems.

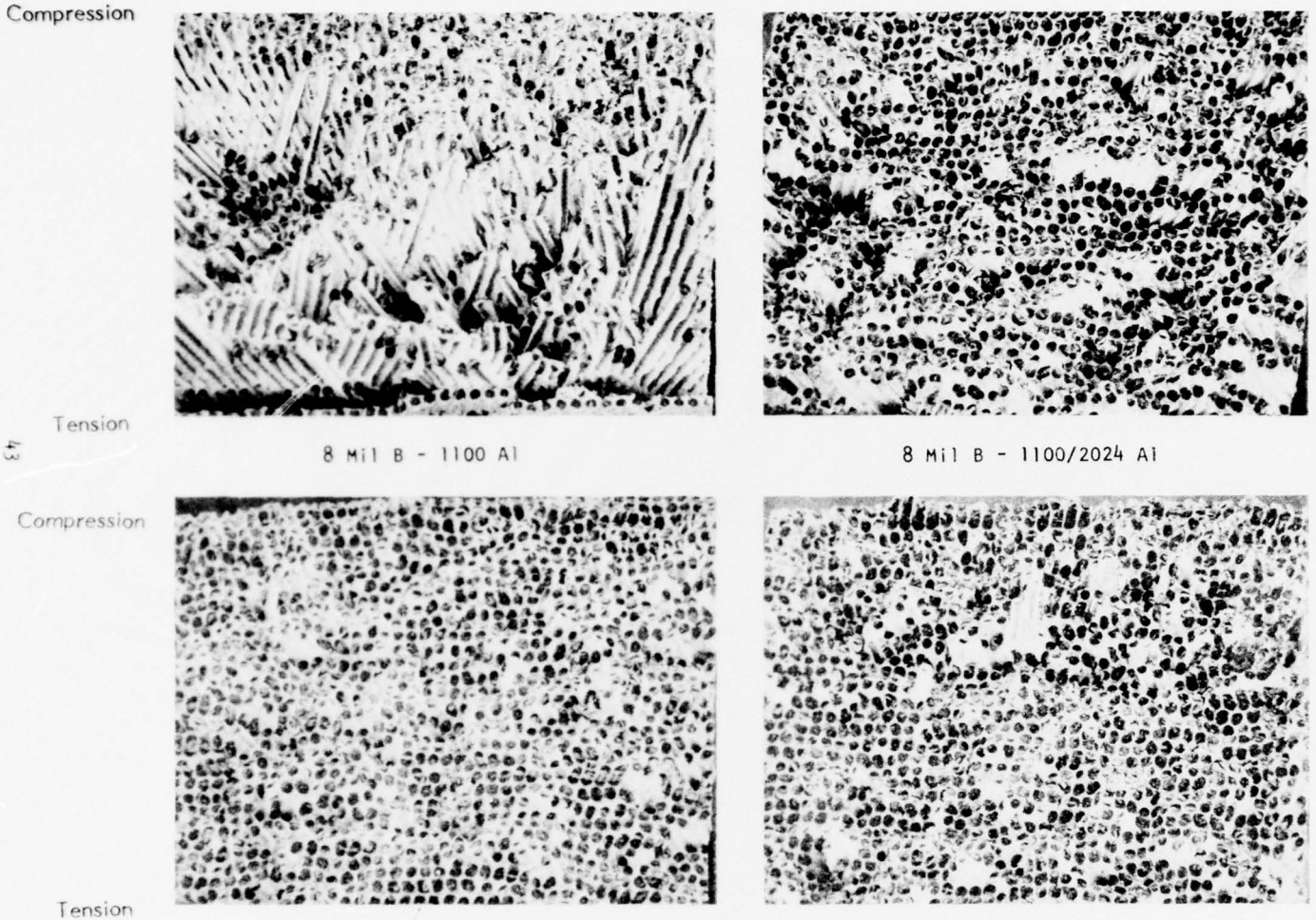

Figure 17. Scanning Electron Micrographs of Full Size Charpy Fracture Surfaces of ±15° Air Bonded Specimens. Longitudinal Orientation 10X.

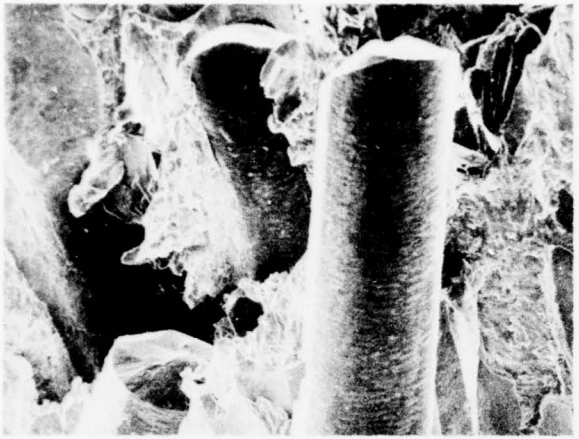

8 Mil B - 1100 Al

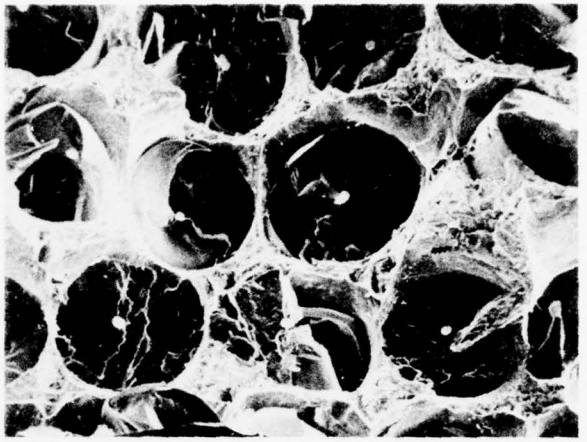

8 Mil B - 1100/2024 Al

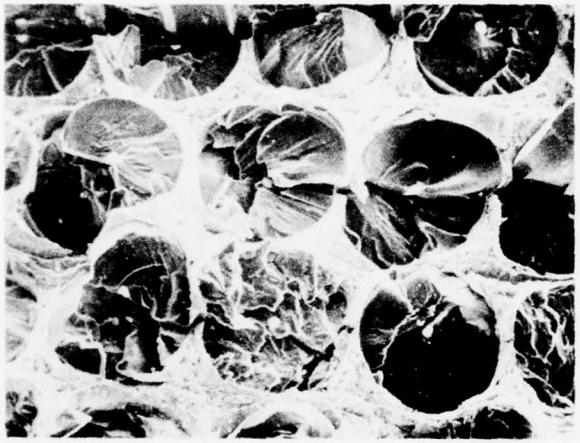

8 Mil B - 1100/2024 Modified Hybrid

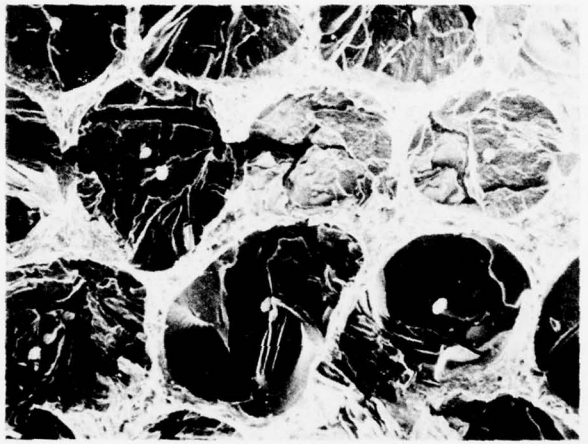

8 Mil B - 6061 Al

Figure 18. Scanning Electron Micrographs of Full Size Charpy Fracture Surfaces of ±15° Air Bonded Specimens. Longitudinal Orientation 100X

Ballistic impact testing was performed on the 1100 and 1100/2024 systems. The specimen used is illustrated in Figure 19 which simulates a root attachment bladelike shape. The specimen was originally designed to measure the effectiveness of various root wedge and splay geometries as well as material and processing variations. The specimen has since been found effective in providing a measure of resistance to so-called gross or structural damage. Like most ballistic impact tests, maintaining specimen geometry, projectile velocity, and projectile energy constant will produce a ranking of material resistance to damage.

The ballistic impact testing facility is illustrated in Figure 20. The system consists of a launch tube operated by helium gas pressure, a RTV rubber projectile which is carried by a styrofoam sabot, and a timing circuit employing photodiode sensors. The projectile mass was about 5-1/4 grams and the two test velocities used were nominally 550 and 900 feet per second. The test specimens were held at the root end and hit 3/4 inch from the free end with the projectile. The projectile mass and velocity determined the kinetic energy and it is assumed that all the energy is transferred during normal incidence impact. Impact energies were approximately 56 and 143 ft-lb for the two tests. Velocities were measured from firing pressure calibration curves for this sequence of tests. Specimens were examined after test to determine the extent of deformation, evidence of fracture or broken filaments, and any unusual fracture or behavior characteristics of the air bonded material.

Specimens after test are shown in Figure 21. Included for comparison are vacuum bonded specimens run under similar but not identical conditions.[4] The degree of deformation in the 1100 is consistent with the vacuum bonded material. The 1100/2024 did not deform as much. Both specimens underwent a gross or structural form of damage. Damage was confined primarily to the root area except for the 145 ft-lb 1100 specimen which also had some local deformation. On the basis of these tests, the air bonded or vacuum bonded material would produce equivalent resistance to structural damage.

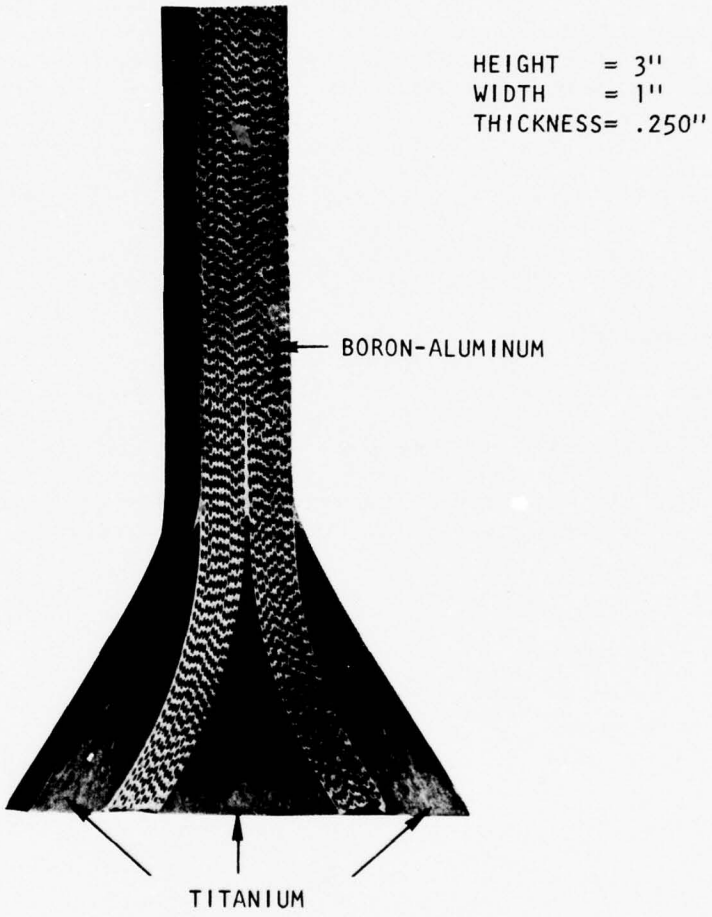

Figure 19. Ballistic Impact Test Specimen.

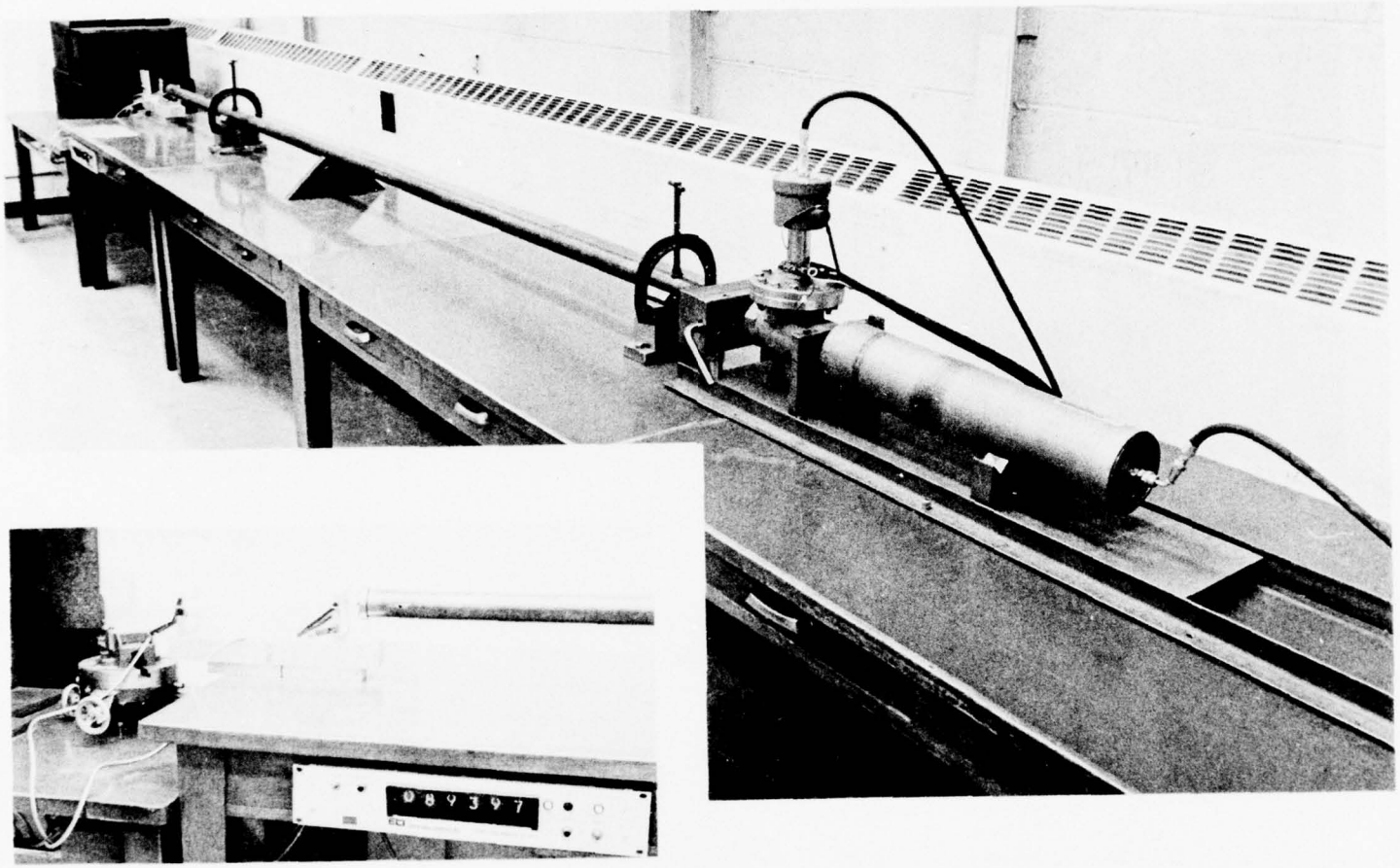

Figure 20. TRW Ballistic Impact Facility.

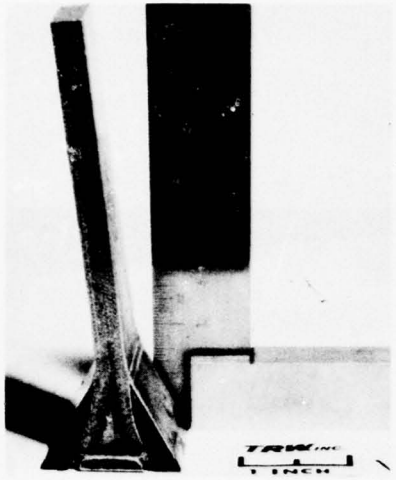

1100
667 Ft/Sec 84 Ft-Lbs
Vacuum Bonded

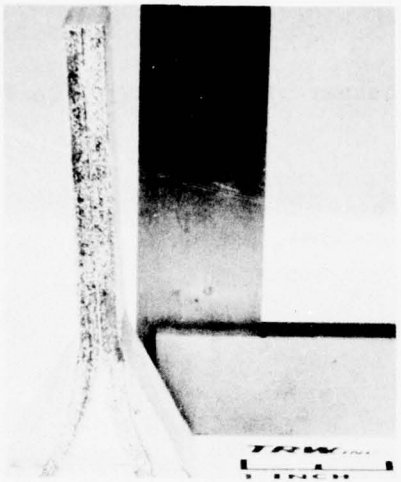

1100
560 Ft/Sec 56 Ft-Lbs
Air Bonded

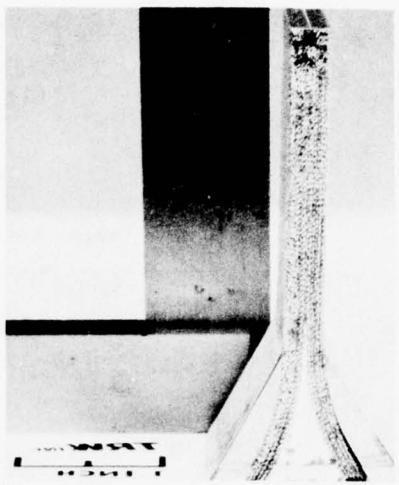

1100/2024
560 Ft/Sec 57 Ft-Lbs
Air Bonded

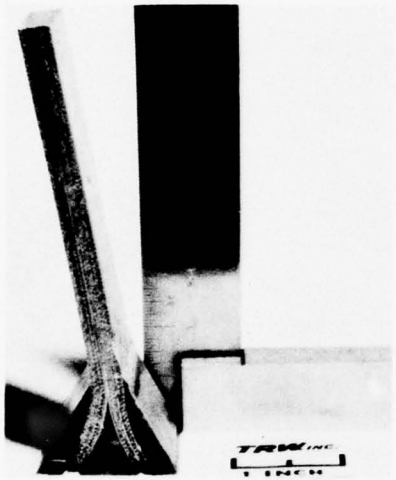

5.6B-1100
621 Ft/Sec 74 Ft-Lbs
Vacuum Bonded

1100
885 Ft/Sec 145 Ft-Lbs
Air Bonded

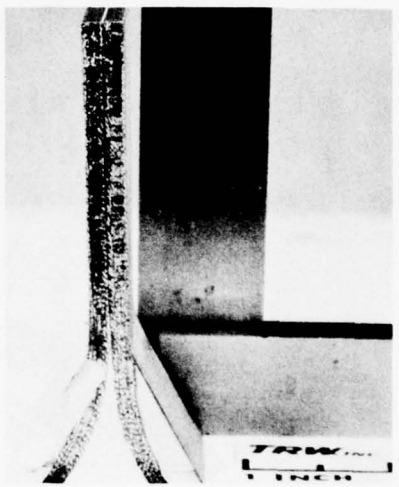

1100/2024
885 Ft/Sec 141 Ft-Lbs
Air Bonded

Figure 21. Ballistic Impact Specimens After Testing. All ±15° Filament Orientation and 8 Mil B Unless Noted.

D. SYSTEM SELECTION

System selection was based upon the material which would provide the highest projected impact properties while meeting other design requirements of the blade. In examination of the Charpy impact energy, in Table 10, it is apparent that the 8 mil boron-1100 aluminum system had the highest pendulum impact resistance. While the actual stress, velocity, and dynamic response produced by a bird impact of a fan blade differ from the Charpy test, materials with improved Charpy values have provided improved whirling arm impact of actual blades.(5) For this reason, the 8 mil boron-1100 system was selected for material evaluation. The longitudinal and transverse tensile strength are adequate for the J-101 blade steady state stresses. The shear strength of the 1100 system may be below the level required locally although use of the measured double notch value in this regard is a conservative estimate.

E. MATERIAL EVALUATION

Panels of ±15° 8 mil boron-aluminum were prepared using the following conditions:

monotape fabricated at 900°F 15 minutes 8 KSI
secondary bond in air at 925°F 15 minutes 15 KSI

Panels were evaluated for elevated temperature tensile, shear, bend strength, fatigue and room temperature sub-size impact, room temperature modulus and resistance to salt corrosion. The modulus measurements were made on specimens sectioned from previous panels.

Mechanical properties are summarized in Table 11. The low longitudinal tensile strength is the result of a shear failure in the grip. However, three point bend tests produced much higher values of strength than the tensile tests. Extensive filament pullout was noted in both longitudinal and transverse tensile tests. The load-deflection curves of the bend test showed non-linearity almost immediately so the presence of shear failure was difficult to determine. Interlaminar shear tests using the double notch specimen were run at both room temperature and 350°F. While the shear strength was low, it is interesting to note that the failure in flexure could reach such a maximum stress without some evidence of a shear failure. Flexural and torsional fatigue strengths were higher than the room temperature values, either because of improved panel quality or an actual temperature effect.

Sub-size impact testing was performed using a specimen 0.4 inch x 2.16 inch x 8 inch ply. This is the standard Charpy width with the thickness reduced and the specimen unnotched. The specimen thickness is comparable to an actual fan blade airfoil. In past work at TRW these specimens have worked well for material or process ranking but the specimen is sensitive to variations in size and simply normalizing for various sizes is difficult. The first two specimens were from current panels while the second two were produced earlier in the program. The impact values are quite high.

Room temperature modulus measurements were performed with strain gaged specimens. A longitudinal specimen of 1/4 inch width and a transverse specimen of 1/2 inch width had strain gages attached to each side and wired to cancel bending moments. Specimens were step loaded in an Instron Tensile Tester and strain gage readings taken. Transverse results are plotted in Figure 22. The modulus was messured as 20.6×10^6 psi. The longitudinal results are plotted in Figure 23 and the modulus was 22.8×10^6 psi. The longitudinal modulus was lower than anticipated.

Resistance to salt corrosion was determined by salt spray testing. Tests were run in accordance with ASTM specification B-117. Two types of tests were employed. In the first case, duplicate tensile specimens were prepared and one exposed to the salt spray fro 168 hours. In the second case, a specimen was examined before and after a 500 hour exposure.

No loss in tensile strength was obtained after the 168 hour salt exposure. The weight gain of the specimen exposed for 500 hours was 0.015 mg/mm^2. The

TABLE 11

PROPERTIES OF ±15° AIR BONDED 8 MIL B-1100 Al

350°F Tensile (psi)	Longitudinal	40,600	grip shear failure
		38,600	grip shear failure
	Transverse	3,300	
		3,600	
		4,400	
350°F 3 Point Bend (psi)	0.350" Span	61,000	
		57,900	
	0.510" Span	58,242	
		50,900	
Interlaminar Shear Double Notch Specimen (psi)	RT	4,300	
		5,300	
	350°F	2,200	
		2,500	
Unnotched Thin Panel Charpy	RT	25.6 in-lb (71 ft-lb/in^2)	
		23 in-lb (64 ft-lb/in^2)	
	RT	25 in-lb (69 ft-lb/in^2)	
		26.2 in-lb (101 ft-lb/in^2)	
Elastic Modulus (psi)	RT	Longitudinal 22.8 x 10^6	
		Transverse 20.9 x 10^6	
Flexural Fatigue	350°F	45 ksi	Runout
		50 ksi	Runout
		55 ksi	Runout
		60 ksi	2 x 10^6 cycle
	350°F	51.6 ksi	306,000 cycle
Torsional Fatigue	350°F	20	Runout
		25	Runout
		30	Runout
		35	Runout
		40	5 x 10^6 cycle
	350°F	20	Runout
		25	Runout
		30	Runout
		34	5 x 10^6 cycle

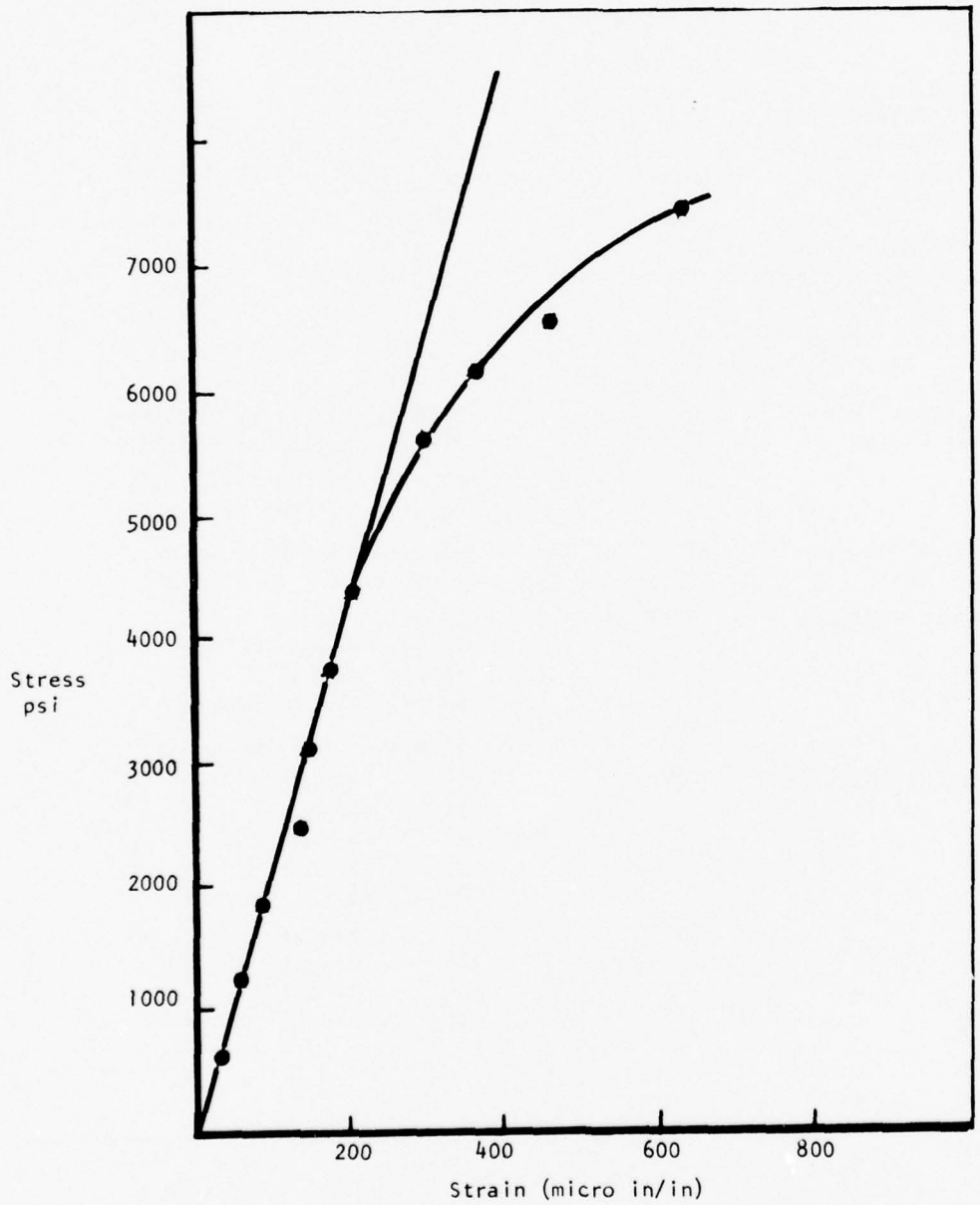

Figure 22. Transverse Stress-Strain Curve of Air Bonded ±15° 8 mil B-1100 Al

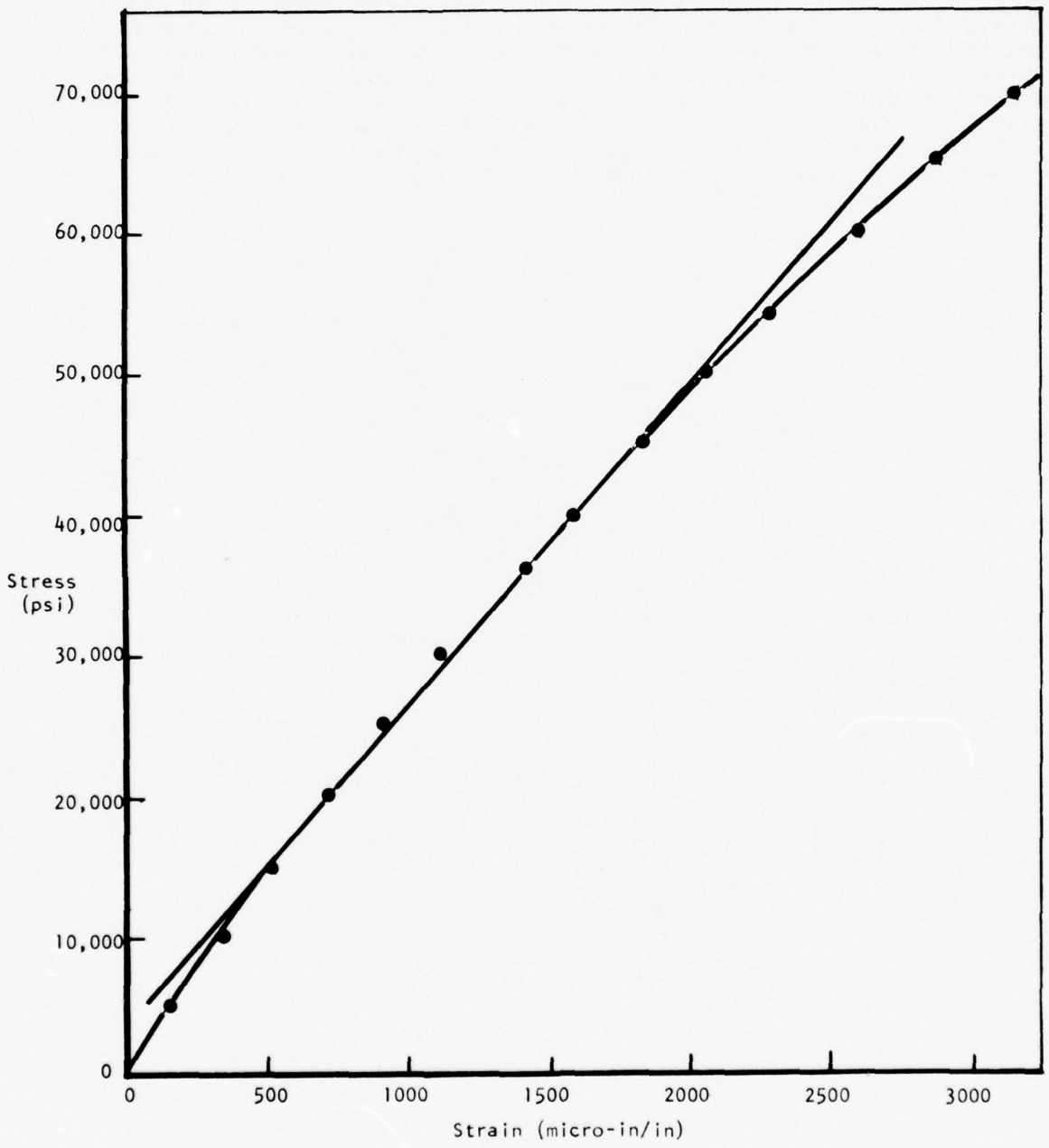

Figure 23. Longitudinal Stress-Strain Curve of Air Bonded ±15° 8 mil B-1100 Al

specimen appearance was similar to a piece of unreinforced aluminum exposed during the same cycle. Some salt was still adhering to the side of the specimen in roughened areas where the fibers came to the surface which contributed to the weight gain.

While material evaluation was limited to panel shapes in the present program, TRW has applied air bonding to more complicated forms. Figure 24 illustrates diamond cross section panels fabricated to evaluate localized ballistic impact resistance. This program was performed for NASA under a GE subcontract.(6) Two J-101 fan blades fabricated under a NASA purchase order and one under TRW IR&D are shown in Figure 25 and a typical microstructure in Figure 26. TRW is also currently air bonding CF6 fan blades for a feasibility demonstration(6) and to produce blades for whirling arm test.(7) Prototype F-404 blades are also being fabricated for whirling arm test.(8)

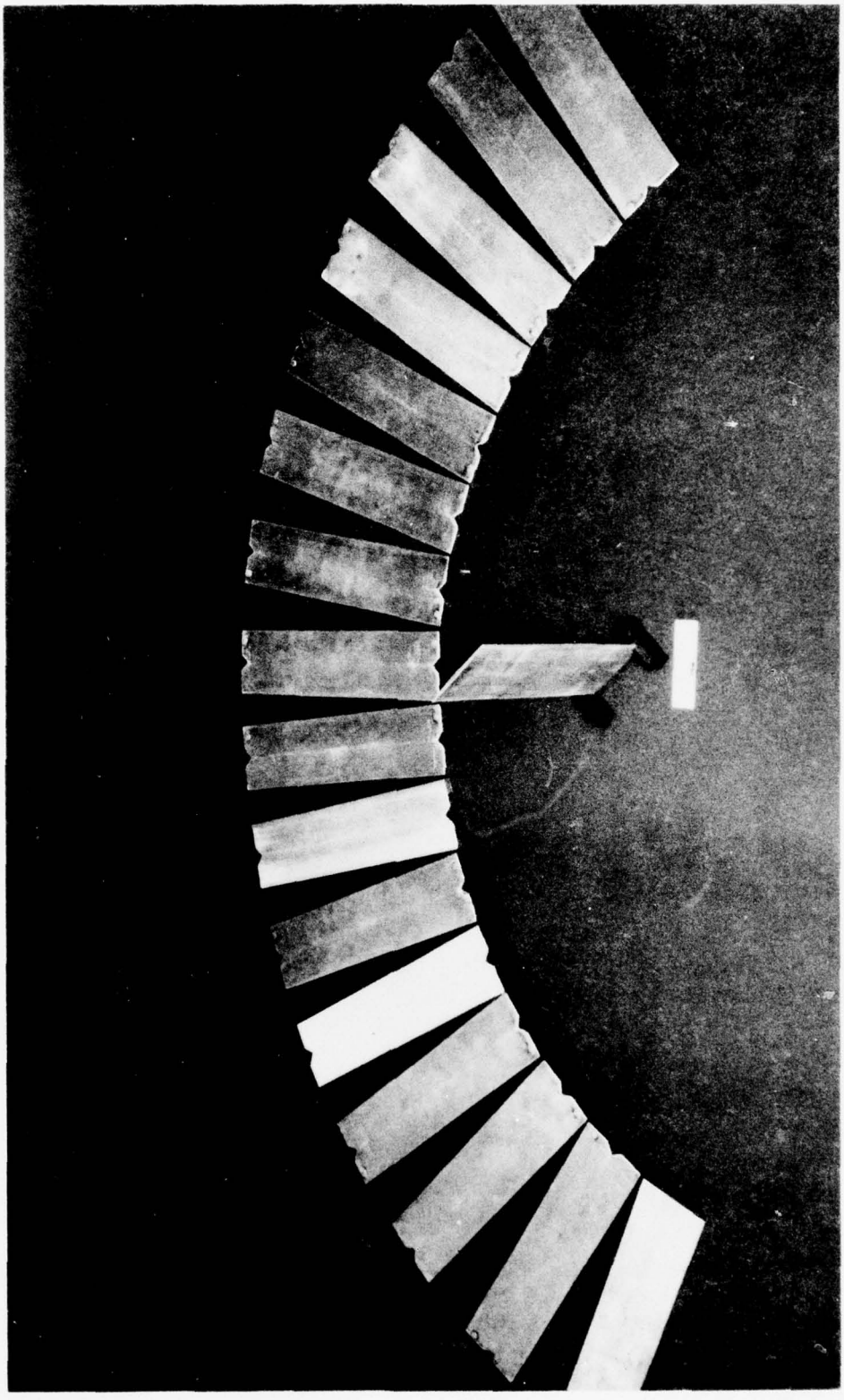

Figure 24. Air Bonded Blakelike Shape Specimens Produced for FOD Testing.

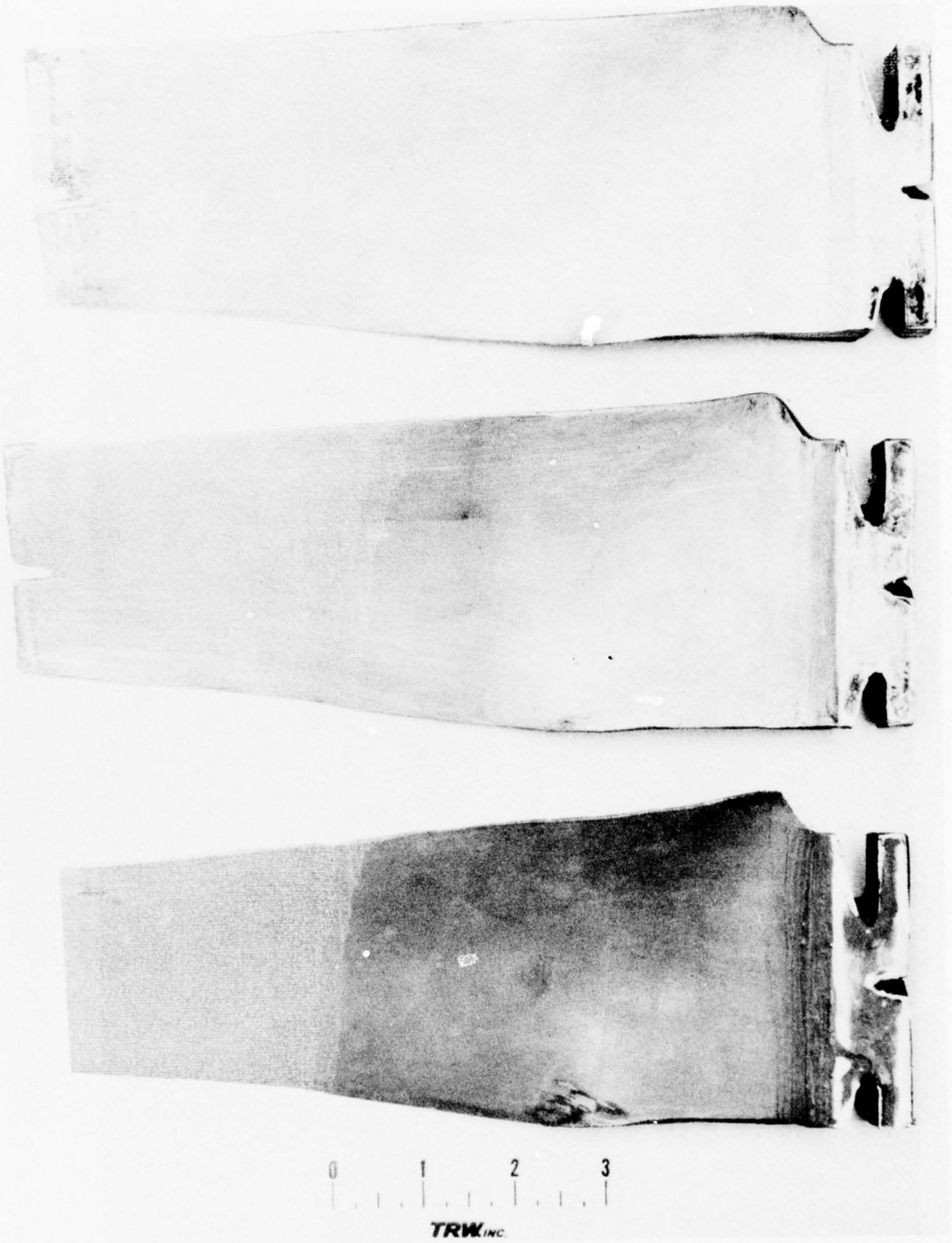

Figure 25. Air Bonded Boron-Aluminum J101 Fan Blades Fabricated by TRW.

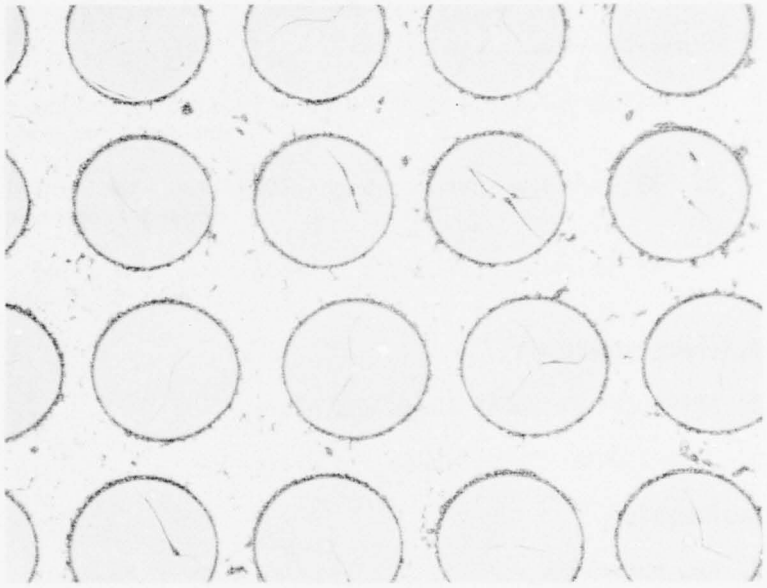

Figure 26. Microstructure of Air Bonded Boron-Aluminum J101 Fan Blade.

F. PRELIMINARY PROCESSING SPECIFICATION

PRELIMINARY PROCESSING SPECIFICATION FOR AIR BONDED BORON-ALUMINUM

1. SCOPE

This specification presents preliminary requirements for boron-aluminum fabricated in air into panel and blade form from fully dense monotapes. Its purpose is to summarize the recommended processing for these materials.

1.1 Classification

A. 45-55 volume percent boron-1100 aluminum alloy diffusion bonded from monotapes.

B. 45-55 volume percent boron-2024/1100 aluminum alloy diffusion bonded from monotapes.

C. 45-55 volume percent boron-6061 aluminum alloy diffusion bonded from monotapes.

2. APPLICABLE DOCUMENTS

2.1 AMS 4026 6061 sheet and plate

2.2 QQ-A-250 4E 2024 sheet and plate

3. REQUIREMENTS

3.1 Raw Materials

3.1.1 Filament

The filament shall have a minimum UTS of 450 KSI and a diameter tolerance of ±0.0001 inch for 5.6 mil and 0.0002 inch for 8 mil.

3.1.2 Foil

The foil shall conform to applicable AMS or QQ specification. Foil shall be clean of grease or visible stains. Thickness tolerance shall be ±0.0001 inch. Preferred starting thickness is 2.3 mils for 5.6 mil fiber and 3.1 mils for 8 mil fiber.

3.2 Monotape

3.2.1 Monotape Fabrication

Monotapes shall be fully dense diffusion bonded from foil.

Monotape fabrication shall be performed at the lowest temperature consistent with the intended applications. Recommended is

Class A	900°F ±10°	15 minute	8 KSI
Class B	850°F ±10°	15 minute	8 KSI
Class C	850°F ±10°	15 minute	8 KSI

3.2.2 Monotape Requirements

3.2.2.1 Gaps between filaments.

Gaps shall not exceed 1/32 of an inch.

3.2.2.2 Cross-over Filaments

Single or multiple filament cross-over is not permitted.

3.2.2.3 Surface of Monotape

The surface shall be clean, smooth and free of contamination.

3.2.2.4 Fiber Alignment

The angular tolerance of fibers shall be ±2°.

3.2.2.5 Consolidated Tape Quality

There shall be no voids, delamination, stray fibers, broken fibers, or foreign material that degrade the mechanical properties.

3.2.2.6 Volume Fraction

The volume fraction percent of the fiber shall be maintained within ±2-1/2%.

3.2.2.7 Formability

The buyer may establish a monotape formability requirement.

3.2.2.8 Filament Spacing

The average filament spacing will be 6.9 mils for 5.6 mil fiber and 9.6 mils for 8 mil fiber.

3.2.2.9 Thickness Control

The final thickness shall be held to ±0.0001 inch.

3.2.2.10 Organic Binder

The filament mat shall employ a polystyrene binder applied as a solution of xylene and polystyrene.

3.3 Panel or Blade Fabrication

3.3.1 Surface Treatment

Prior to bonding monotapes will be given a surface treatment described in TRW Patent Application S/N 685,812.

3.3.2 Bonding

Parts shall be bonded by hot pressing in air with preheated dies. Cooling shall be by withdrawal and air cooling.

3.3.3 Bonding Parameters

Bonding parameters shall be governed by the final application. Recommended are insertion into hot dies and the following bonding cycle when the composite is at temperature.

Class A	925°F	15 minutes	12 KSI
Class B	910°F	15 minutes	10 KSI
Class C	900°F	15 minutes	10 KSI

4. QUALITY CONTROL

4.1 Mechanical Properties

4.1.1 Tensile

Tensile specimens taken from the part shall be capable of demonstrating the tensile properties specified for the application. Minimum panel tensile strength shall be:

Class A	110,000
Class B	150,000
Class C	150,000

4.1.2 Single Filaments

Single boron filaments extracted from a trim section of the part shall average 350 KSI UTS.

4.1.3 Shear

Shear test and properties shall be agreed upon by vendor and customer.

4.2 Structure

Metallographic examination shall show no evidence of significant interstitial contamination and full metallurgical bond at matrix interface.

4.3 Ultrasonic Inspection

Ultrasonic standards for inspection will be as agreed upon by vendor and customer. A mutual ultrasonic standard will be employed in the event of indications for rejection.

4.4 Radiographic Inspection

Radiographic inspection shall be per MIL-I-86700 May 8, 1975.

G. PRELIMINARY COST ANALYSIS

Boron/aluminum is considered a viable material for blade application in terms of both properties and cost. As TRW internal commitments grew in this materials area and as external funding was gained, considerable effort has been expended upon cost analysis of metal matrix composites. In addition to the present program, these analyses have been performed in support of a National Materials Advisory Board committee on metal matrix composites to justify internal IR&D support of metal matrix composites, as contract requirements on various externally funded programs, and more recently, to quote production quantities of boron/aluminum fan blades for an advanced engine of a major engine manufacturer. Major conclusions from these efforts are that the use of fully consolidated monotapes offers advantages in cost and properties, that boron/aluminum composites can be produced at almost half the cost of a titanium blade, and most important, that air bonding offers significant savings.

It should be pointed out that the B-Al blades fabricated to date were not produced by a production process since no such facility exists for B-Al blades. Therefore, in projecting the cost of B-Al blades in production quantities and in order to assess its cost competitiveness with currently used blades or vacuum processing, certain assumptions must be made based on two major factors: a) material/process characteristics established in the laboratory, and b) prior experience in scaling up fan blade material/process combinations from the laboratory to the factory for production volume manufacture. The value of fan blade production experience and a widely based knowledge of the turbine engine blade business must not be underestimated. Without the identification of those assumptions and prior experience in scaling up fan blade material/process combinations, one cannot have much confidence in the projected cost.

Cost savings due to air bonding have been estimated by analogy with two production processes presently used by TRW, precision investment casting and heat treatment. TRW has extensive and sophisticated facilities for vacuum casting and heat treating which are used to produce high tolerance turbine components from nickel and cobalt base superalloys. For a given part and with considerable automation of the vacuum process including vacuum interlocks, it costs four times as much to case a part in vacuum than in air. TRW also heat treates in both vacuum and air and the relative cost of vacuum heat treatment is 1-3 times heat treating in air. Both of these examples are mature widely used industrial production processes and illustrate the magnitude of the differential cost to be expected between air and vacuum bonding.

The effect of such a reduction on blade cost may be estimated by comparison with fabrication costs of a typical blade fabricated by bonding in inert atmosphere. The various costs associated with the fabrication of typical fan blades from B-Al diffusion bonded monotapes were recently analyzed and presented to the NMAB Committee on Metal Matrix Composites. The assumptions used in the cost analysis are summarized in Table 12.

Air bonding would reduce monotape cost, assembly cost and blade molding cost. The monotape raw material is a large fraction of the estimated blade cost. The lower limit for the monotape cost at $25/lb is projected on the basis of post-1980 boron prices and the use of the Air Force/TRW process of roll diffusion bonding in air.(1) Air bonding would further reduce the molding costs to $5/blade and the blade assembly cost to $8/blade compared to vacuum bonding. The cost reduction in molding and assembly is due to the elimination of vacuum encapsulation.

TABLE 12

ASSUMPTIONS FOR B/AL BLADE COSTING

1. $25/hour was used for labor plus overhead. This relatively high labor cost also included normal amortization of facilities.

2. Material and labor cost elements were marked up by 20% G&A.

3. The blade fabrication process is based on the use of (fully consolidated) diffusion bonded monotape through a one-step hot pressure bonding approach for the blade molding.

4. Blade data:

   length = 10"; chord width = 2.5"; thickness = 1/8"-1/4"

   average airfoil pitch thickness = 0.187"

   average airfoil volume (0.187 x 2.5 x 10) = 4.7 in^3

   B/Al airfoil weight (4.7 x 0.1) = 0.47 lb

   Ti airfoil weight = 4.7 x 0.16 = 0.75 lb

5. Assume that actual reduction in airfoil volume due to chord taper is equivalent to material waste.

6. Root blocks are fabricated from Ti alloy powder by precision P/M forging.

7. Wedges are made from titanium alloy. The design is similar to Figure 19.

8. Stretch formed and plated stainless leading edge inserts are used.

9. Ply-preform generation and blade assembly is done on mechanized equipment.

10. Blade molding by hot pressure bonding in inert atmosphere (no vacuum). Bonding time 10 minutes for B/Al.

11. At the 10,000 blade level, it is assumed that the plant is producing a total of 50,000 similar parts.

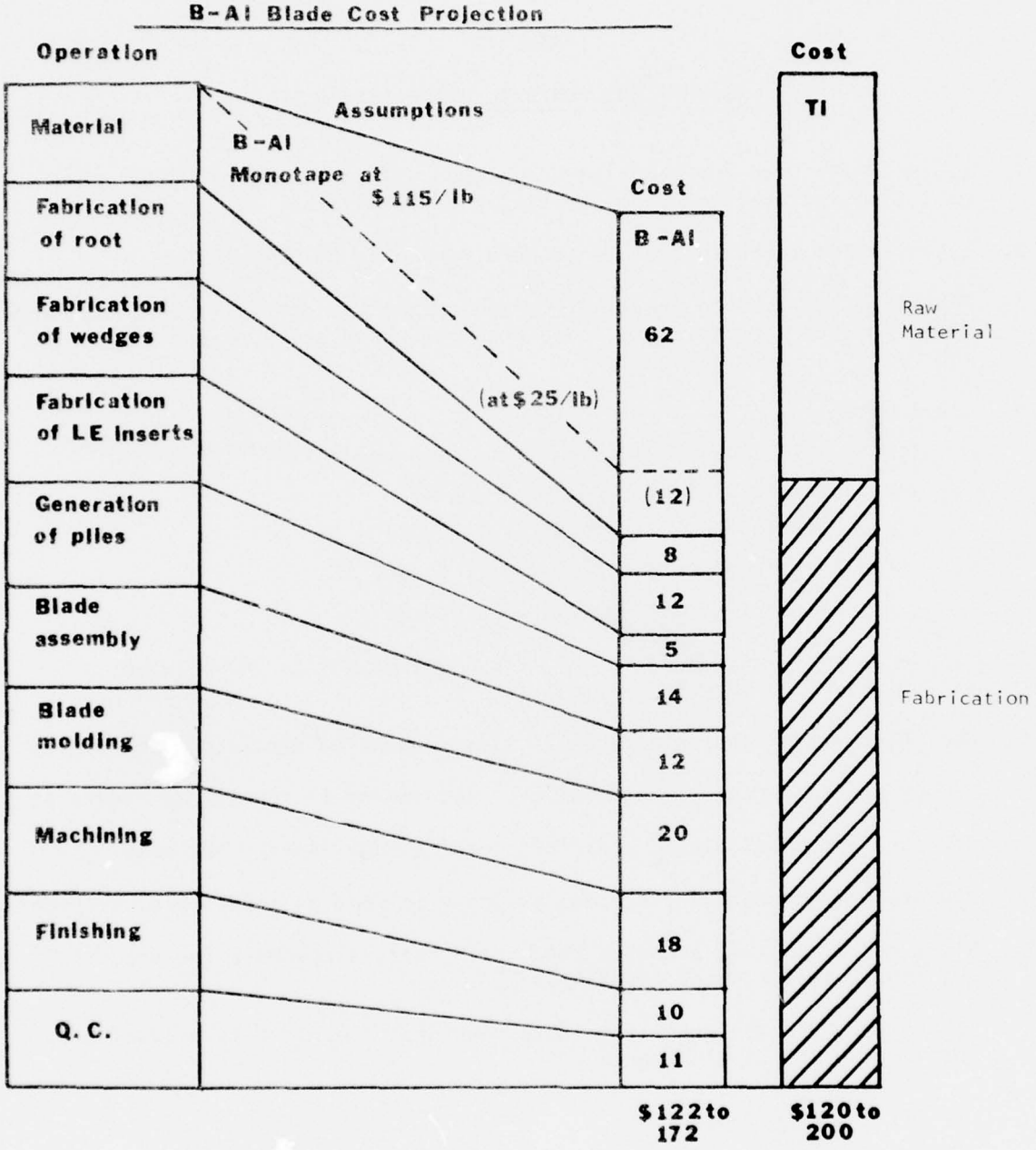

Figure 27. Cost Projection for Vacuum Bonded Boron-Aluminum Blade

H. BLADE STRENGTH REQUIREMENTS

Analytical studies have been performed to determine the operating stresses of the J101 B-Al stage 1 fan blade during engine design point operating conditions and during bird impacts. The results of these studies have been compared with material strength data obtained from test specimens to ascertain which material candidates best satisfy the J101 fan blade strength requirements.

The J101 engine system is an advanced, high thrust to weight design with supersonic operational capability. Incorporation of B-Al is compatible with the high fan inlet temperature requirements of this application. Additionally, the use of B-Al fan blades will further improve the engine thrust to weight ratio. Selection of the first stage fan blade incorporates lightweight composites where the maximum weight reduction exists, 14 pounds for the J101 design. Figures 28 and 29 compare a titanium and B-Al blade, respectively.

NORMAL OPERATION ANALYSIS

The purpose of this analytical study was to identify the boron/aluminum material strength requirements for the J101 blade normal operating conditions. Four three-dimensional finite element analyses (TAMP) were run to determine the blade aeromechanical stability characteristics and stresses as a function of boron filament orientation.

Approach

The TAMP three-dimensional finite element computer program was used to calculate blade natural frequencies, steady state and alternating stresses. Four runs were made, two with each boron filament orientation. These outputs were then used to determine that both designs have acceptable aeromechanical stability characteristics. Next, calculated steady state and alternating tensile stresses were used to construct a Goodman diagram, from which factors of safety were estimated and material design stresses predicted. These values were compared with material specimen test results obtained for several B-Al composite materials. Figure 30 schematically shows the approach used in this task.

J101 Fan Blade Geometry

Table 13 summarizes and compares the J101 B-Al stage 1 fan blade geometric characteristics with those of its titanium counterpart. Note that the B-Al blade geometry is identical to that of the titanium blade except the mid-span shroud has been eliminated. Preliminary design efforts had been done on the NASA SCAR program(9) to define the blade preliminary design. The blade geometry was constant during all studies performed during this program.

Material Properties

Material properties were calculated for two material designs; i.e., 8 mil diameter boron with a $\pm 15^{\circ}$ orientation and 8 mil diameter boron with a $0^{\circ}/20^{\circ}$ orientation. The two filament orientation angles were selected on the basis of preliminary aeromechanical stability calculations and impact resistance results

Figure 28. J101 First Stage Titanium Fan Blade.

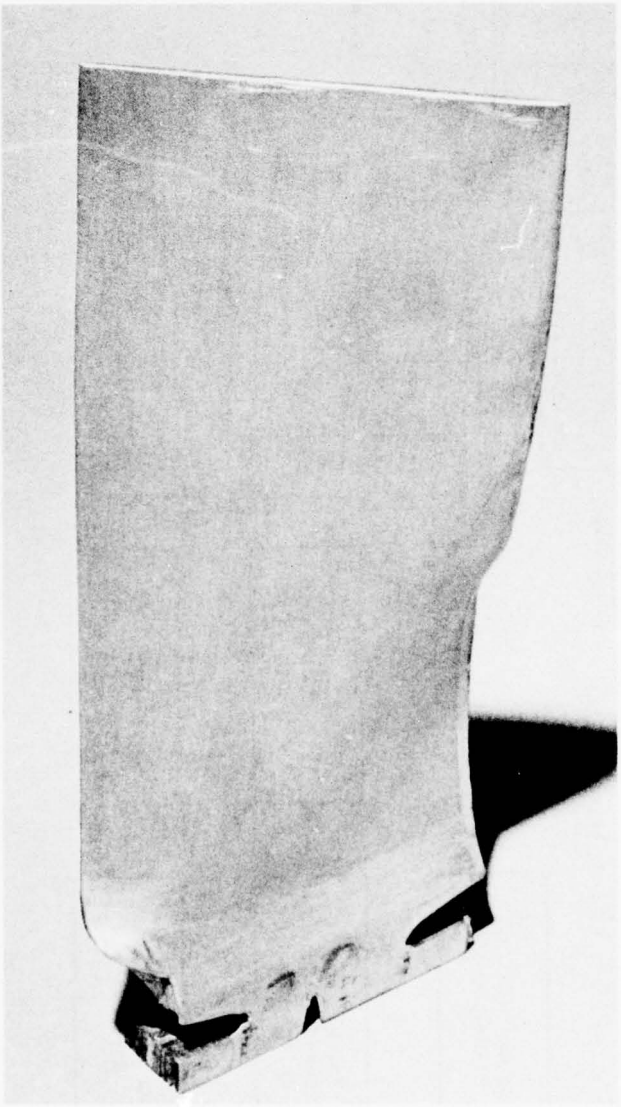

Figure 29. J101 Stage I Air Bonded Boron/Aluminum Fan Blade

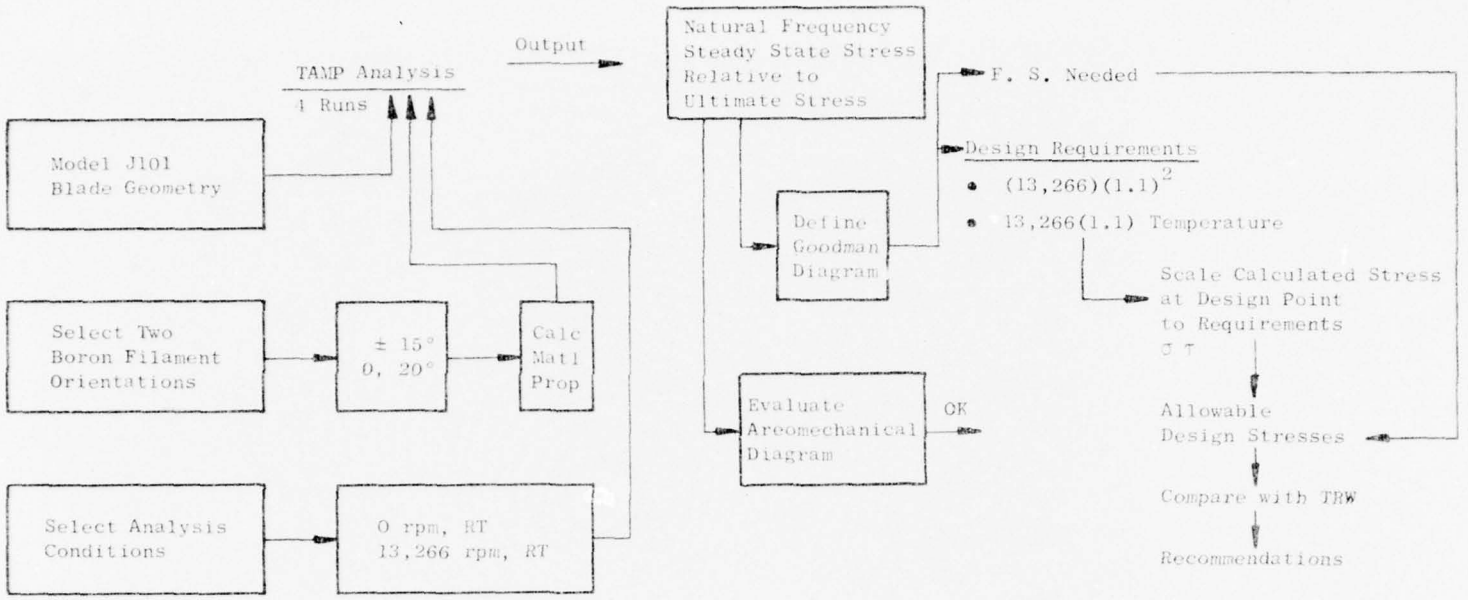

Figure 30. Schematic of Normal Operation Analysis Analytical Approach.

TABLE 13

BLADE SUMMARY, J101 STAGE 1 FAN BLADE

Parameter	Present Metal Blade	Composite Blade
N_b No. of Blade	32	32
Materials	6-4 Ti	B/Al
Temperature, °F	175	175
C_o	3.52	3.52
C_t	3.60	3.60
T_M/C_o	0.068	0.068
T_M/C_T	0.025	0.025
$Solidity_o$	2.62	2.62
$Solidity_t$	1.40	1.40
R_t (Inlet)	13.16	13.16
R/R (Inlet)	0.45	0.45
β_o*	18.72	18.72
β_t*	60.89	60.89
ϕ	1.094	1.50
θ_o	99.7	99.7
θ_t	2.93	2.93
Mid-Span Location	50%	No Mid-Span

C_o = Chord at root, inches

T_M/C_T = Airfoil maximum thickness/chord at tip, dimensionless

R_t = Radius at tip, inches

R/R = Airfoil root radius/tip radius, dimensionless

β* = Airfoil stagger angle from tangential, degrees

ϕ = Tip untwist, degrees

θ = Airfoil camber, degrees

Subscript

o = root

t = tip

obtained on the SCAR program which indicated these two orientations had good Charpy impact strength.

Table 14 summarizes the B-Al material physical properties of the 57 percent volume fraction B-Al material used in the analysis. Note that, for the two filament orientations, the modulus of elasticity and Poisson's ratios are quite similar. Further, there is very little change in properties due to temperature. The largest change due to temperature is in the shear modulus (G). Figures 31 and 32 show, for the two orientations, the effective three-dimensional material properties used in the region of the blade which is nickel plated. These data are shown as a function of the thickness of the combined material.

Design Point Operating Conditions

The J101 engine specifications were used to define the design point operating conditions as summarized below.

Condition	RPM	Temperature (^{o}F)
Hot Day Takeoff	13,266	175
Max. Steady State Operation	13,935	350
Max. Design Overspeed	14,215	350
Burst Speed	16,345	Room Temperature

The blade must be designed to have infinite life (10^{7} cycles) at the maximum steady state operating condition. The maximum design overspeed and burst conditions represent low cycle requirements.

For this program, the TAMP analyses were performed at the hot takeoff condition for two rotor speeds, zero and 13,266 rpm. Stresses at other conditions were scaled from the TAMP results.

Analytical Model

Figure 33 shows the three-dimensional finite element (TAMP) model of the J101 B-Al blade, using one element through the blade thickness. TAMP is a multipurpose finite element computer program capable of calculating the steady state stresses and lowest forty natural modes of vibration of composite blades.

The program utilizes an eight-noded isoparametric box element, shown in Figure 34, of practically any shape. This is a nonconstant strain element with 33 degrees of freedom (24 internal to minimize strain energy). The present modeling limits provide up to 900 nodal points, 580 elements, and 10 different materials. The program accounts for the inertial forces of rotation and vibration. Thermal stresses can also be computed. The root can be restrained by both friction and springs. Distributed pressures or point forces can be applied as external loads to the structure.

The material property input to the program consists of the bulk elastic properties, including different moduli in the radial, chordwise and thickness directions; different Poisson's ratios between these three directions; and different shear moduli between these three directions. Thus, nine constants are used to describe the elastic properties of the materials.

TABLE 14

B/AL MATERIAL PROPERTIES

(Calculated from Advanced Composite Design Guide, Program AC-3)

		(±15) Layup		(0/20) Layup	
		Temperature (°F)		Temperature (°F)	
		175	350	175	350
Tension	E_x	31.5	30.5	31.9	30.9
	E_y	21.6	20.7	21.8	20.9
	G_{xy}	7.7	6.0	7.5	5.8
	M_{xy}	.236	.184	.220	.171
	M_{yx}	.163	.140	.152	.130
Compression	E_x	31.5	32.5	31.9	32.9
	E_y	21.6	18.1	21.8	18.3
	G_{xy}	7.7	6.0	7.5	5.8
	M_{xy}	.236	.127	.220	.127
	M_{yx}	.163	.163	.152	.163
Bending	E_x	31.5	31.5	31.9	31.9
	E_y	21.6	17.4	21.8	19.6
	G_{xy}	7.7	6.0	7.5	5.8
	M_{xy}	.236	.155	.220	.145
	M_{yx}	.163	.151	.152	.141

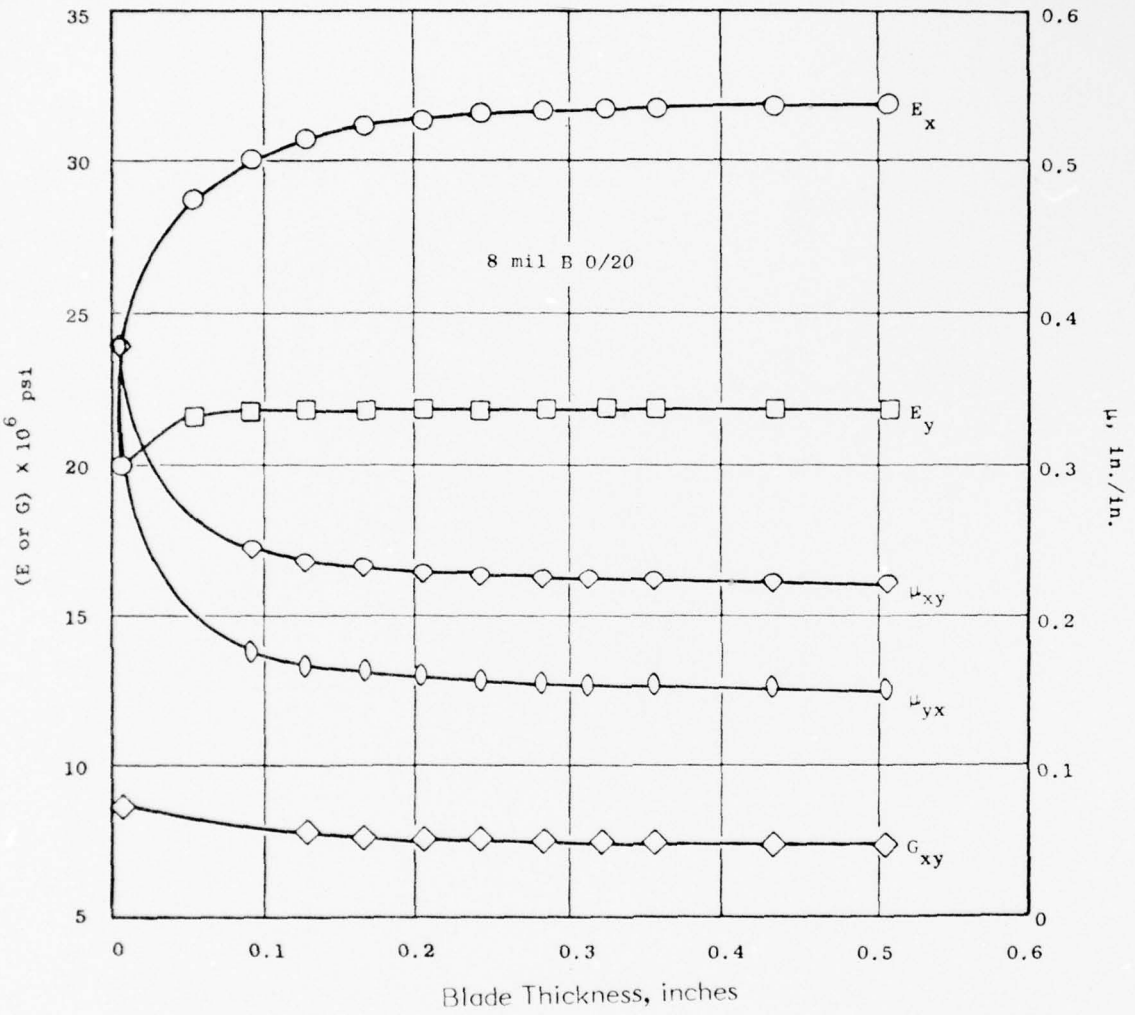

Figure 31. Influence of Nickel Plating on Elastic Properties of 0^o, 20^o B/Al at Various Blade Thicknesses.

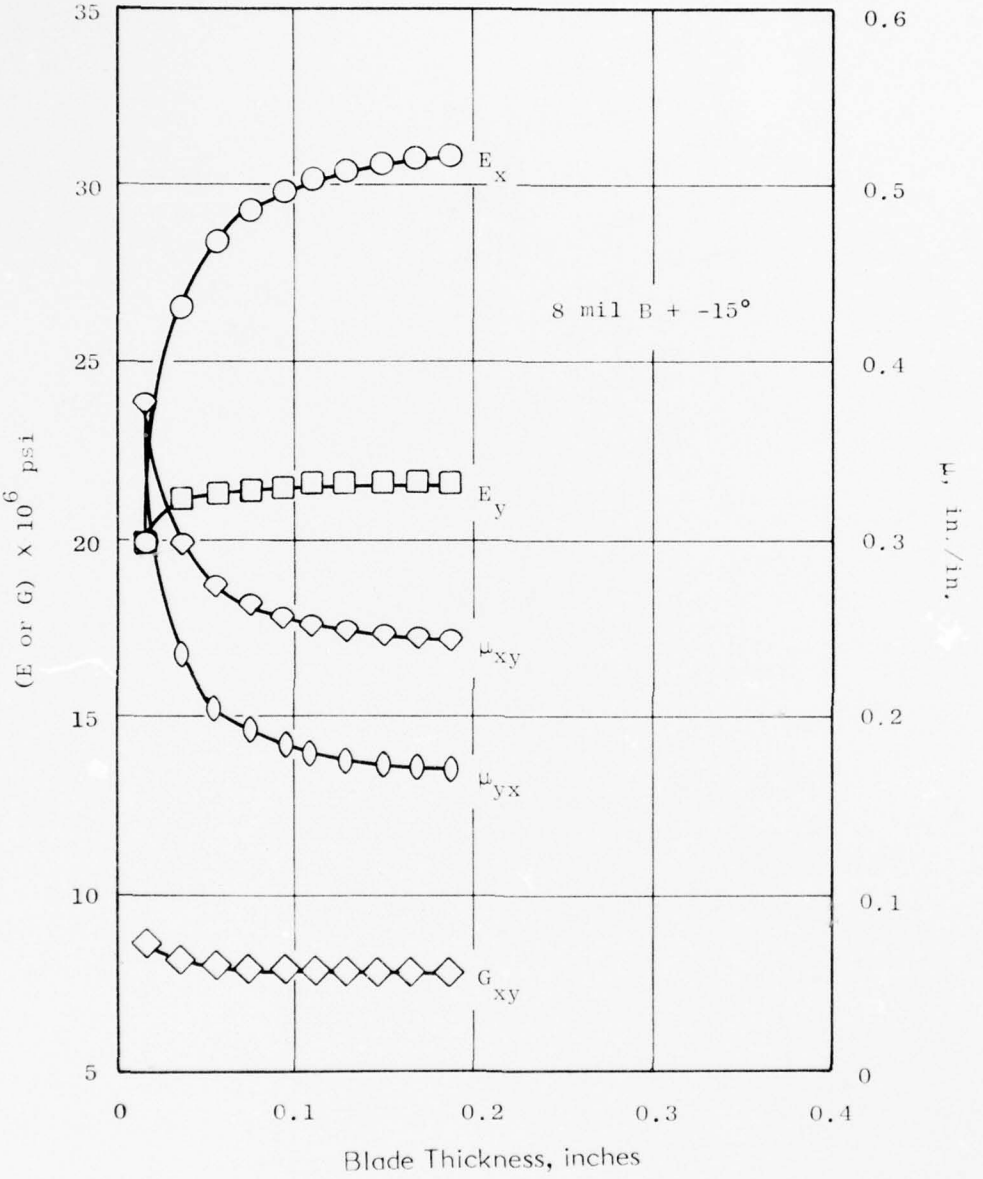

Figure 32. Influence of Nickel Plating on Elastic Properties of $\pm 15^{\circ}$ B/Al at Various Blade Thicknesses.

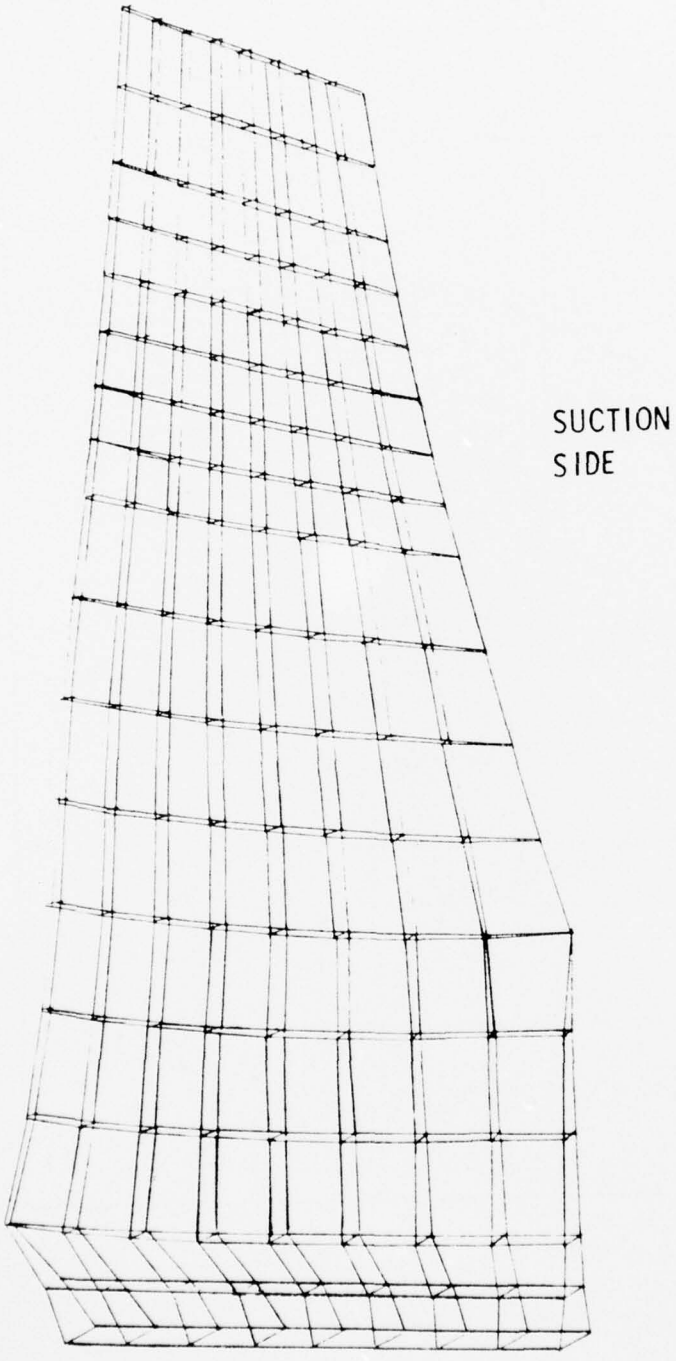

Figure 33. J101 B/A1 Blade, TAMP Model.

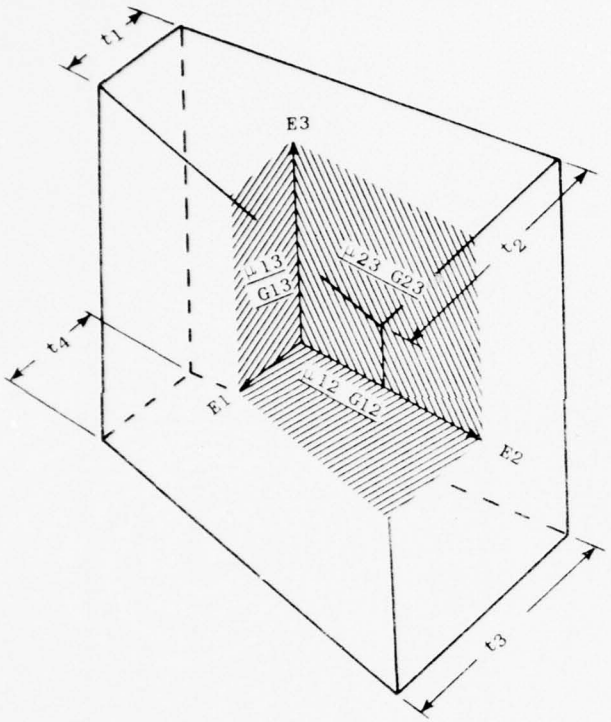

MATERIAL PROPERTY ORIENTATION

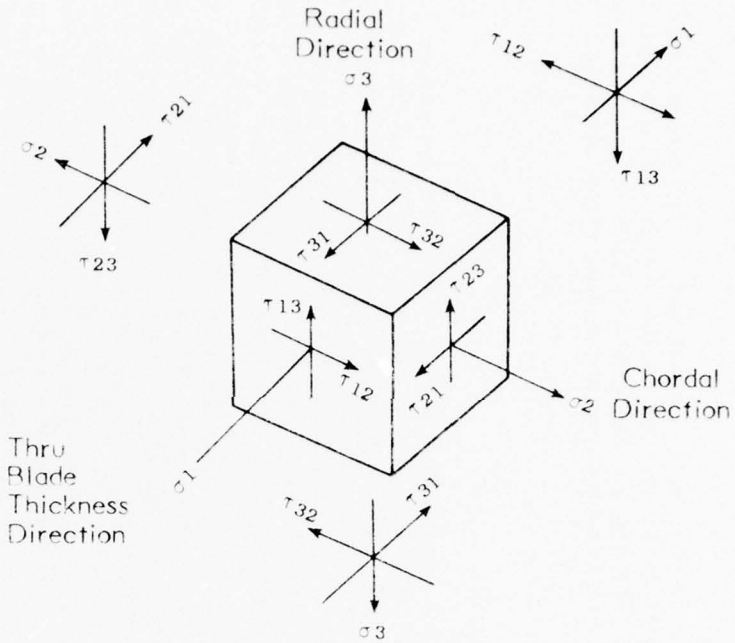

TAMP POSITIVE SIGN CONVENTION

Figure 34. TAMP Computer Finite Element Notation.

A recent modification to the three-dimensional finite element computer program allows the output to be placed on file for later use in a general purpose plotting routine. The use of the plotter allows stresses and deflections to be plotted in contours for both concave and convex blade surfaces.

Analytical Results

Aeromechanical Stability

The first forty natural frequencies of the blade were determined for each filament orientation. The calculated modal patterns (points of zero deflection on the blade) at each of these frequencies were obtained. The first four modes are identified as the first and second flexural, the first torsional and the third flexural. The higher orders are generally complex, coupled modes without specific identification. These higher order modes are not used to study the blade stabiliy characteristics, but are used later in the impact analysis.

The first three J101 B-Al blade frequencies of interest for blade stability characteristics are indicated on the Campbell diagram, Figure 35. The calculated first flexural frequency is about 1% below the objective. Blades fabricated and tested in the NASA SCAR program had an average measured static first flexural frequency about 2% above the objective. The calculated second flexural natural frequency has good separation from the first torsional mode and does not cross any significant excitation lines within the engina operating range.

The first torsional frequency of the J101 B-Al blade has adequate margin over the 6/rev excitation at the engine design point. Furthermore, the J101 B-Al blade first torsional frequencies are essentially the same as the titanium blade which it replaces.

Th 18 inlet guide vanes and 68 first stage stator vanes produce a 3980 cps and a 15035 cps stimuli, respectively. These excitations are well out of the area of concern.

Instability prediction techniques have been developed through an integration of analytical techniques and engine test data. Certain guidelines have been established for predicting flutter by what is known as the reduced velocity parameter defined as follows:

$$V_R = \frac{V}{b\omega}, \text{ where}$$

V = relative air velocity (ft/sec) at 87% span

b = chord/2 (ft) at 87% span

ω = first torsional frequency (rad/sec)

A plot of $V/b\omega$ versus incidence angle for the J101 Stage 1 fan blade is shown in Figure 36. Sufficient stability margin exists for inlet distortion and for the capability of sustaining repeated stalls throughout the J101 operating regime.

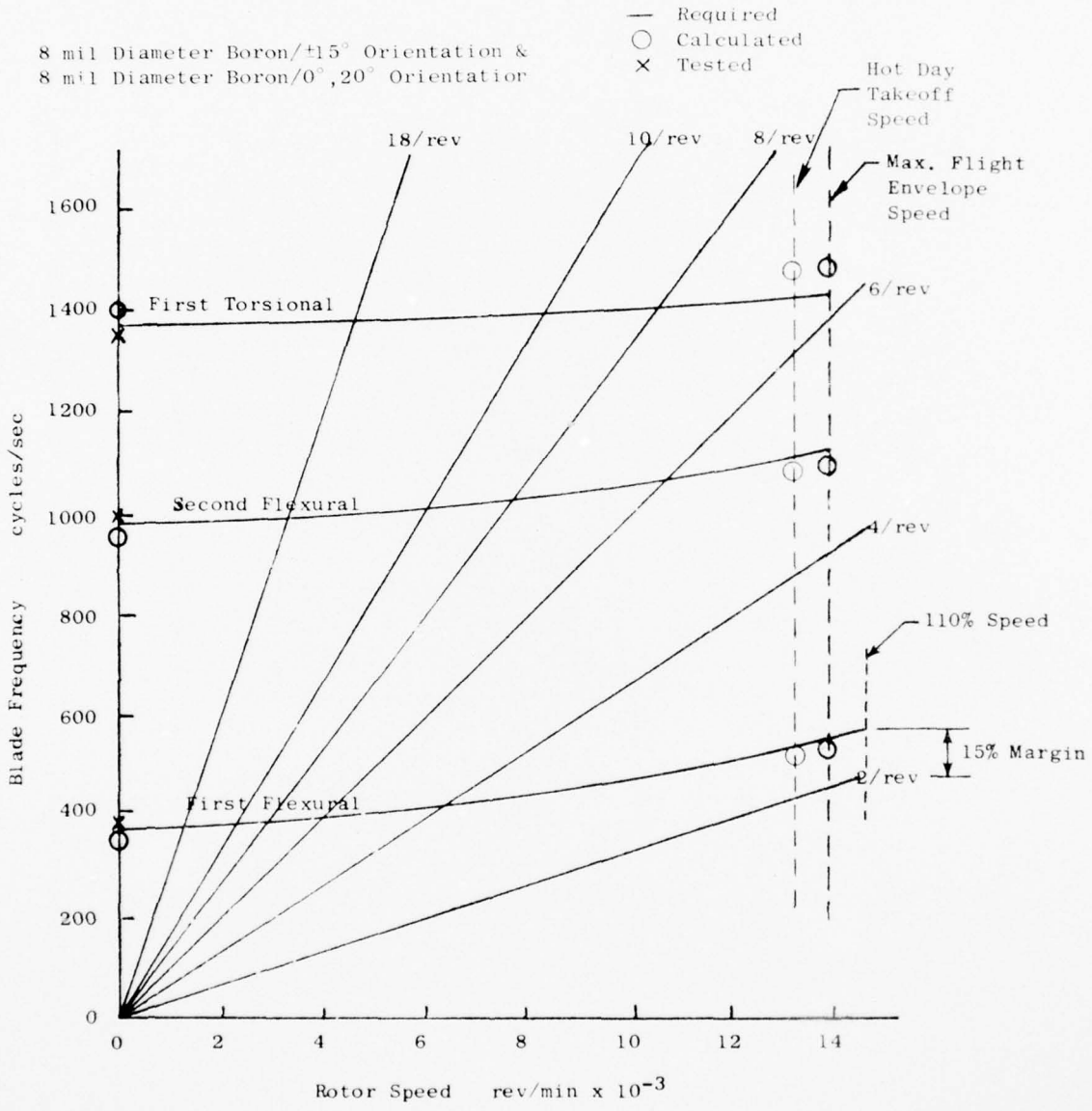

Figure 35. Campbell Diagram, J101 Stage 1 B/Al Fan Blade.

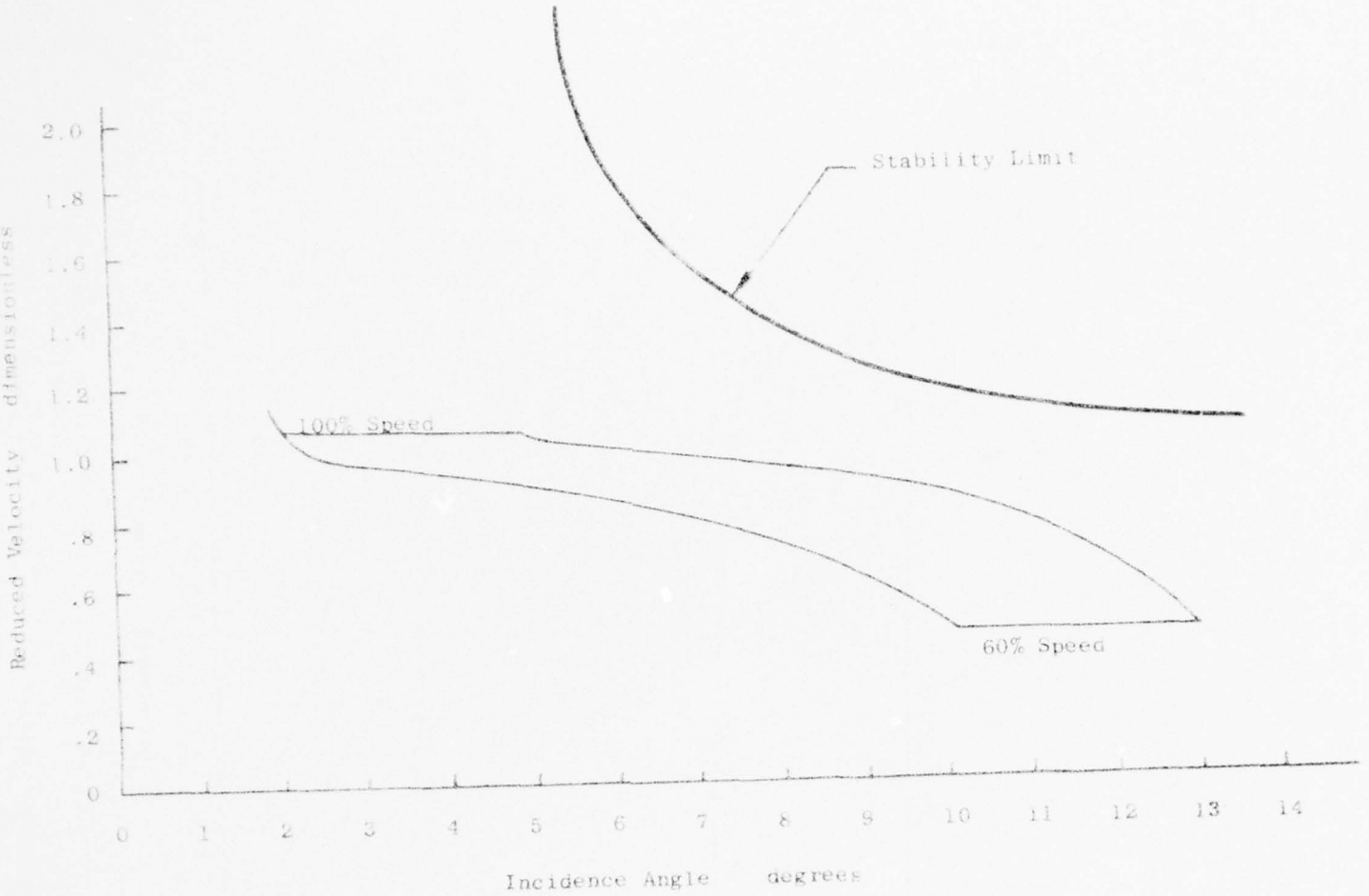

Figure 36. J101 Stage 1 B/Al Fan Blade, Torsional Stability Map.

Steady State Stress Analysis

A steady state stress analysis of the J101 Stage 1 B-Al fan blade was also obtained from the finite element (TAMP) computer program. Two analyses were performed, one each for the $[\pm 15^{O}]$ layup and the $[0/20^{O}]$ layup, at the hot day takeoff conditions and 100% rated speed of 13,266 rpm. Both of these analyses utilized the same blade geometry and the material property variations were small. The resulting calculated stress distirbutions were nearly identical and the stress amplitudes of the $[\pm 15^{O}]$ layup were approximately 3% higher than the $[0/20^{O}]$ layup. Consequently, only the stress distributions from the $[\pm 15^{O}]$ layup analysis are presented.

The steady state stress distributions in the J101 B-Al blade are shown in Figures 37 through 44. All of the stress components are at Gaussian quadrature points and are located approximately halfway between the centerline and the surface. The maximum radial tensile stress (σ_3) is 55,300 psi, located at 35% span, chordwise at the maximum airfoil thickness, and on the convex surface. The radial ultimate strength of 8 mil boron with a $[\pm 15^{O}]$ orientation is estimated at 120,000 psi which is approximately two times greater than the maximum calculated radial stress.

The maximum calculated chordwise interlaminar shear stress (τ_{12}) of 1780 psi is located at the airfoil trailing edge root. The maximum radial shear stress (τ_{13}) of 6774 psi is located on the dovetail forward face concave. The other high radial shear stresses of 5764 psi in the trailing edge 35% span location and 5644 psi in the airfoil leading edge root should be noted. Short transverse tensile stress (σ_1) are low, Figures 43 and 44. From the radial and chordwise shear stress components, a maximum principal shear stress of 6815 psi exists at the dovetail forward face, 6010 psi in the airfoil trailing edge "dog leg" area, and 5805 psi in the overhung airfoil leading edge root, shown in Figure 45.

Vibratory Stress Analysis

The next two steady state finite analyses were to determine the vibratory stress distributions in the first flexural and first torsional blade resonant modes with unit applied stimuli. These analyses were run at 13,266 rpm to include the centrifugal stiffening effects; however, the centrifugal stress components were then subtracted to obtain the vibratory stress components. The steady state stress components and the vibratory stress components were then plotted on the Goodman diagram, Figure 46. The vibratory stresses were scaled until the maximum combination of steady state and vibratory stresses reached the assumed material limit of 10^7 cycles (infinite life). The Goodman diagram presented in Figure 46 was extrapolated from test data obtained from other General Electric programs.

The vibratory stress distributions in the first flexural mode shown in Figures 47 and 48 extrapolate to a maximum surface radial bending stress (σ_3) of 32,600 psi near the mid-span and the maximum airfoil chordwise thickness, and a maximum interlaminar shear stress (τ_{13}) of 4260 psi at the airfoil leading edge root. The maximum radial bending stress (σ_3) in the first torsional mode of 17,703 psi occurs at the dovetail trailing edge; however, it should be noted that a rather

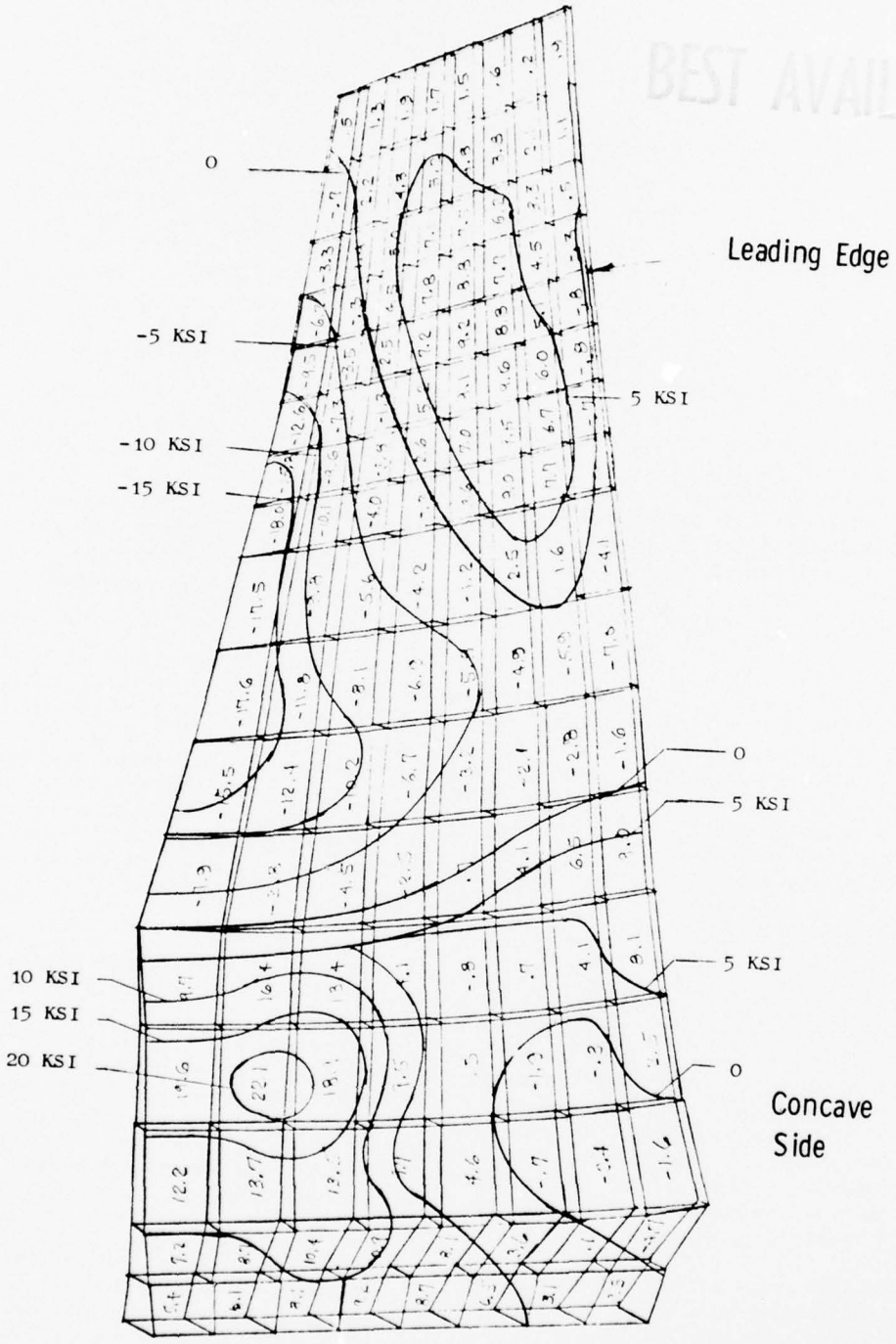

Figure 37. J101 B/Al Blade TAMP Analysis, Radial Stress, Concave (σ_3).

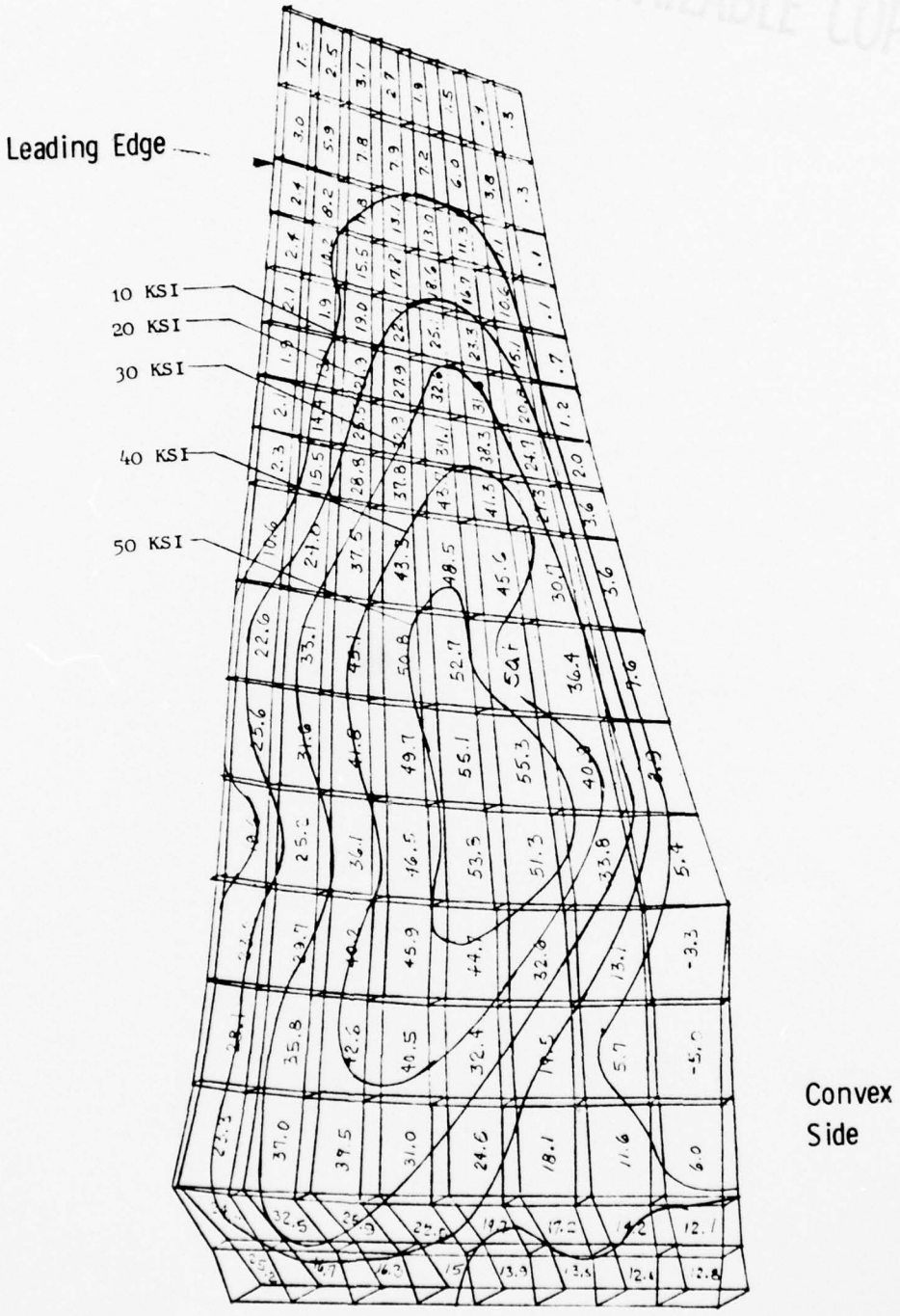

Figure 38. J101 B/A1 TAMP Analysis, Radial Stress, Convex (σ_3).

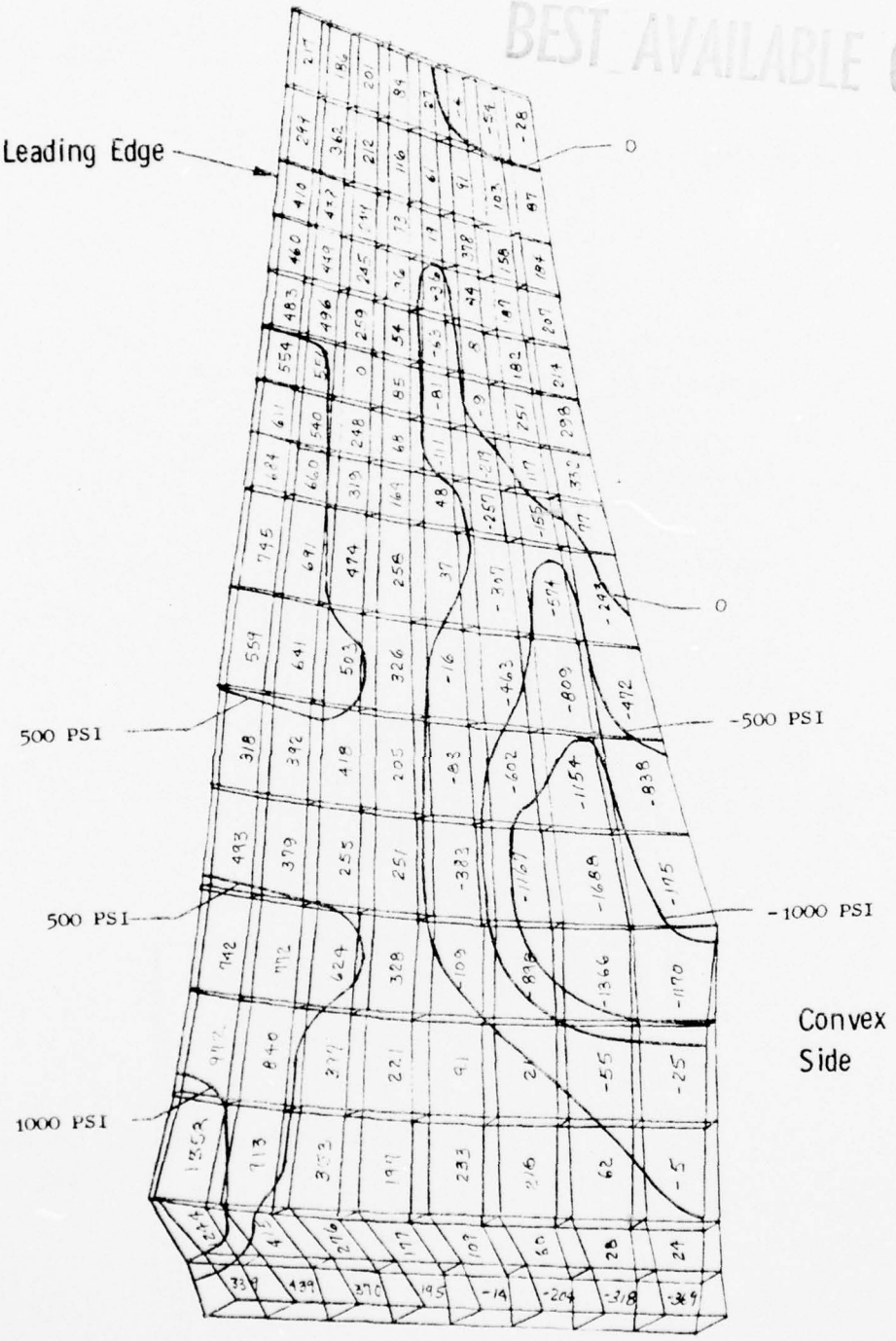

Figure 39. J101 B/A1 Blade TAMP Analysis, Chordwise Shear Stress, Convex (τ_{12}).

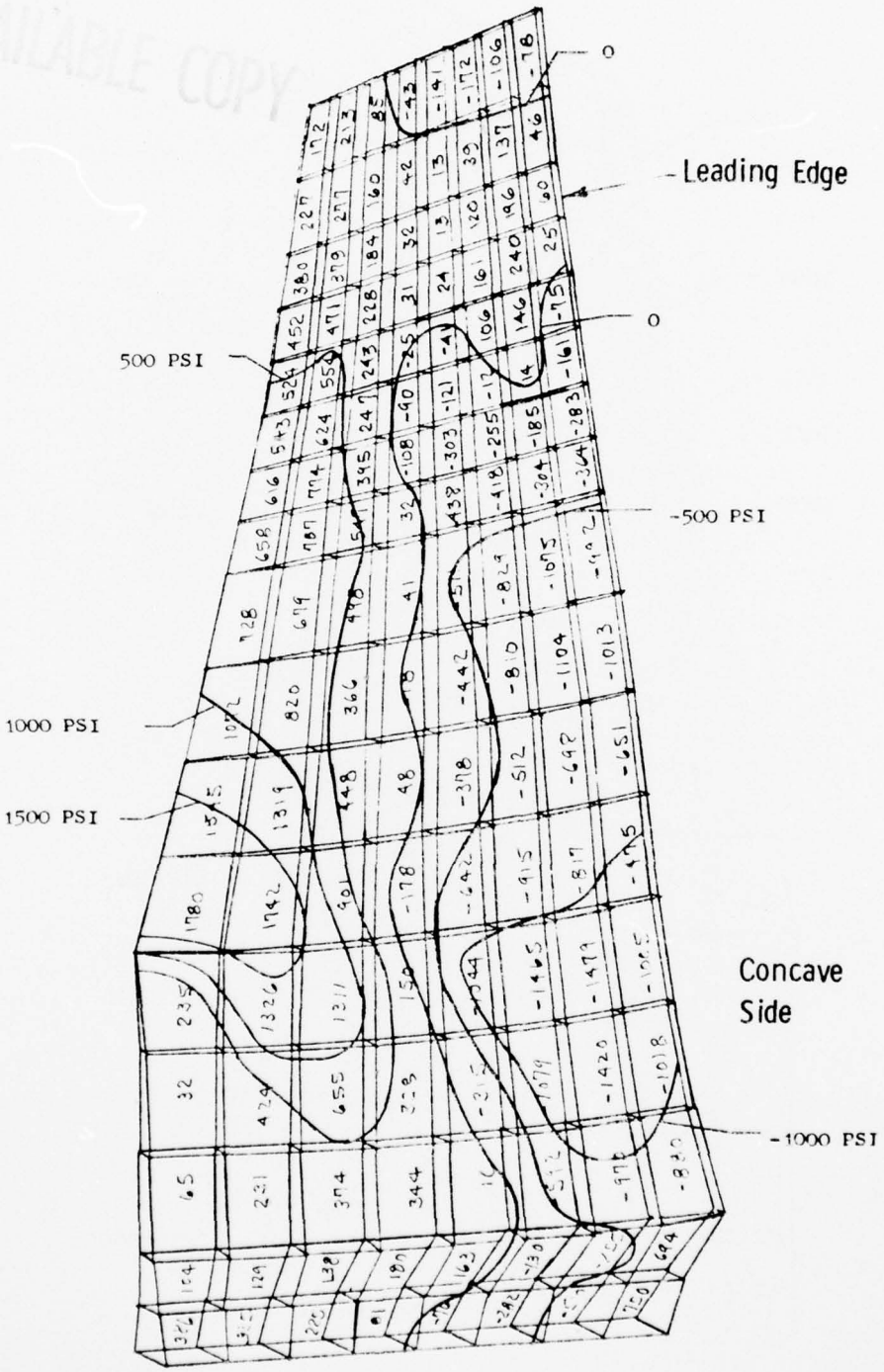

Figure 40. J101 B/A1 Blade TAMP Analysis, Chordwise Shear Stress, Concave (τ_{12}).

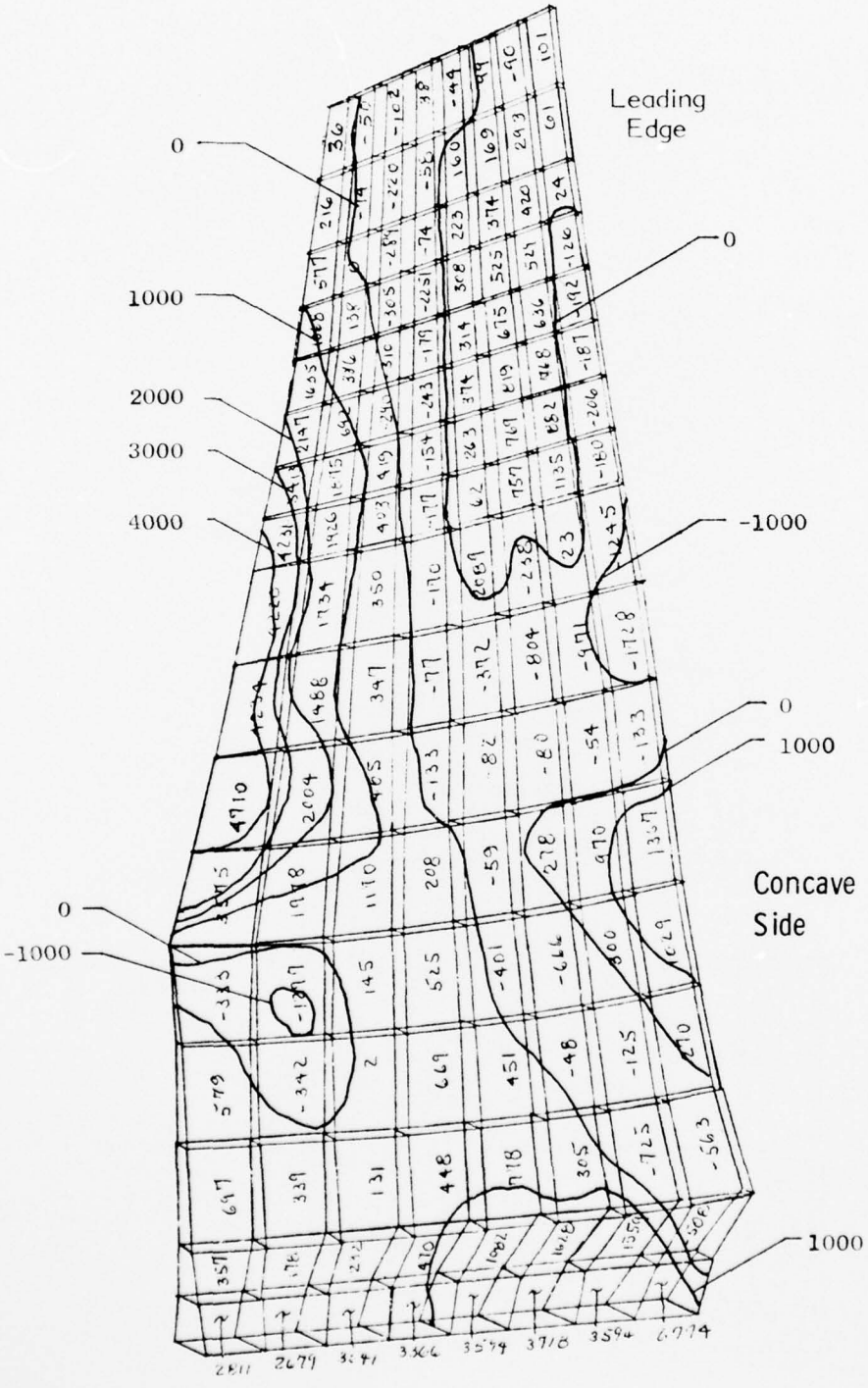

Figure 41. J101 B/Al Blade TAMP Analysis, Radial Shear Stress, Concave (τ_{13}).

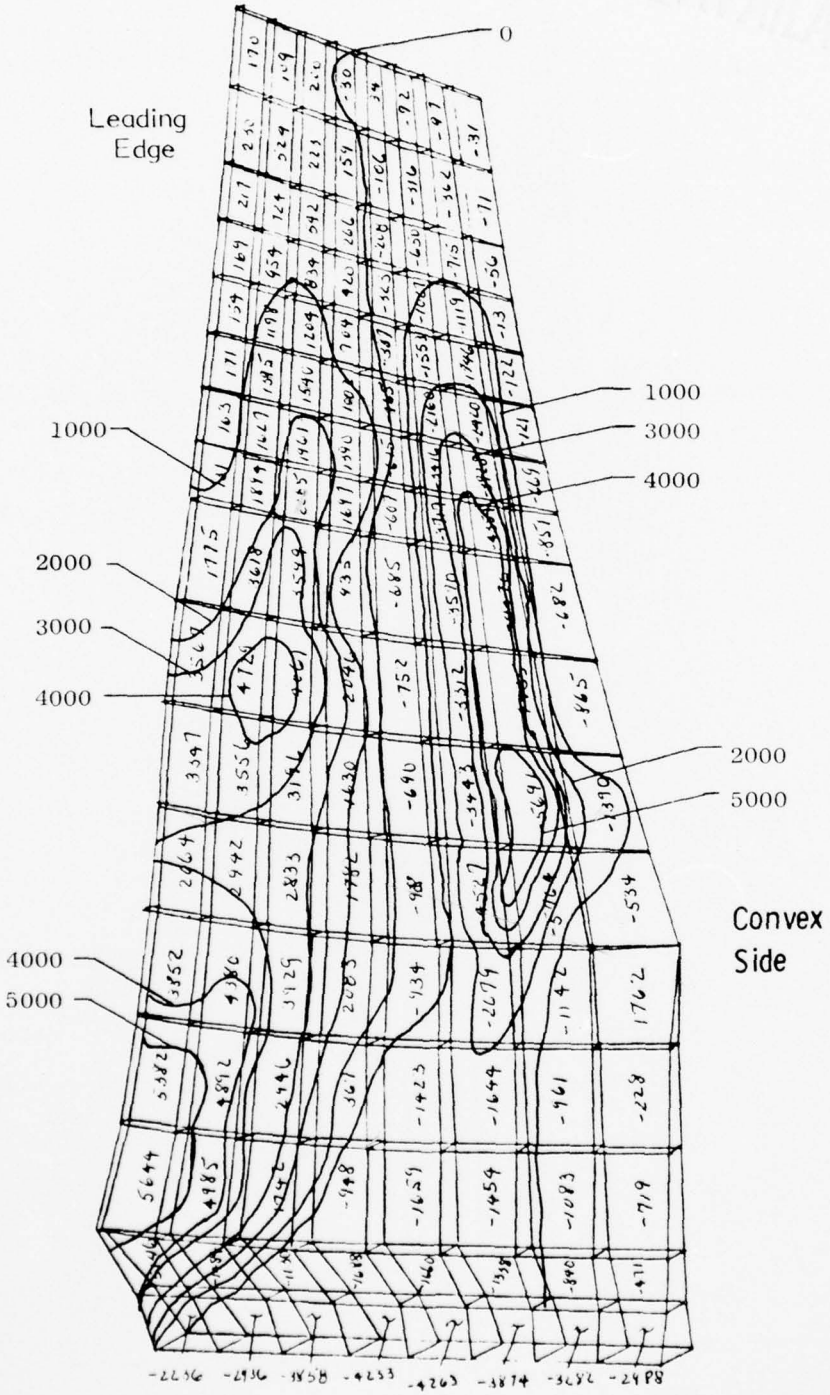

Figure 42. J101 B/Al Blade TAMP Analysis, Radial Shear Stress, Convex (τ_{13}).

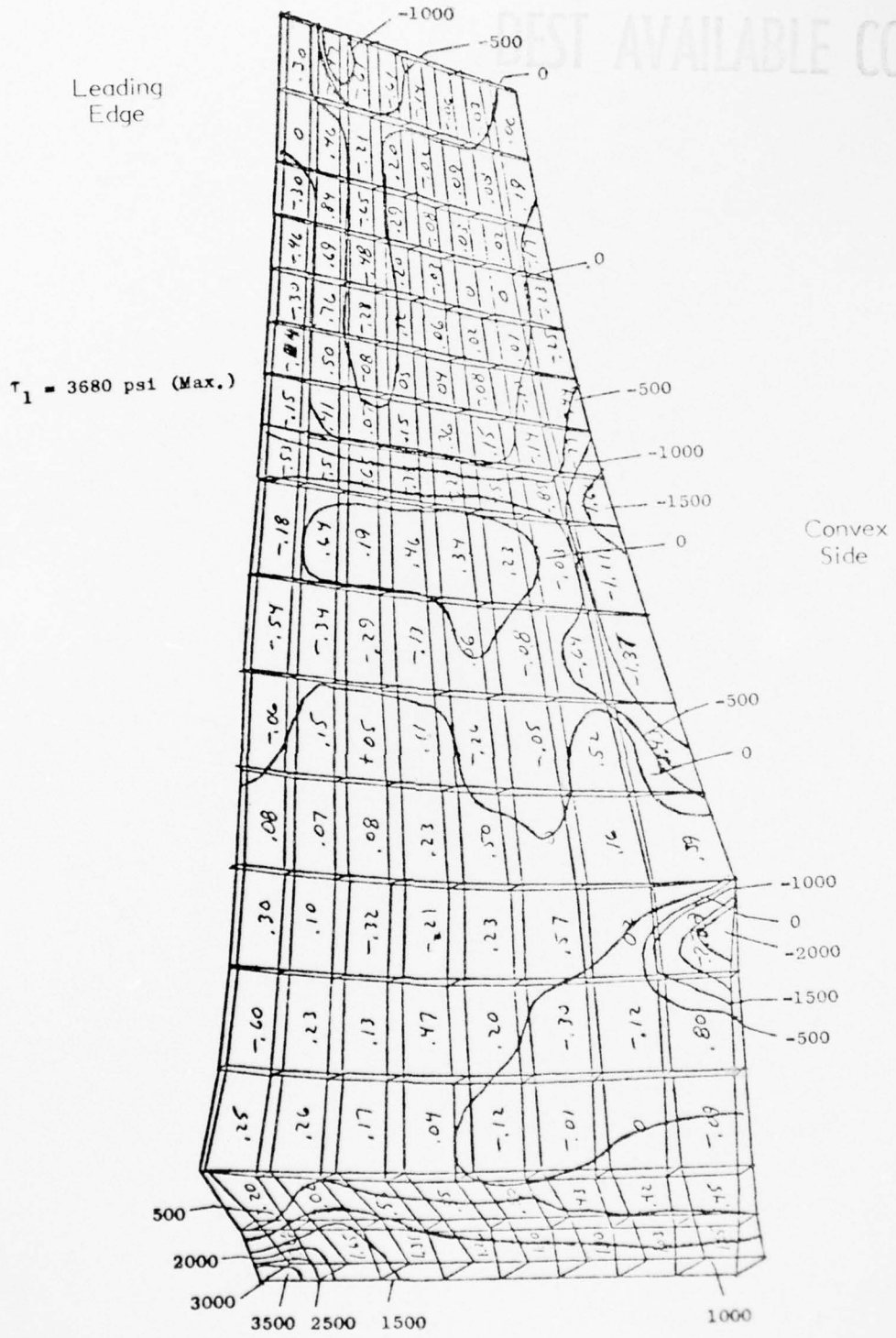

Figure 43. J101 B/Al TAMP Analysis, Suction Side, Transverse Tensile Stress (σ_1).

AD-A041 492 TRW INC CLEVELAND OHIO MATERIALS TECHNOLOGY F/G 13/8
AIR BONDED, FOD RESISTANT METAL MATRIX FAN BLADES.(U)
SEP 76 G S DOBLE, P MELNYK F33615-75-C-5222

UNCLASSIFIED ER-7850-2 AFML-TR-76-218 NL

2 OF 2
ADA
041492

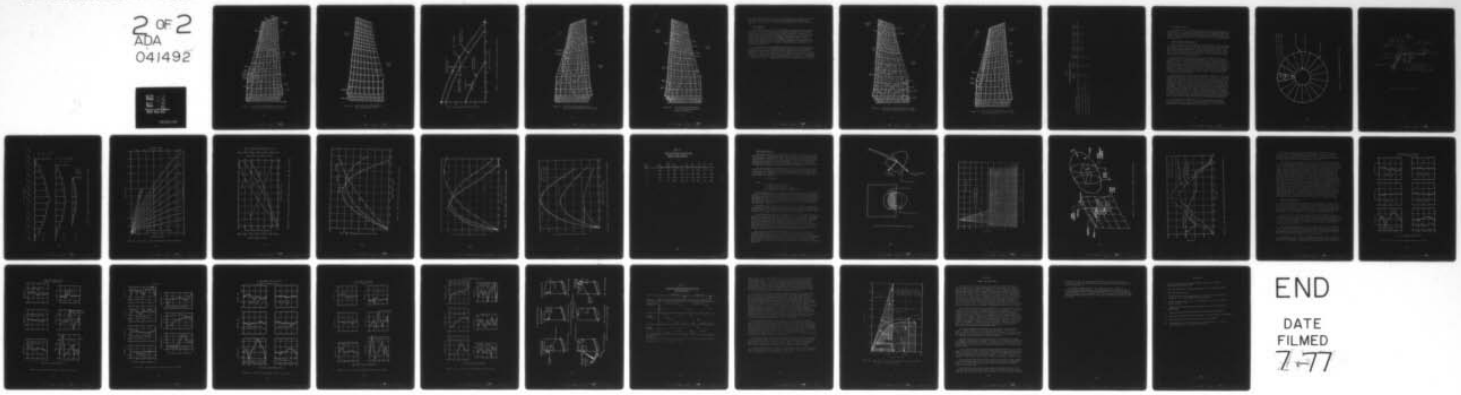

END
DATE
FILMED
7-77

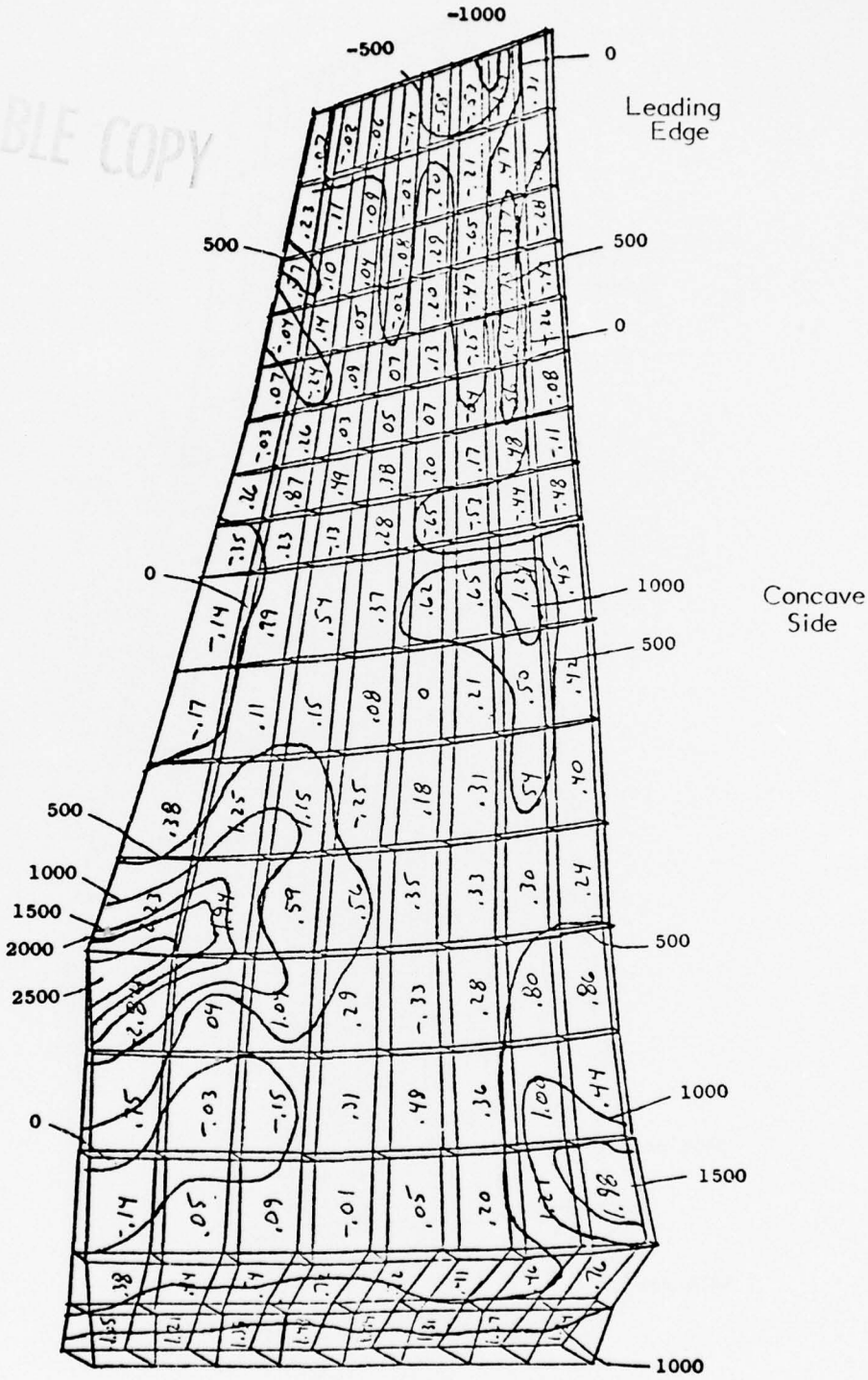

Figure 44. J101 B/Al Blade TAMP Analysis, Pressure Side, Transverse Tensile Stress (σ_1).

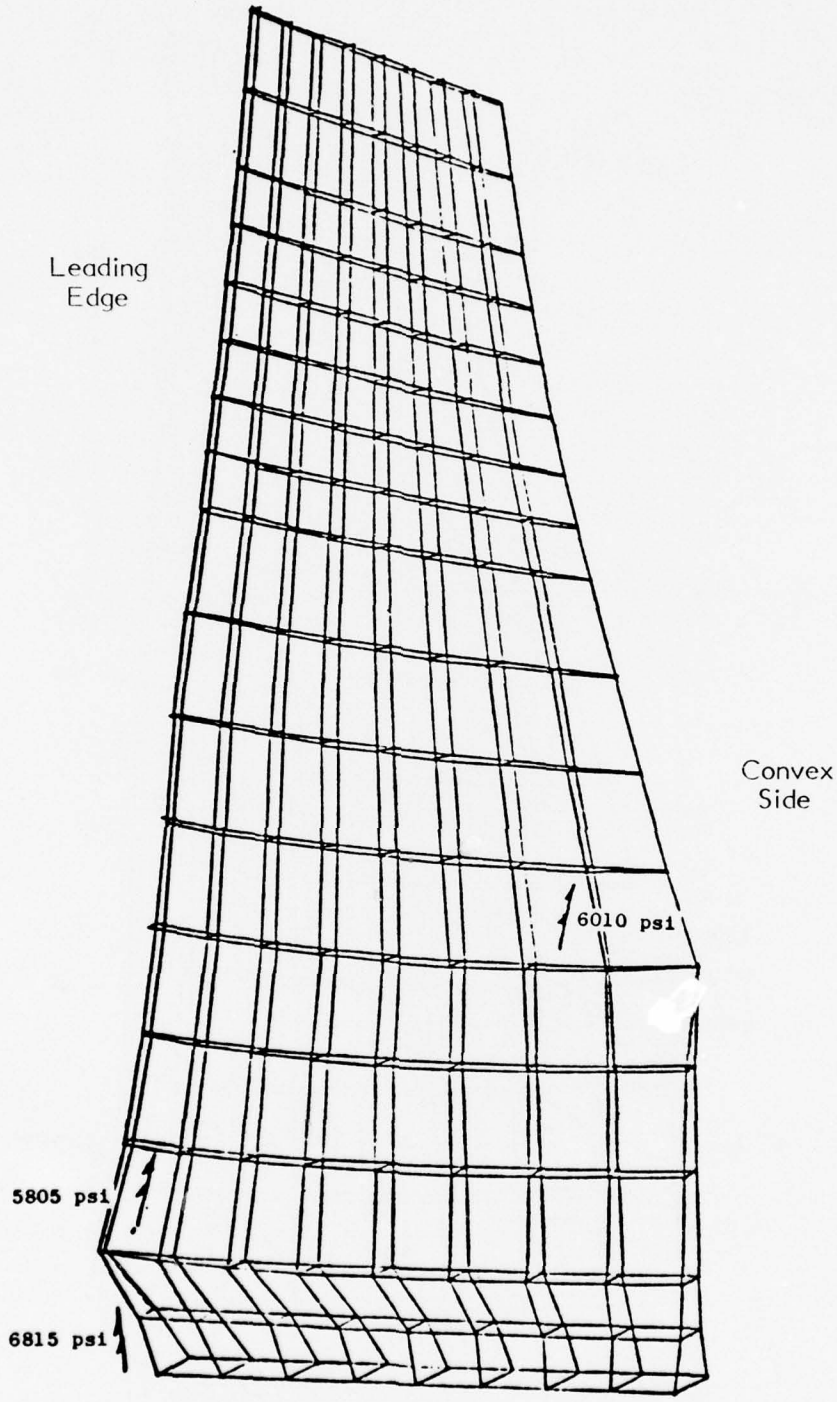

Figure 45. J101 B/Al Blade TAMP Analysis,
Max Principal/Shear Stress.

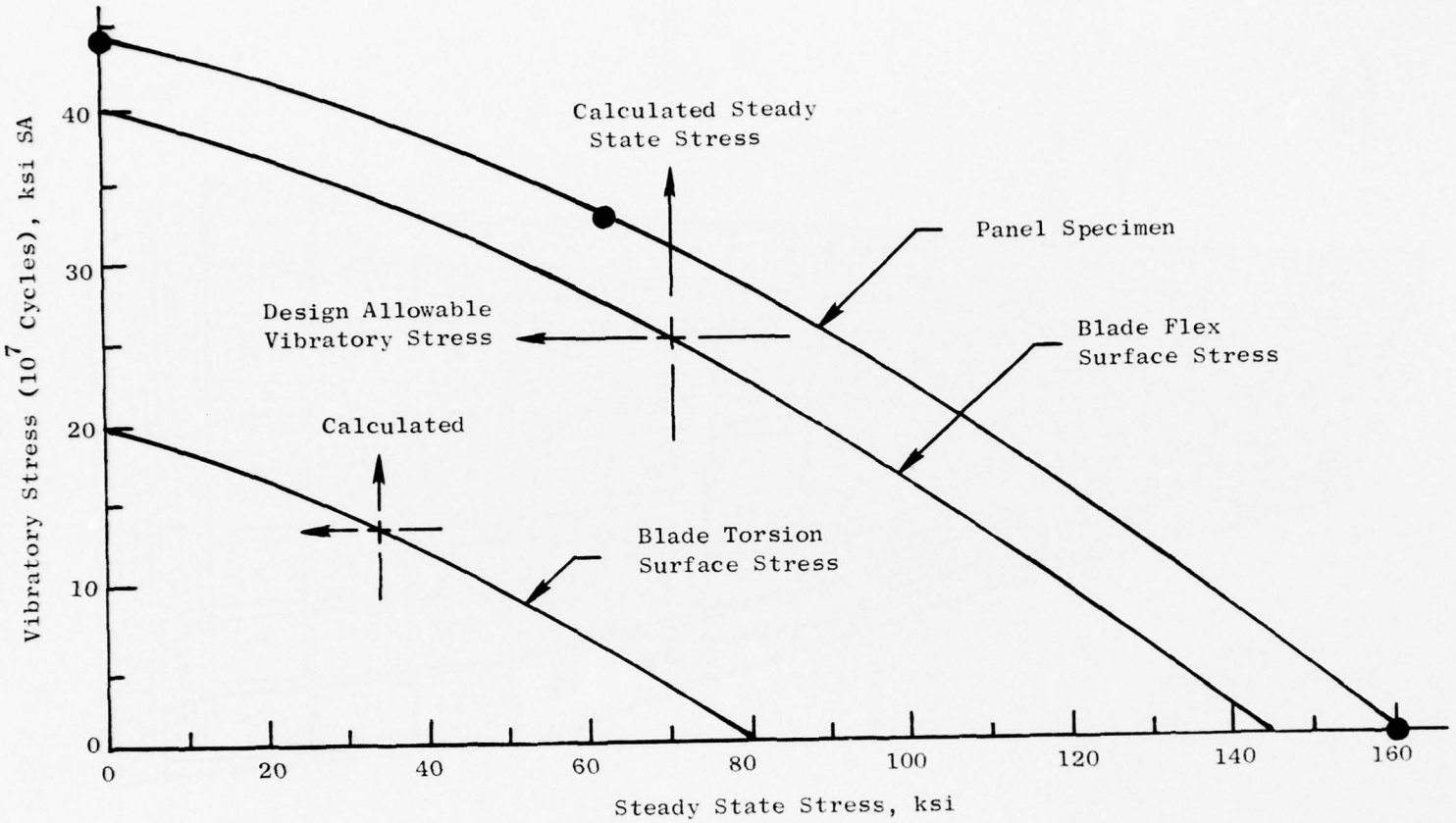

Figure 46. J101 B/Al Blade TAMP Analysis, Goodman Diagram.

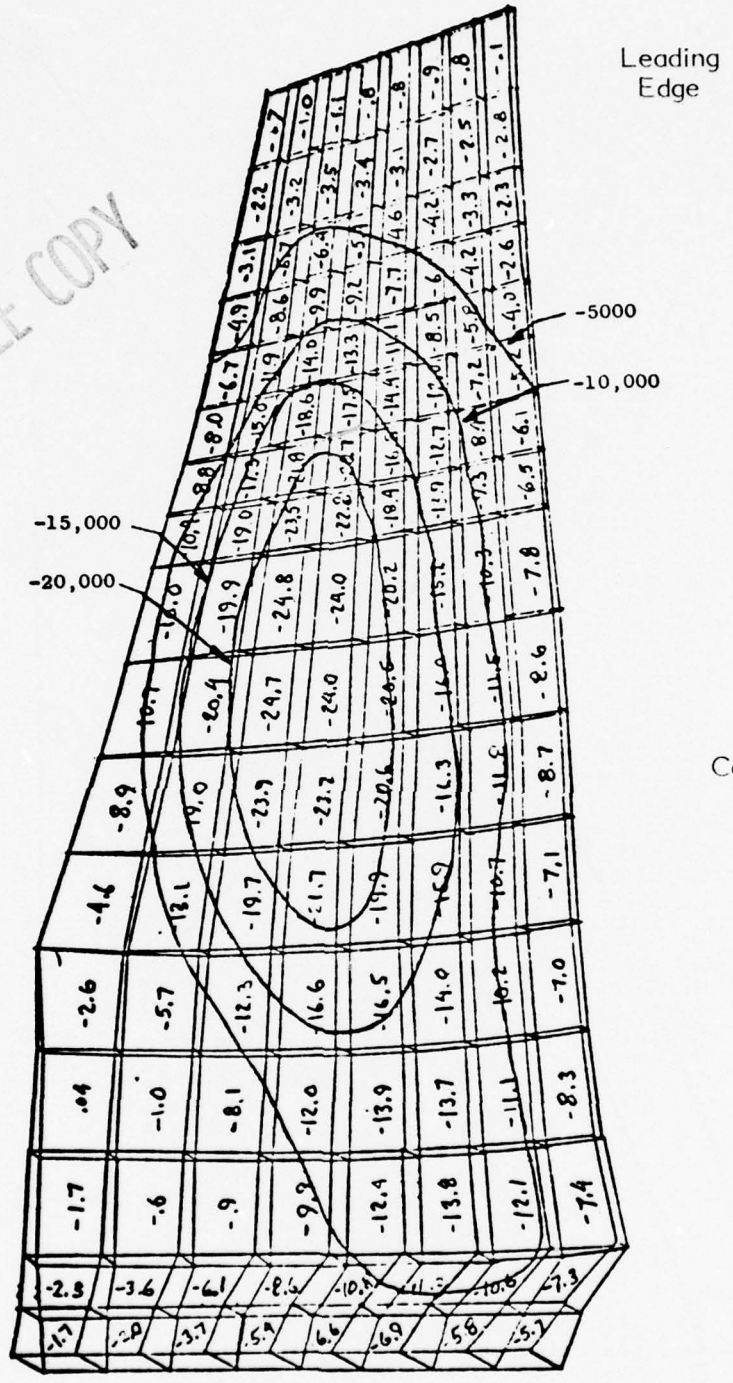

Figure 47. J101 B/Al Blade TAMP Analysis, Firs. Flex, Radial Bending Stress (σ_3).

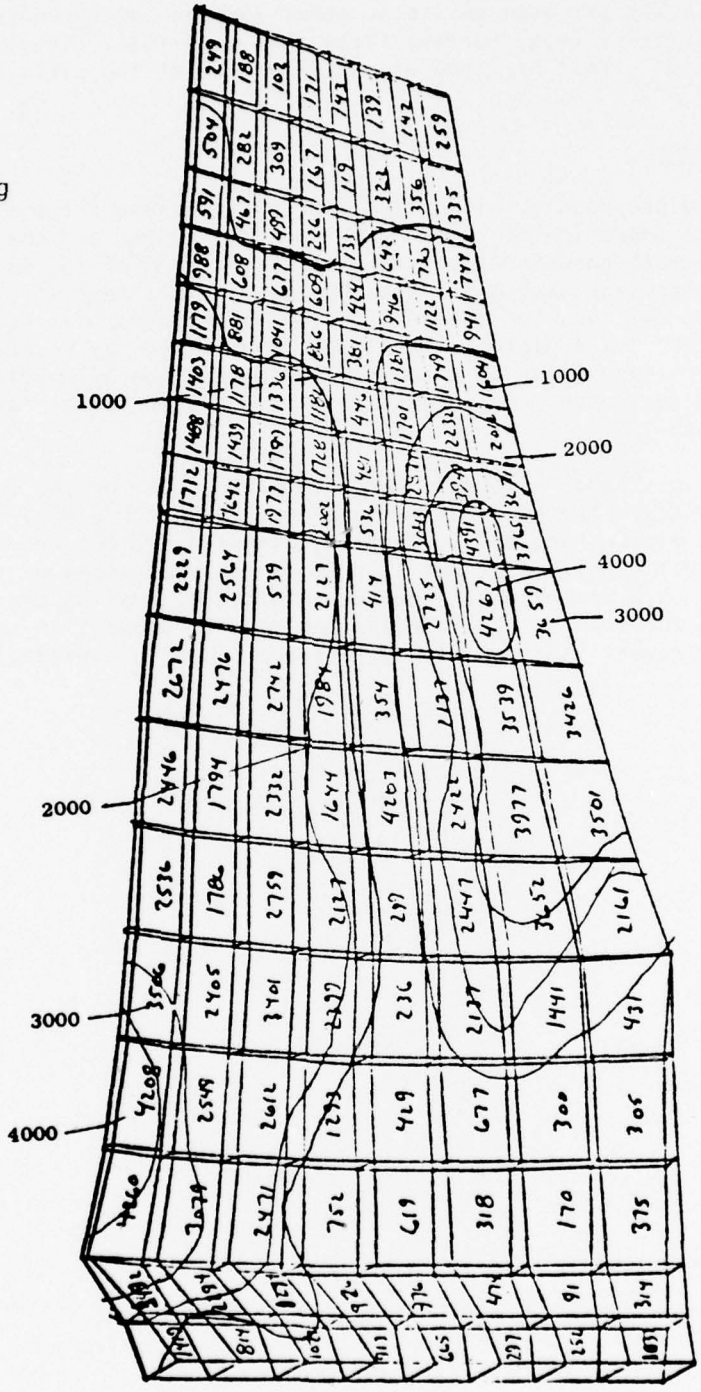

Figure 48. J101 B/Al Blade TAMP Analysis, First Flex, Radial Interlaminar Shear Stress. (τ_{13})

high stress of 14,713 psi also exists at about 70% span as shown in Figure 49. The radial shear stress (τ_{23}) for the first torsional mode, Figure 50, indicates a maximum stress of 7,900 psi at about 60% at the airfoil leading edge.

Stress Summary

As indicated previously, all of the TAMP finite element results present Gaussian stresses approximately halfway between the center and the surface calculated at takeoff conditions and a rated rotor speed of 13,266 rpm. The maximum surface stresses were calculated by assuming a linear stress distribution across the thickness of the blade. The adjusted maximum surface stresses are 70,500 psi radial and 15,000 psi chordwise. By increasing the steady state operating stress on the Goodman diagram, the allowable vibratory stresses must be decreased. A summary of these adjusted stress levels is presented in Table 15.

It was also desirable to obtain stresses at all four of the design point operating conditions. The additional three conditions would have required five more finite element analyses (vibratory stresses are not required for overspeed and burst conditions), but this was beyond the scope of this program. However, a reasonable approximation can be obtained by scaling the stresses up in proportion to the rotor speed increase and down in proportion to the modulus of elasticity decrease. These scaled stresses are also presented in Table 15.

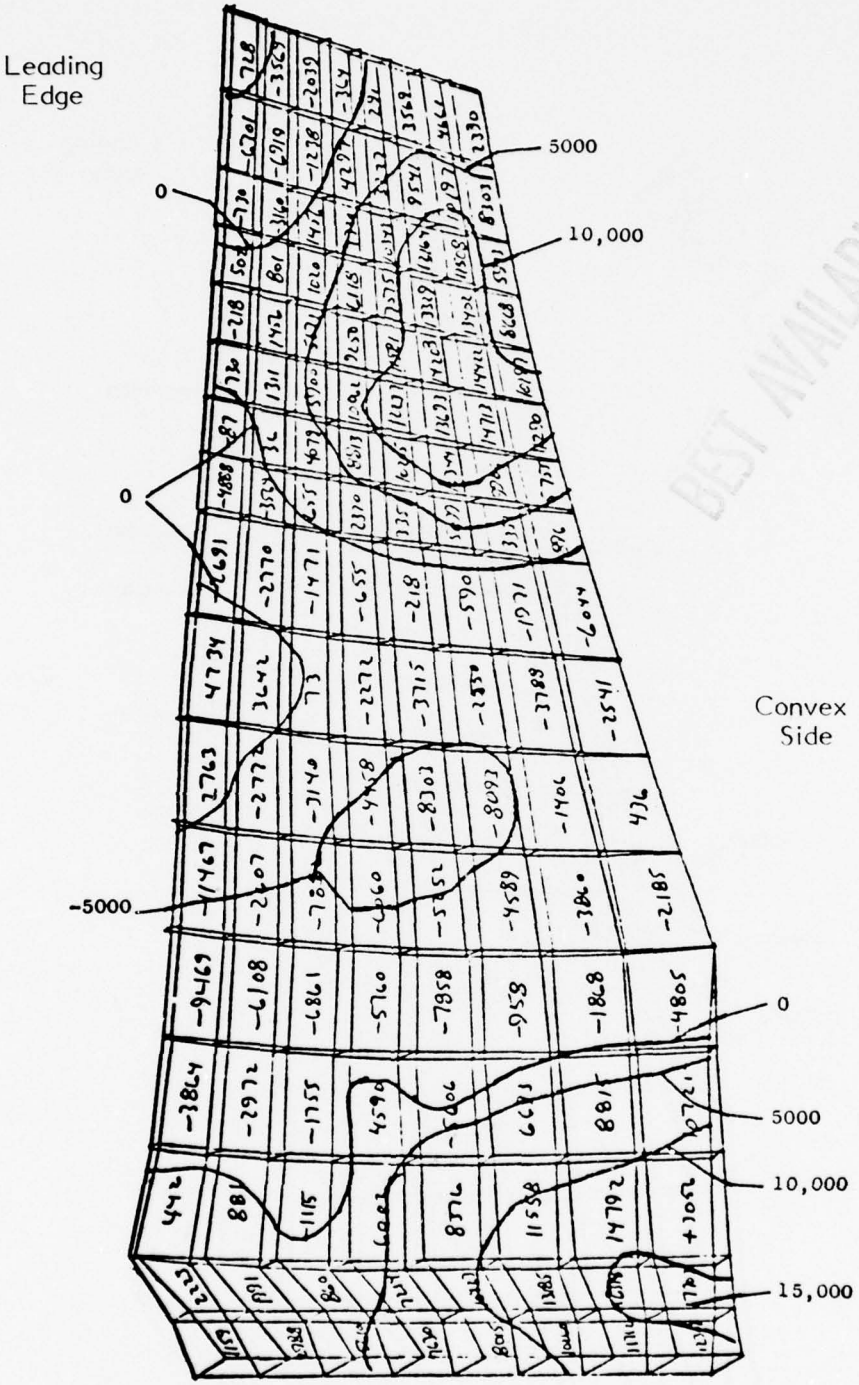

Figure 49. J101 B/Al Blade TAMP Analysis, First Torsional, Radial Bending Stress (σ_3).

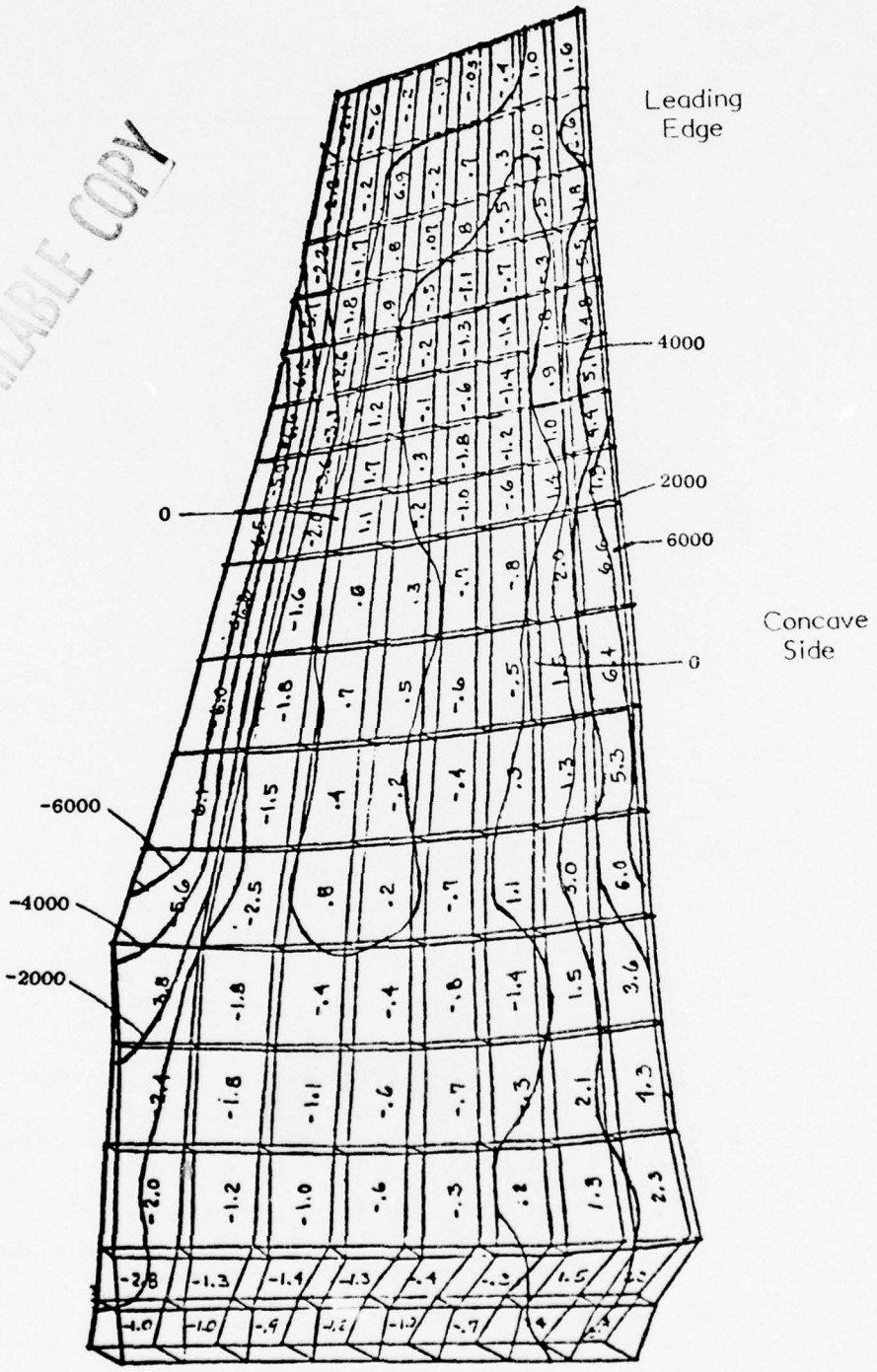

Figure 50. J101 B/Al Blade TAMP Analysis, First Torsional, Radial Shear Stress (τ_{13}).

TABLE 15

STRESS REQUIREMENT SUMMARY

Operating Condition	Radial Tensile σ_3	Chordwise Tensile σ_3	Principle Shear τ_{max}	1st Flex Radial σ_3	1st Flex Shear τ_{13}	1st Tors Radial σ_3	1st Tors Shear τ_{13}
Hot Day Takeoff, 13,260 rpm 175°F	70.5	15.0	6.8	-26.0	3.7	14.8	5.7
Max. Steady State, 13,935 rpm 350°F	75.3	16.0	7.3	-27.8	4.0	15.8	6.1
Max. Design Overspeed, 14,215 rpm 350°F	78.4	16.7	7.6	-	-	-	-
Burst Speed, 16,345 rpm RT	107	22.8	10.3	-	-	-	-

I. BIRD IMPACT ANALYSIS

The purpose of this study was to determine analytically the blade dynamic impact response for various bird impact conditions. The approach taken was to estimate the most severe bird impact conditions for the J101 B-A1 stage 1 fan blade. Using these severe conditions, four cases were identified which would identify stress and deflection as a function of bird size, incidence angle and relative velocity.

J101 Bird Impact Characteristics

The J101 engine has inlet guide vanes (IGV's) upstream of the first stage fan blades. The trailing edge of the IGV's is approximately 0.5 inch upstream of the leading edge of the fan blade. Figure 51 shows a front view of the IGV's and the largest diameter bird that can pass through the IGV's. At the root, adjacent to the spinner, the largest bird that can pass through is 6.5 ounces. At the mid-span and 70% span, the bird sizes which can pass through are 16 ounces and 25 ounces, respectively.

Using the bird sizes identified, the bird-blade impact conditions were calculated at the 17%, 50% and 70% blade heights as a function of aircraft velocity. Figure 52 schematically shows the top view of the blade and the bird velocity vectors. It was assumed that the bird axial velocity was equal to the aircraft velocity and the maximum bird slice would be taken by the blade. The bird was assumed to be an ellipsoid slided perpendicular to its major axis; the slice is taken from the center of the bird. Figure 53 shows the number of blades that could be impacted by various size birds at the 70% span location. In the analysis presented herein, the largest weight sliced perpendicular to the major axis is being considered.

Figure 54 shows the largest bird slice weight as a function of bird weight and J101 aircraft velocity. Also shown are the radii of the birds. Figure 55 shows the bird-blade impact parameters; i.e., bird slice weight (W_S), relative velocity (V_R), incidence angle (θ), and bird slice thickness to diameter ratio (t_S/D_S) as a function of aircraft velocity for a 25 ounce bird impacting the J101 blade at the 70% span location. These parameters were used to calculate the change in bird slice momentum normal to the airfoil at the impact span and the change in bird slice kinetic energy as a function of aircraft velocity for the 17%, 50% and 70% blade span heights. These calculations are summarized in Figures 56 and 57, respectively. Note that the peak magnitude of the change in momentum (ΔMn) is high for all three span locations, however, the peak occurs at different aircraft speeds. The change in bird slice kinetic energy (ΔK) has similar characteristics, but its peaks occur at different aircraft velocities than the ΔMn. Conditions analyzed are summarized in Table 16 and Figure 58.

It has been found in QCSEE blade studies that measured blade impact stresses correlated with changes in bird slice kinetic energy. Since the present effort addresses the calculation of blade impact transient stresses and deflections, a ΔK correlation will also be used.

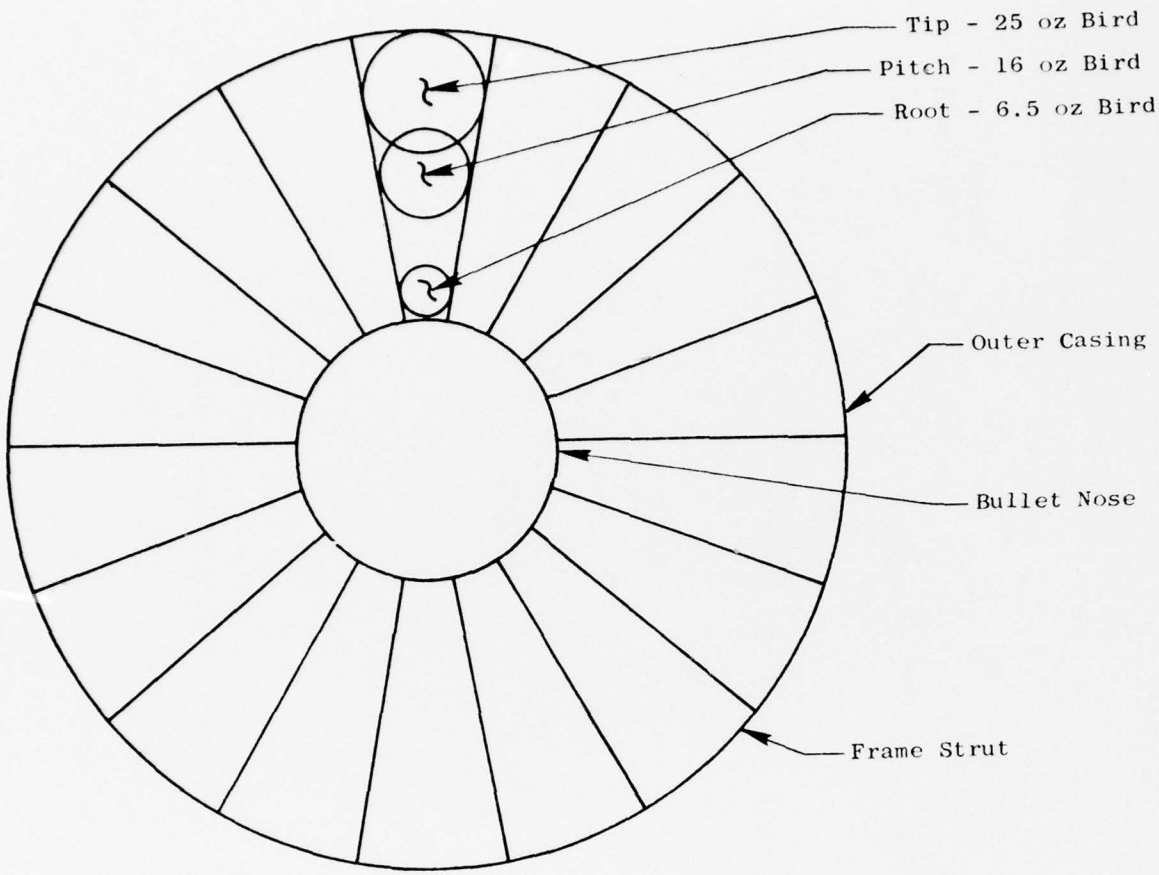

Figure 51. J101 Engine-Ingested Bird Size Limit.

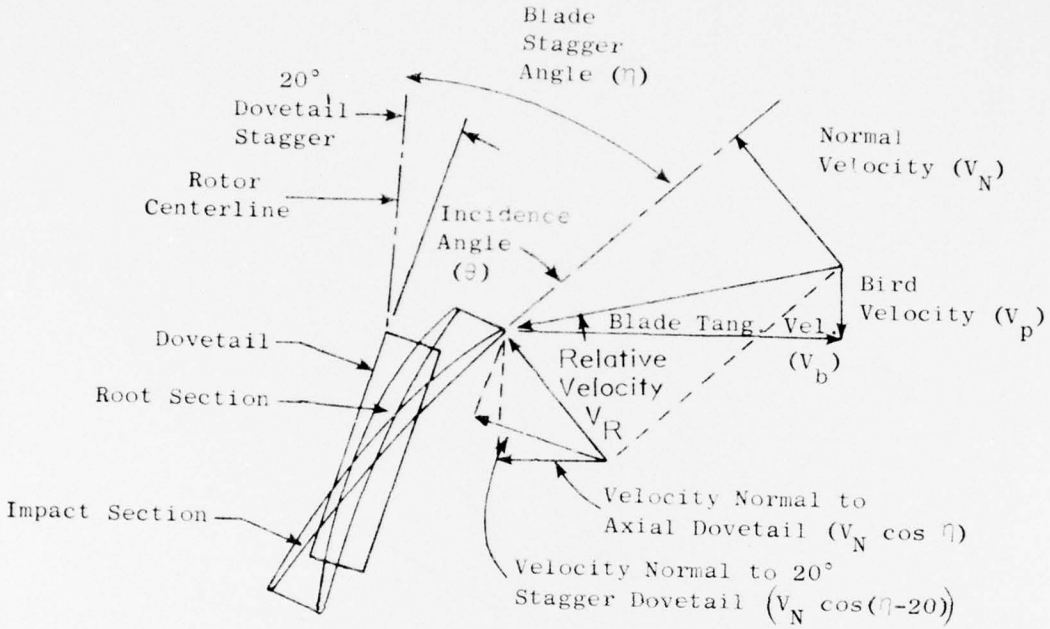

Figure 52. Bird Impact Diagram.

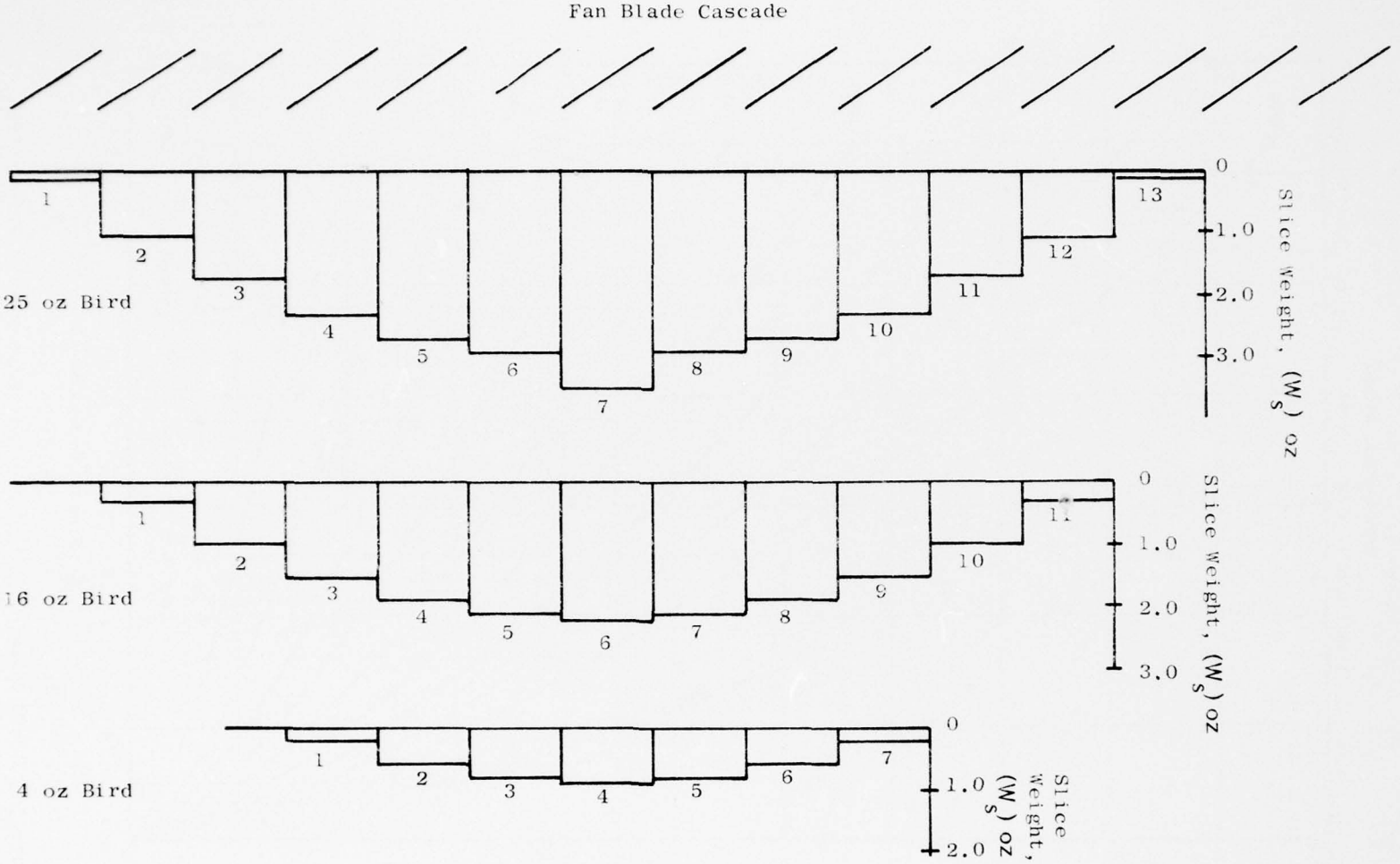

Figure 53. Number of Blades Impacted By Several Sizes of Birds.

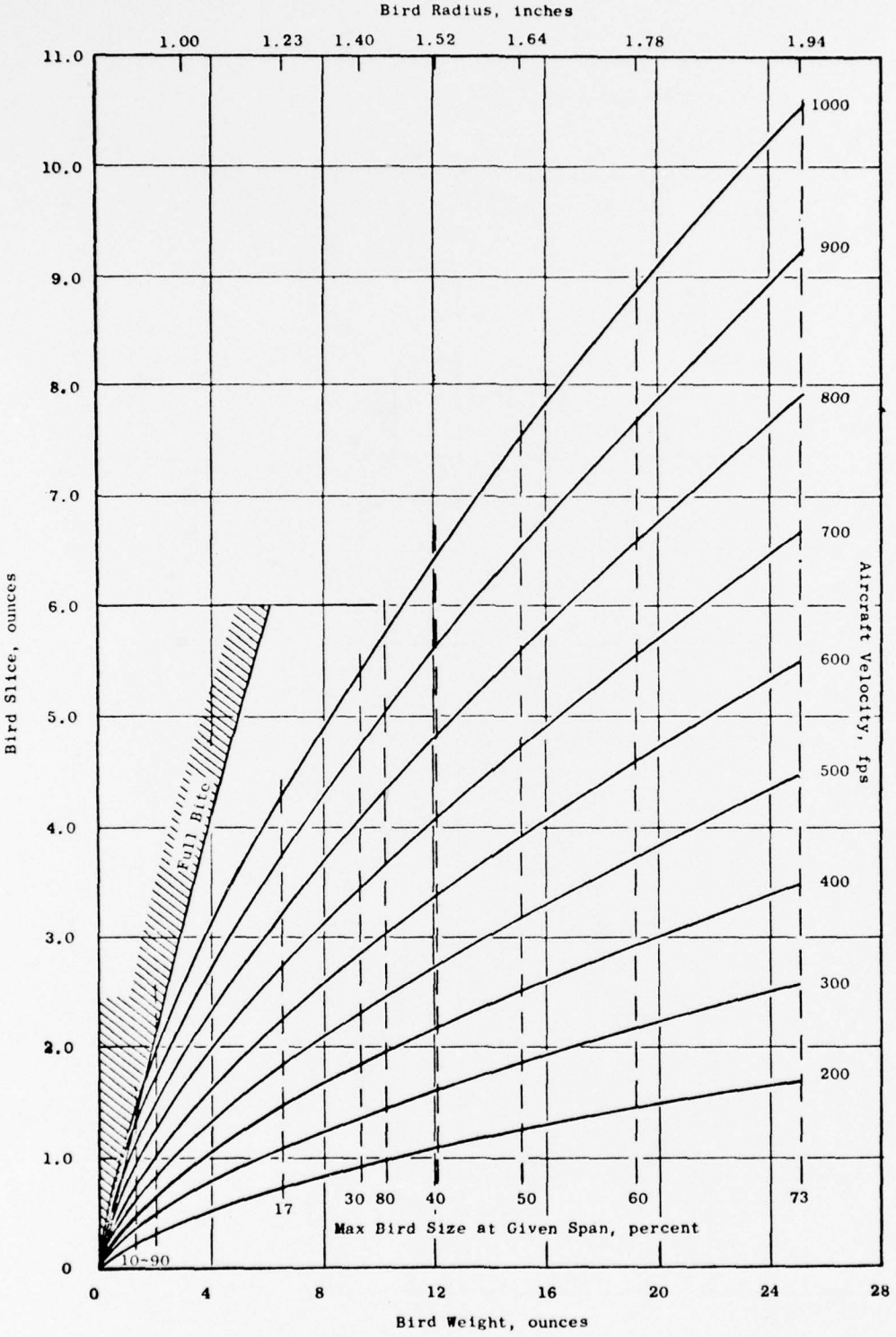

Figure 54. J101 Stage 1 B/A1 Fan Blade Bird Strike Parameters.

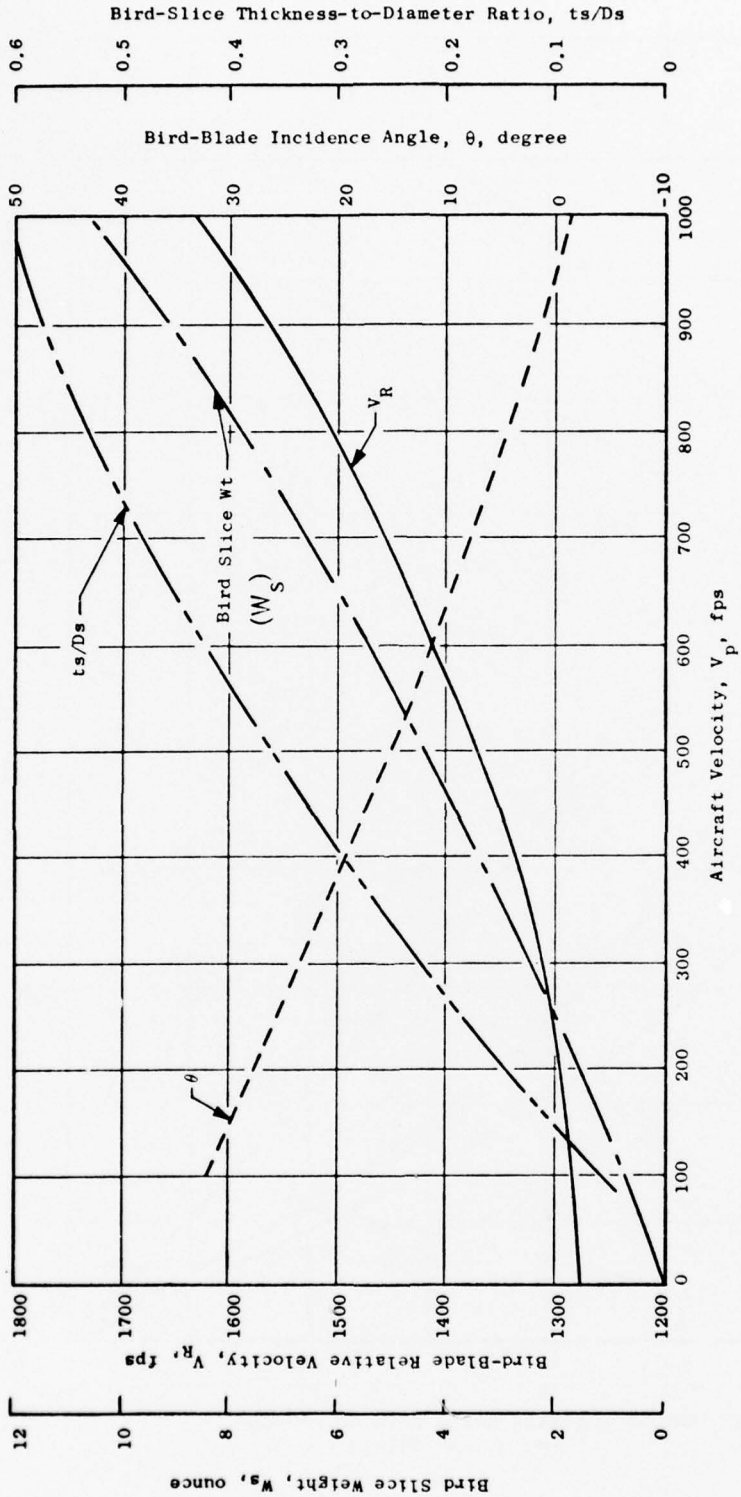

Figure 55. J101 Stage 1 Bird-Blade Impact Parameters for 70% Span, 25 oz Bird.

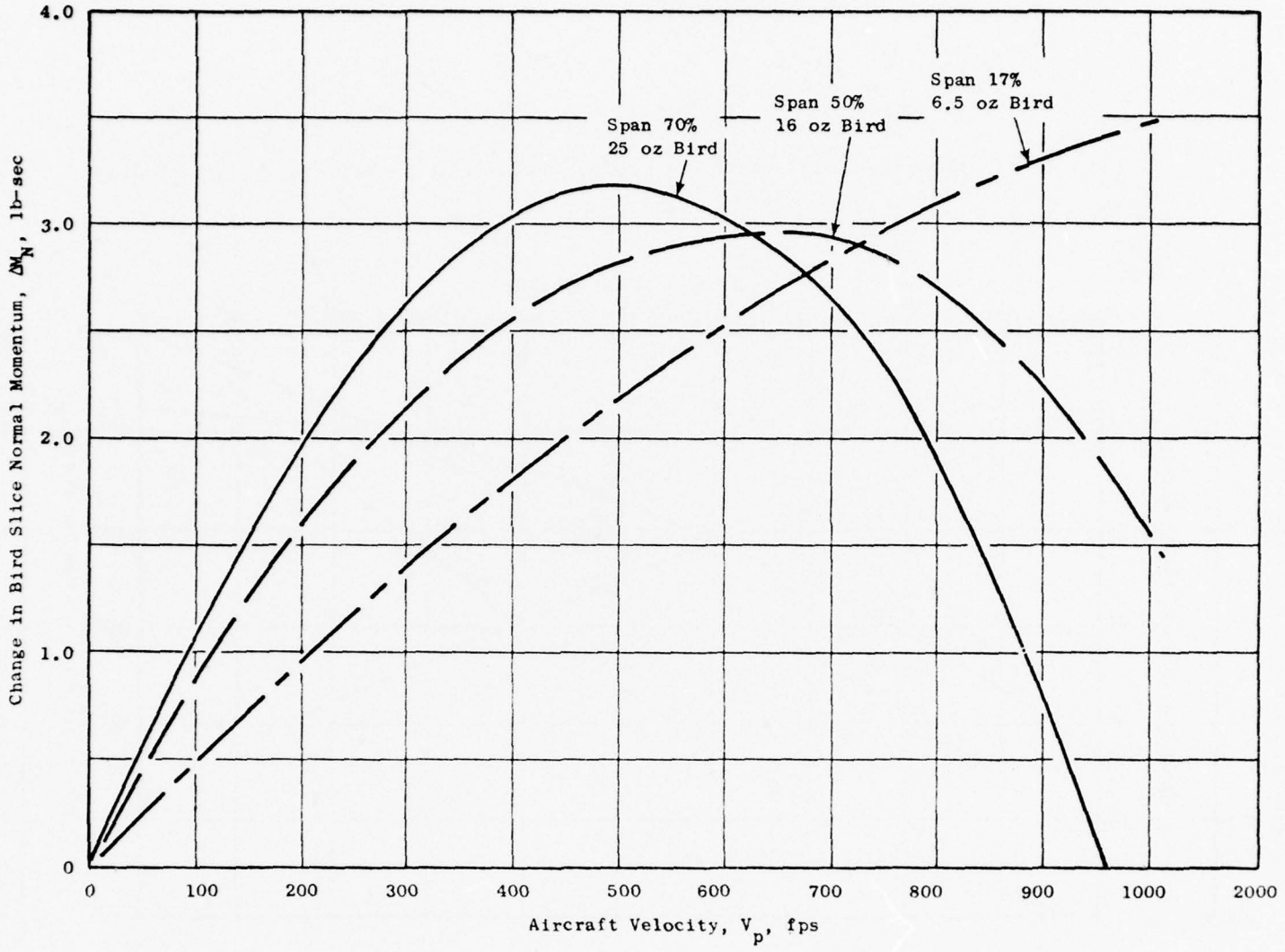

Figure 56. J101 Blade Impact, Change in Bird Slice Momentum.

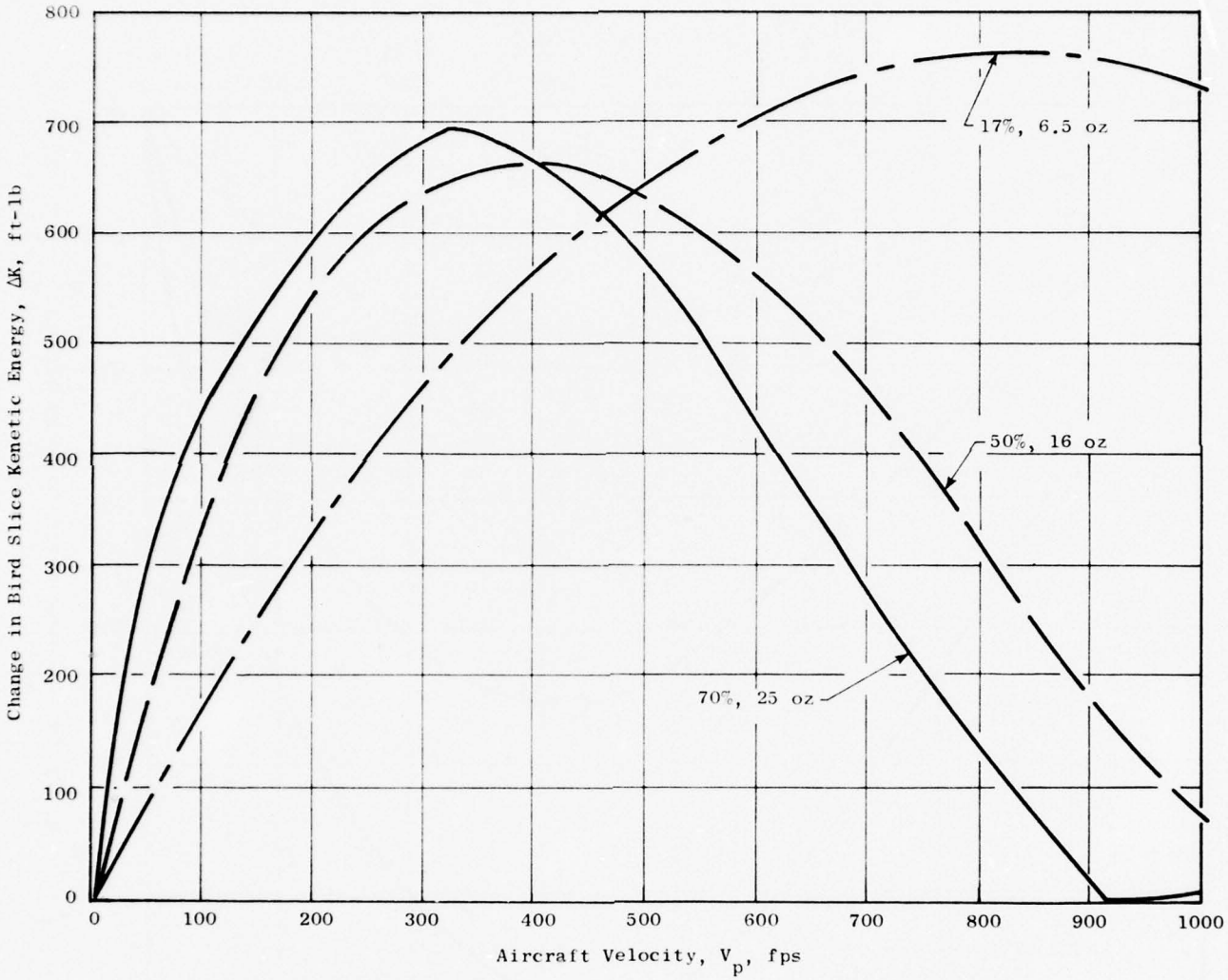

Figure 57. J101 Blade Impact, Change in Bird Slice Kinetic Energy.

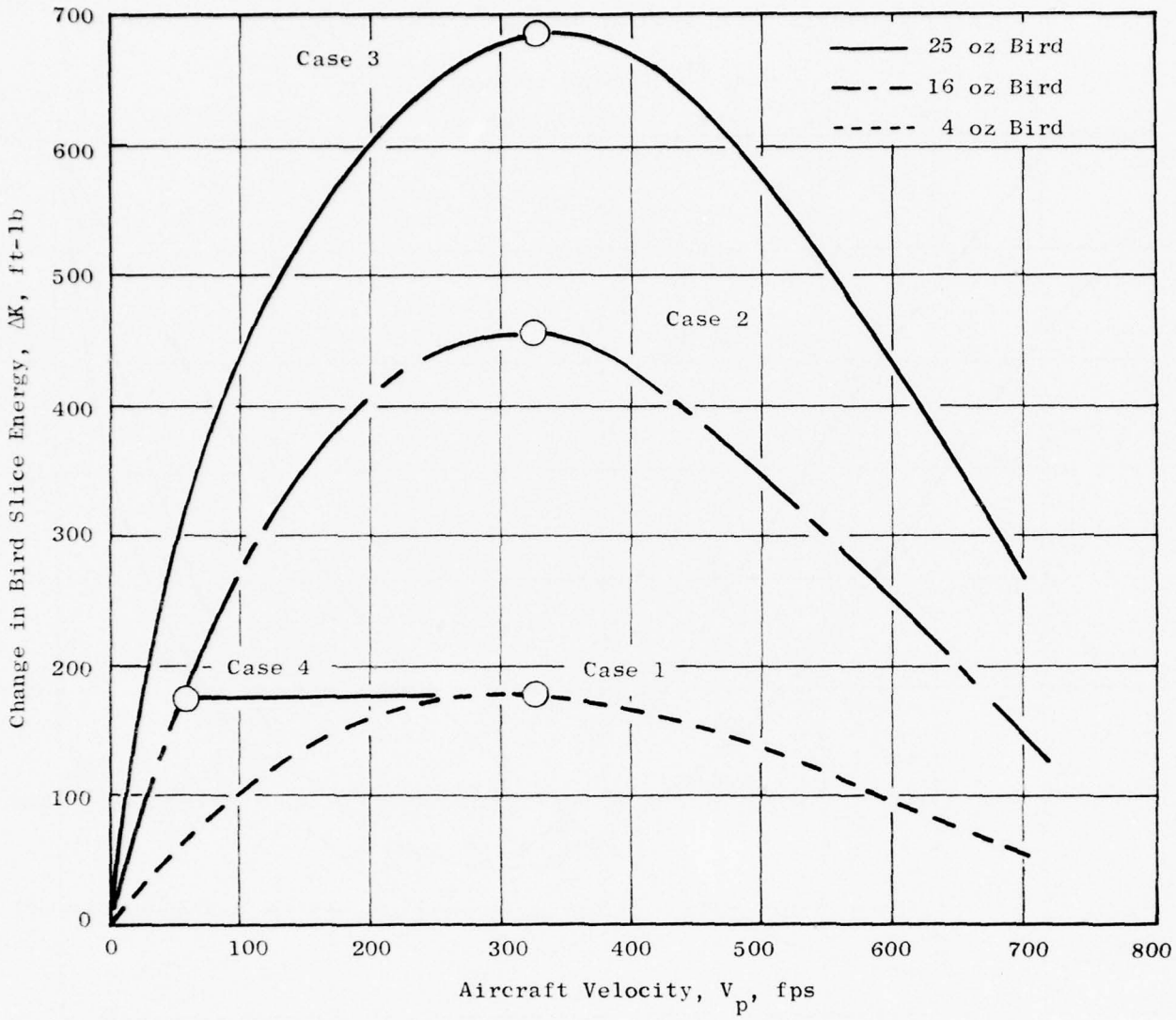

Figure 58. J101 Blade - Change In Bird Strike Kinetic Energy for 70% Impacts.

TABLE 16

IMPACT CONDITIONS SELECTED FOR

DYNAMIC IMPACT ANALYSIS

Case No.	V_p (ft/sec)	Span (0/0)	V_R (ft/sec)	σ (^{o})	W_b (oz)	W_s (oz)	ΔK (ft-lb)	D_s (in.)	τ_s/D_s
1	325	70	1321	22.5	4	.74	182	2.14	.25
2	325	70	1321	22.5	16	1.86	458	3.4	.156
3	325	70	1321	22.5	25	2.82	695	3.94	.134
4	55	70	1281	34.2	16	.36	182	3.4	.027

TAMP Impact Analysis

The bird impulse acting on the blade is a critical consideration in the impact analysis. Investigations have indicated that a real bird behaved like a fluid body when impacted by a blade. The pressure, contact area and forces resulting from a fluid bird were calculated as a function of impact duration. The required parameters were then determined for input into the nonlinear dampened spring, lump mass system in the TAMP finite element computer program to simulate the force-time characteristics of the fluid bird.

Two cases considered a 0.9 ounce slice from a 3.0 ounce bird and a 3.5 ounce slice from a 25.0 ounce bird both impacting the blade at 75% span with a bird velocity of 400 ft/sec. The fluid bird impinging on the blade, shown in Figure 59, is a cylindrical slice. The resultant pressure on the blade is determined by the equation:

$$p = \frac{1}{2} \frac{\rho}{g} V_N^2$$

where

p = pressure on blade, lb/ft^2
ρ = bird density, lb/ft^3
g = gravitational constant, ft/sec^2
V_N = velocity bird normal to blade, ft/sec

The calculated pressure is constant for the impact duration and independent of the bird and slice sizes. An adjusted pressure-time curve was obtained by selecting a profile from literature data[10] and by setting the area under the calculated curve equal to the area under this adjusted curve shown in Figure 60. The area of the bird in contact with the blade for the duration of the impact was calculated. The bird force acting on the blade was then determined from the pressures and contact area.

The TAMP analysis assumes that the bird slice is a lump mass connected to the blade by a nonlinear dampener and a spring as indicated in Figure 61. This system provides a time dependent force function which traverses the blade chord along a line of nodal points at a specified relative velocity.

A total of twelve transient impact cases were run on the TAMP analysis with a matrix of various coefficients of dampening and spring constants. The impact forces as a function of time for the selected system variables are compared to the results of the fluid bird analysis in Figure 62. The area under the two curves is approximately equal although the profiles are different. The differences in the curves are due to the rigid blade assumed in the fluid bird model and the elastic blade considered in the TAMP model. Also, the entire bird slice mass is concentrated in the TAMP model whereas the fluid bird model considers a variable slice mass as the blade cuts through the bird.

The results of the bird-blade interaction study were used to obtain transient impact results for a 3.0 and a 25 ounce bird impact at 75% span of the J101 stage 1 B-Al fan blade. The absolute values of the stresses calculated using the dynamic impact analyses are not significant due to the small deflection elastic material assumptions incorporated in the program. However, it does yield useful information with regard to the relative effects of different impact parameters.

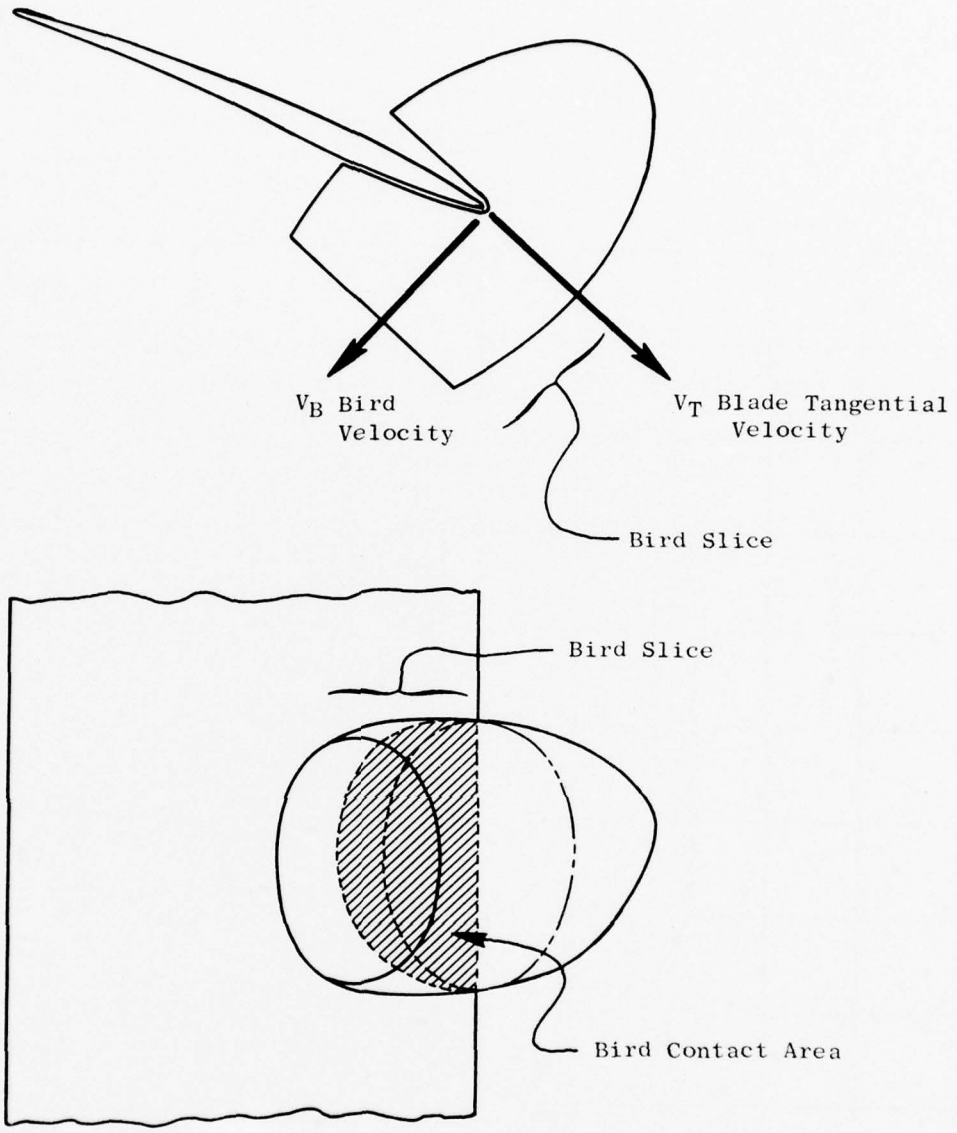

Figure 59. Fluid Bird Impingement on Blade.

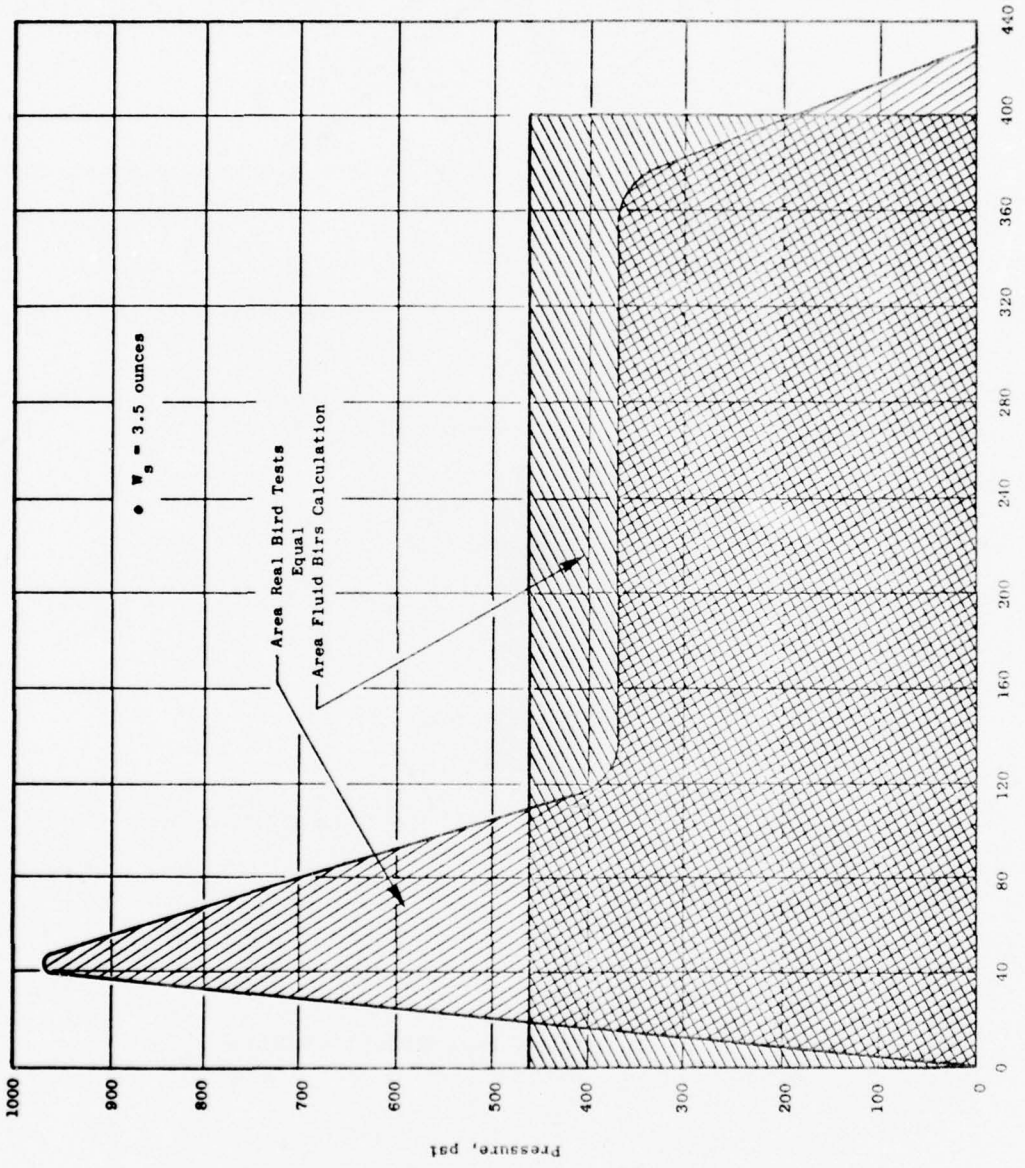

Figure 60. J101 Stage 1 Bird-Blade Interaction Pressure Correction.

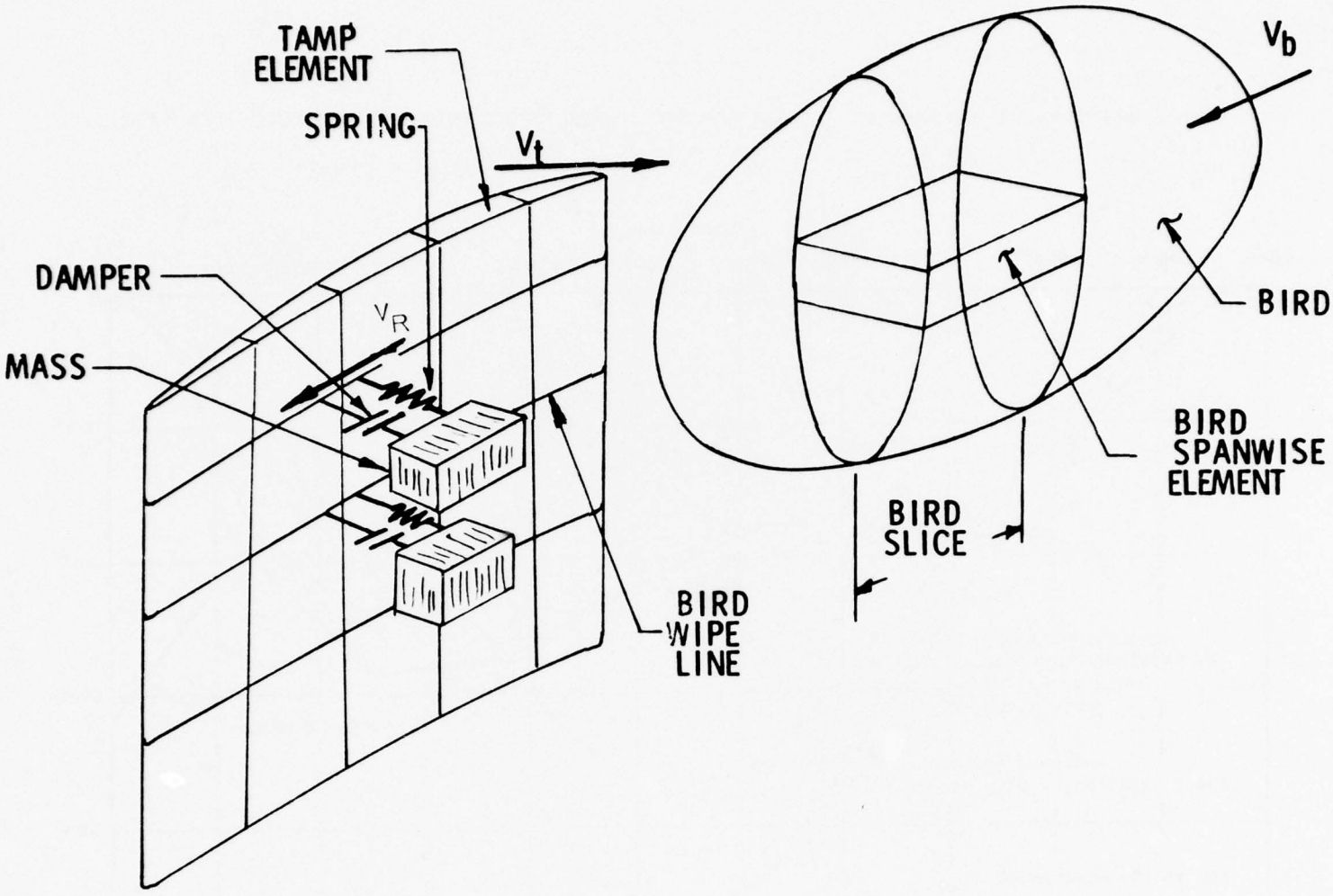

Figure 61. J101 Stage 1 B/Al Blade TAMP Bird Impact Analysis.

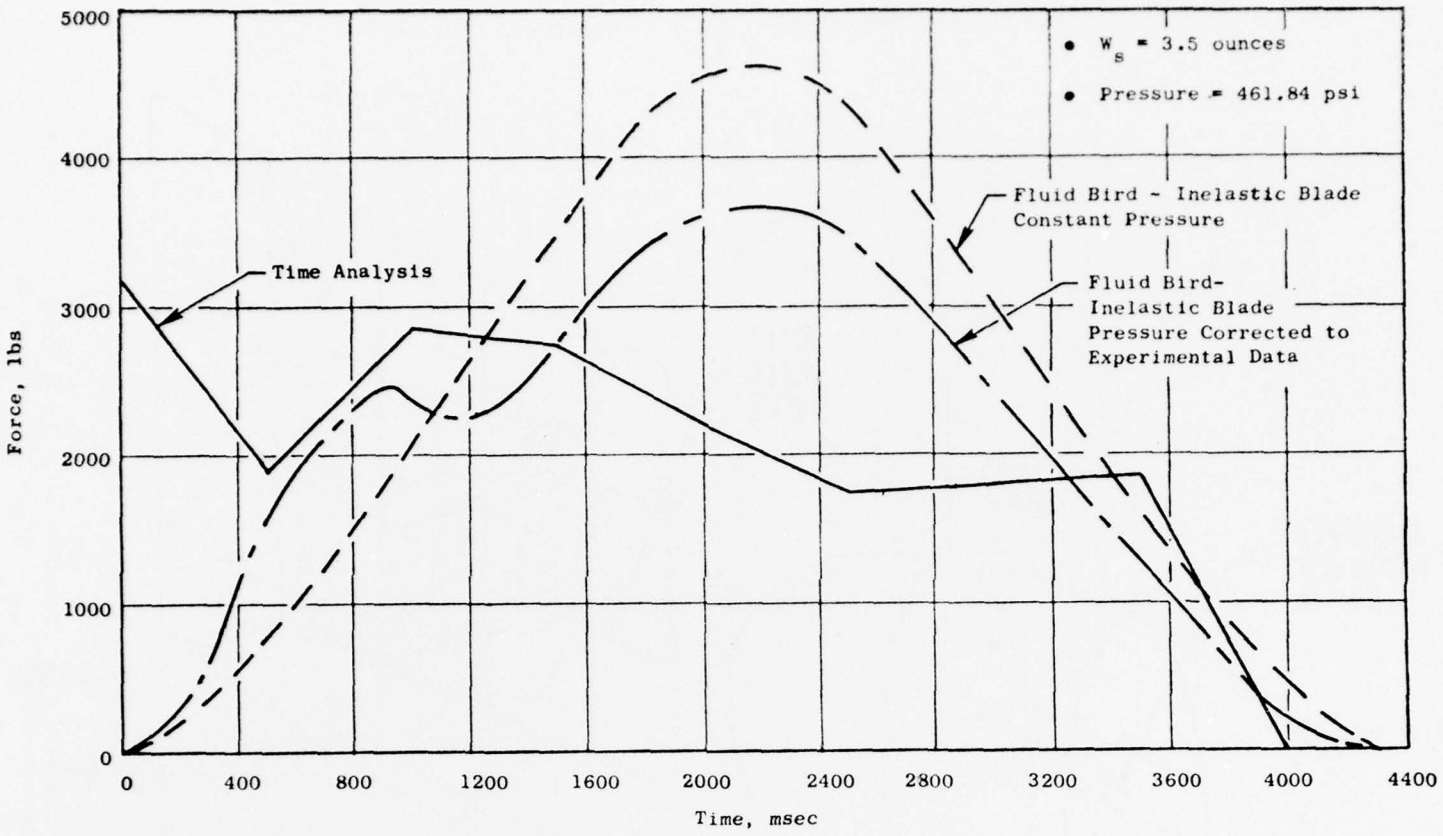

Figure 62. J101 Stage 1 B/A1 Blade TAMP Impact Analysis, Bird-Blade Interaction Force.

The dynamic impact analysis is a subroutine of TAMP which uses the influence coefficients determined in the frequency and steady state stress analysis case. The TAMP finite element program is limited to an elastic analysis based on small deflection theory. This analysis assumed the blade was fixed at the centerline of the dovetail pressure face.

This analysis also assumed that the bird slice was a single concentrated mass traversing along one chord line or "wipe line." The results of the 3.0 ounce starling impact case showed the local and root stresses to be very high; i.e., in the 150,000 psi range. The very high root stresses were not of major concern because the swing root feature had not been incorporated into the model. However, the local stress appeared high. Similar dynamic analysis performed on the QCSEE and F103 fan blades was reviewed in an attempt to determine what may be wrong with the run or model. The only anomaly that could be identified was the method of inputing the bird loading. All earlier work had also used the single wipe line approach, but, in those analyses, the blade was very large compared to the bird. Furthermore, the blade materials were quite soft relative to B-Al. It was concluded that the program had to be refined to allow a more realistic method of wiping the impact force across the blade for the J101 blade. The problem apparently arises because of the short span length of the J101 blade and the stiffness of the B-Al. The starling slice that was being evaluated was 2.14 inches diameter and 0.53 inches thick. As this real slice passes across the blade, it is in contact with approximately 35% of the airfoil span. However, the single line swipe model concentrates the force along a single line which results in steep gradients locally. Simulation of the 25 ounce bird impact was even more pessimistic as the bird is in contact with nearly 55% of the airfoil span.

Impact Analysis Results

The stress components at each nodal point were defined in Figure 34. The results of the dynamic impact analysis are presented in the form of curves of stress and deflection as a function of time. A complete presentation of all stress and deflection components at each nodal point would require approximately 3000 curves per impact case. This massive volume of data makes the presentation and interpretation of the results tedious and difficult.

A few of the more significant results from the 3.0 and 25 ounce bird impact analyses are shown in Figures 63 through 68. The general shape of the deflection and stress curves are the same for both cases except the amplitudes for the 25 ounce bird impact are about 50% to 100% higher than the amplitudes for the 3 ounce bird impact. The 25 ounce bird slice mass is nearly 300% higher than the 3 ounce bird.

The analysis indicates that all of the stress components in the impact area of the blade exceed the B-Al material properties for a 3 ounce starling strike. Due to the limitations and assumptions of the analytical technique, the absolute stress values are pessimistic. It is not certain at this time that the blade would fail locally from a starling impact.

The analysis is most useful in hypothesizing failure modes. As shown in Figure 69 and summarized in Table 17, three critical points during the starling impact were investigated. Approximately 100 microseconds after the initial

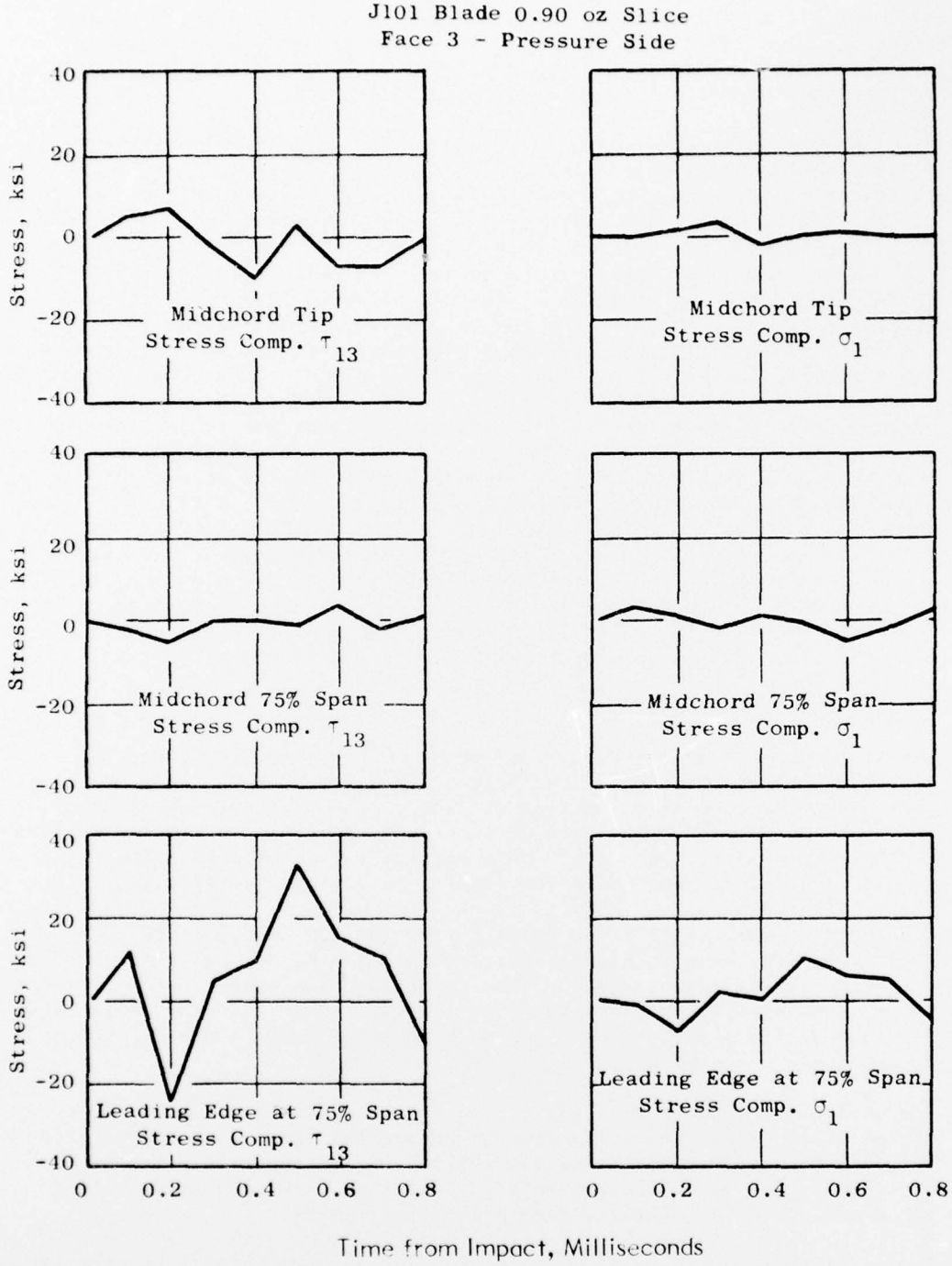

Figure 63. J101 B/Al Blade Impact Results, 3 oz Bird.

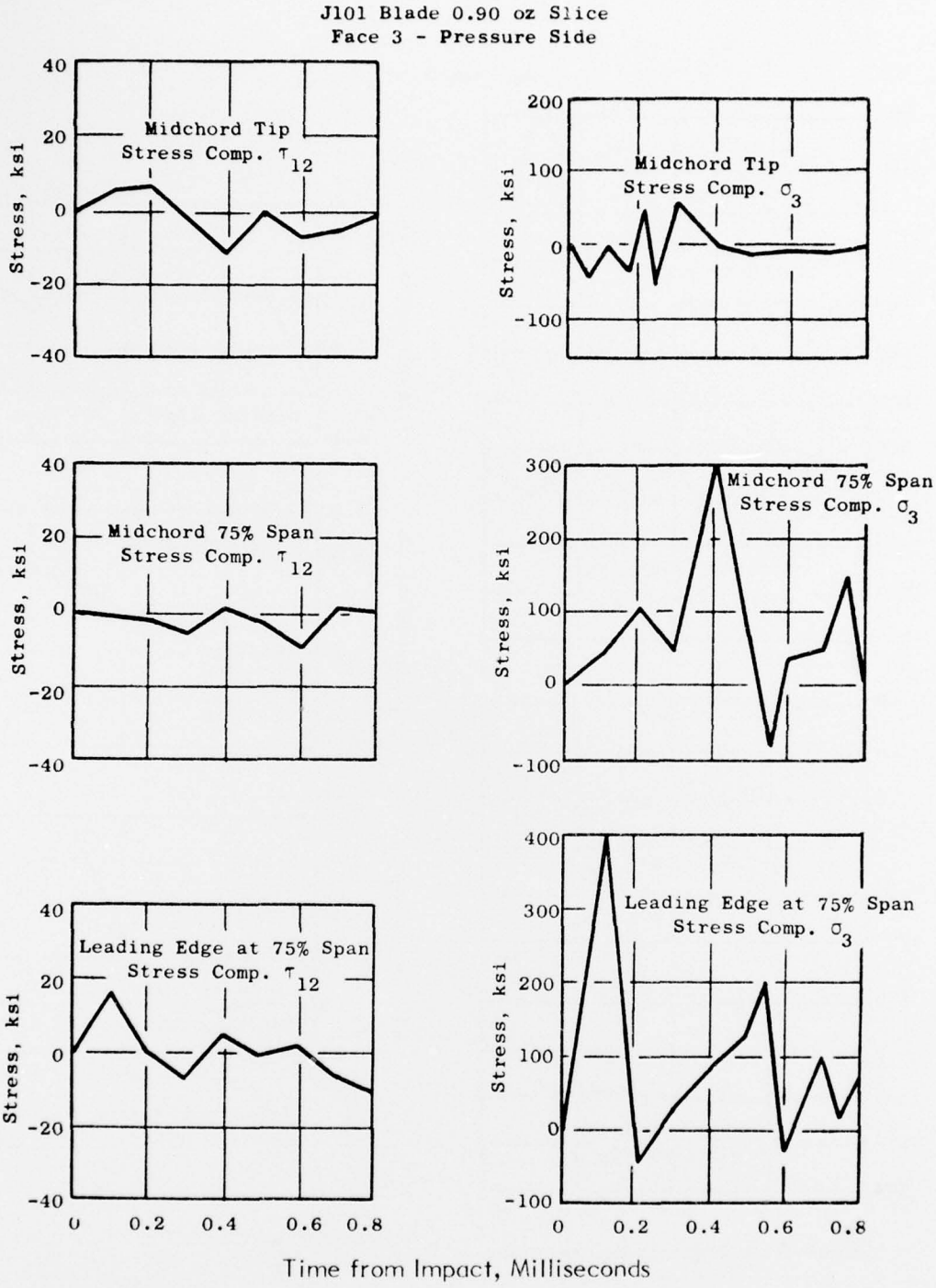

Figure 64. J101 B/A1 Blade Impact Results, 3 oz Bird.

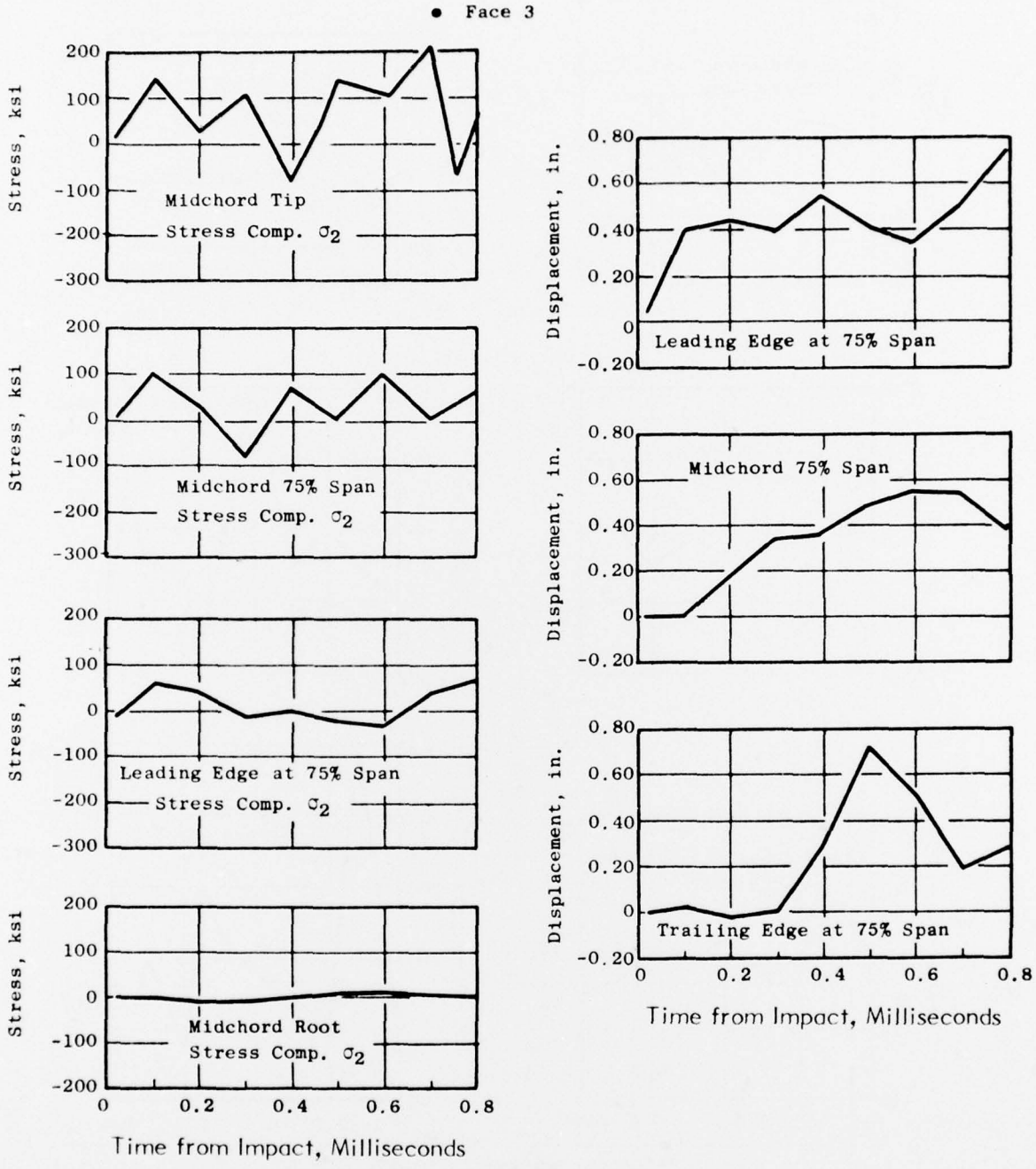

Figure 65. J101 B/Al Blade Impact Results, 3 oz Bird.

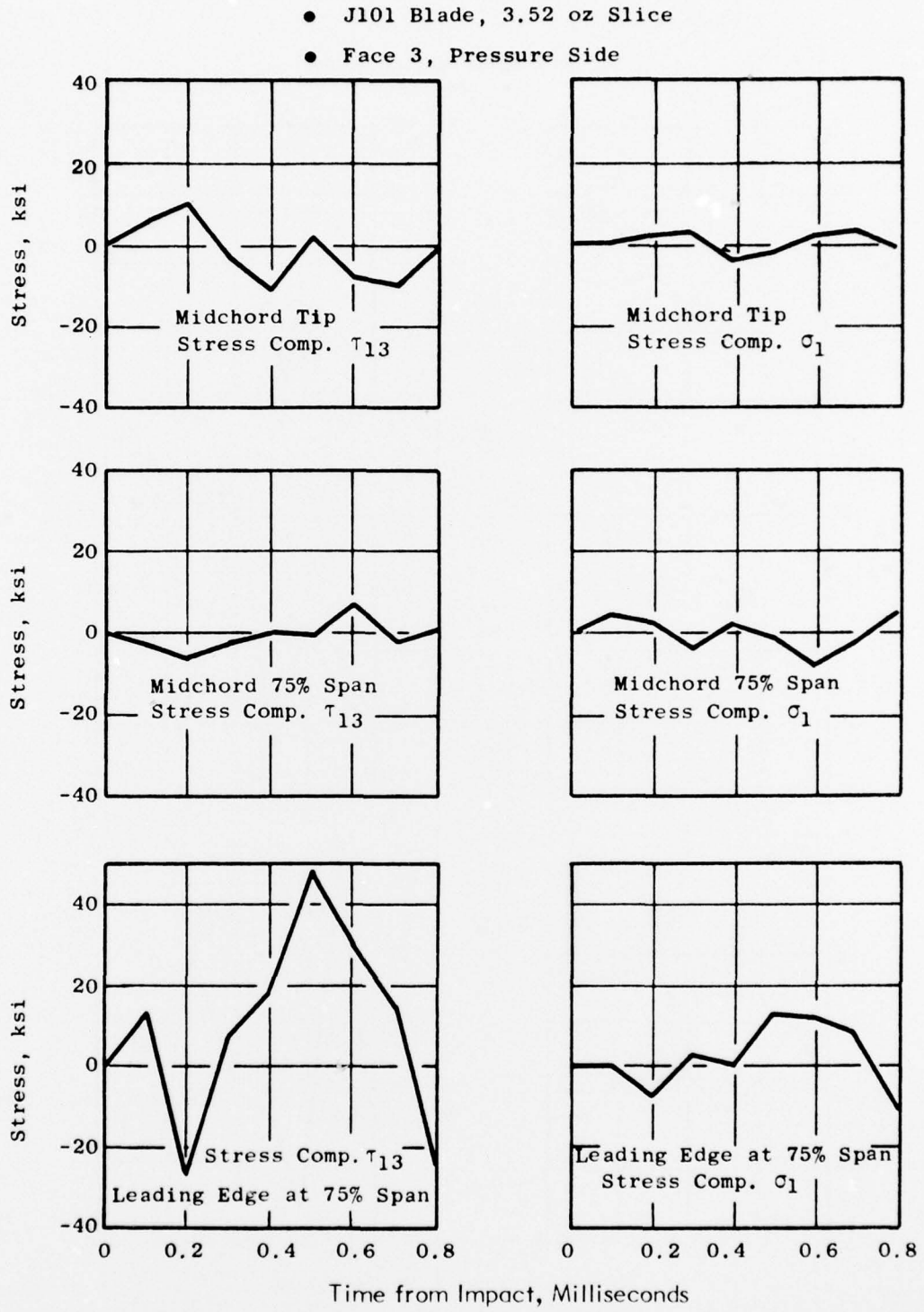

Figure 66. J101 B/Al Blade Impact Results, 25 oz Bird.

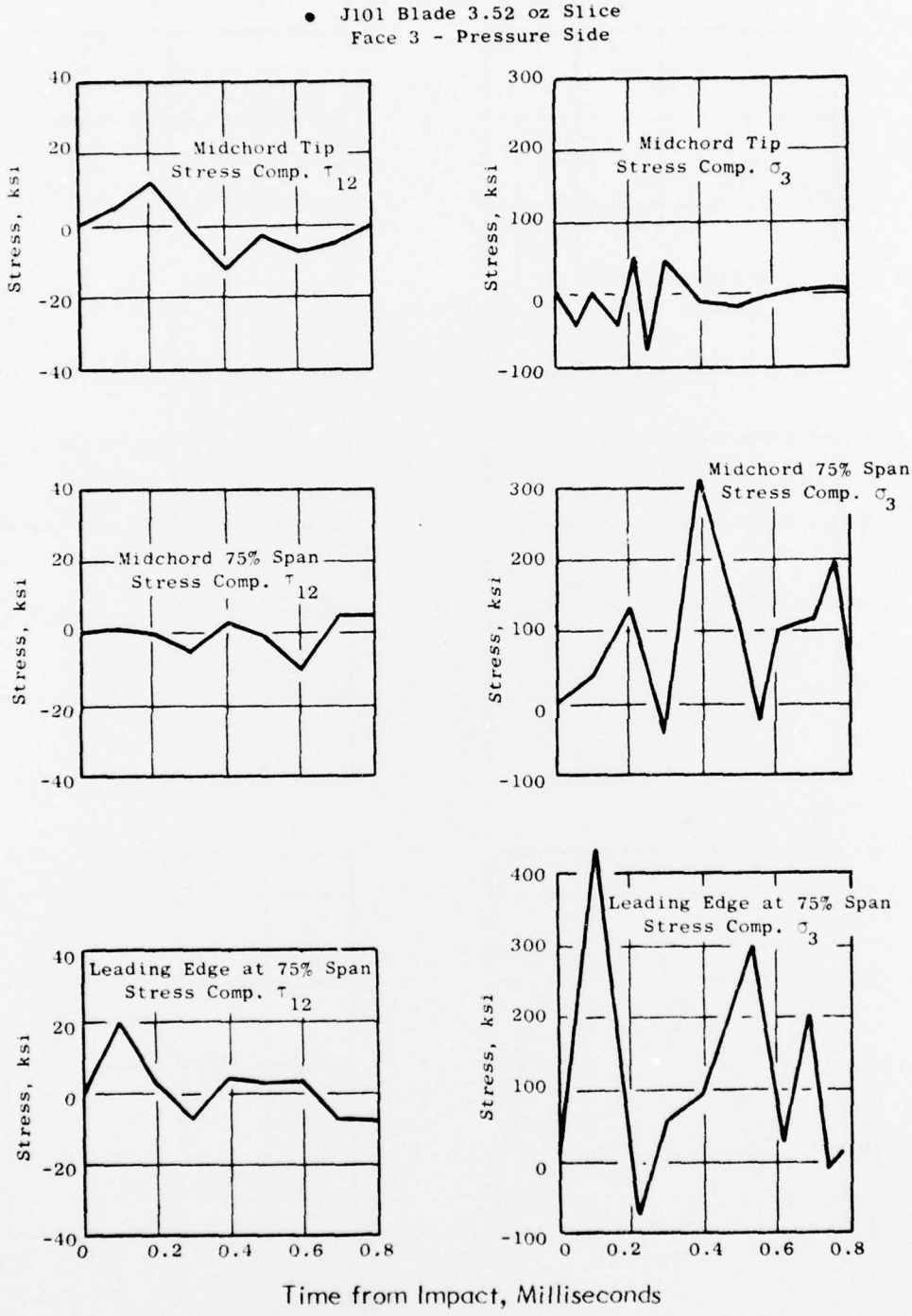

Figure 67. J101 B/Al Blade Impact Results, 25 oz Bird.

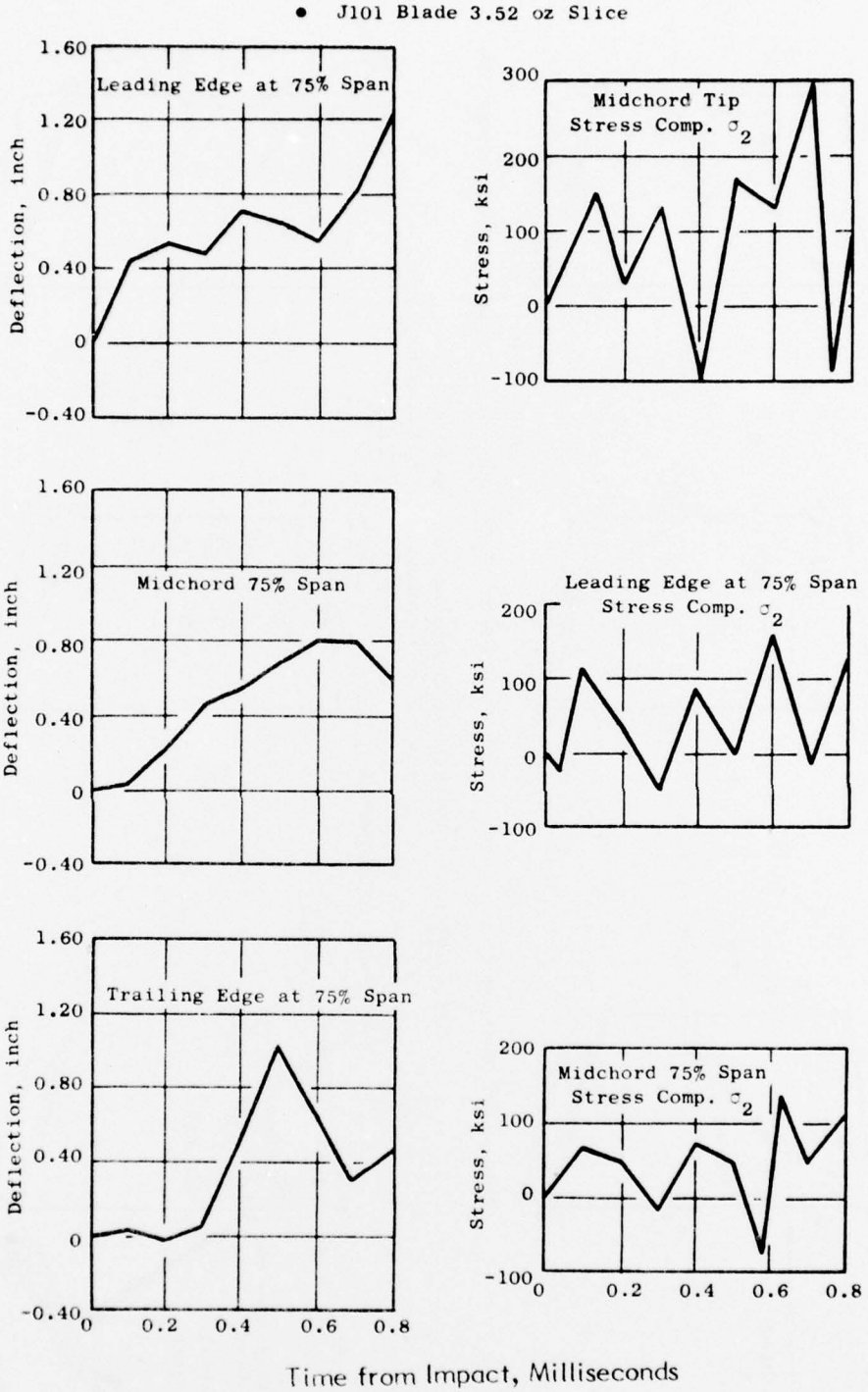

Figure 68. J101 B/Al Blade Impact Results, 25 oz Bird.

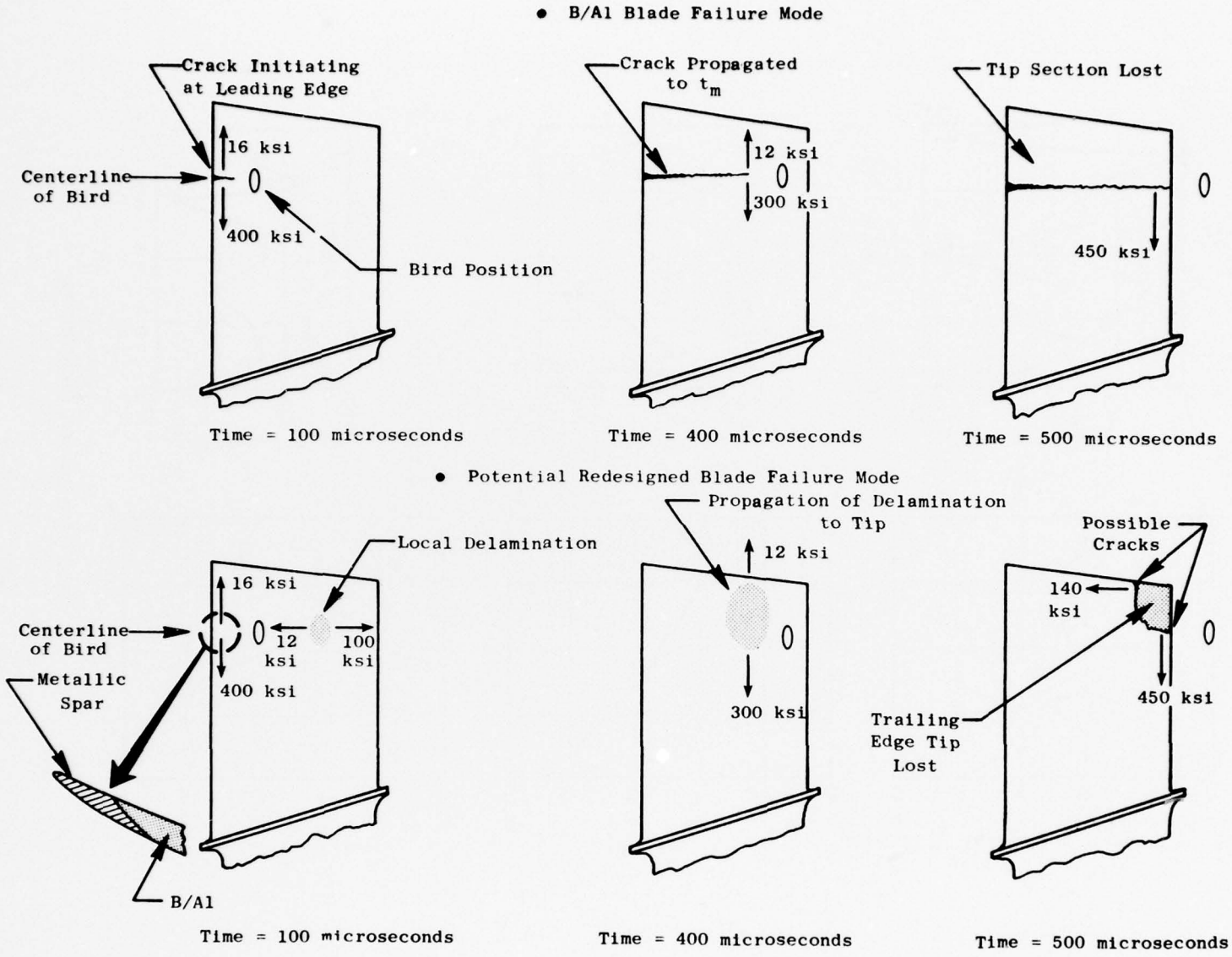

Figure 69. J101 Stage 1 B/Al Fan Blade.

TABLE 17

CALCULATED MAXIMUM STRESS AND DEFLECTIONS

DUE TO BIRD IMPACT

		3 Oz Bird						25 Oz Bird					
Location	Time msec	σ_1 (ksi)	σ_2 (ksi)	σ_3 (ksi)	τ_{12} (ksi)	τ_{13} (ksi)	Max. Def. (in.)	σ_1 (ksi)	σ_2 (ksi)	σ_3 (ksi)	τ_{12} (ksi)	τ_{13} (ksi)	Max. Def. (in.)
Leading Edge 75% Span	.10		60.0	400	16.0				110.0	430	20.0		
	.20					25.0						26.0	
	.30												
	.40						.70						.70
	.50	10.0						12.0					
	.60												
Midspan 75% Span	.1	3.0						4.0					
	.2					5.0							
	.3		-80.0										
	.4			300						320			
	.5												
	.6				10.0		.54		-80		10.0	6	.80
Midspan Blade Tip	.1												
	.2			60						-75			
	.3	3.0											
	.4				12.0	10.0		3.0			12.0	11	
	.5		140						170				
Trailing Edge 75% Span	.50						.70						1.0
Est. Ult. Prop.		4	23	107	7	12							

bird contact, the spanwise bending stresses increase to 400 ksi in the blade leading edge at the center of the bird which would initiate a tensile crack in the leading edge. As the bird traverses the blade, the spanwise bending stresses reach 300 ksi at the airfoil maximum thickness and 450 ksi at the trailing edge. These stresses would propogate the crack across the blade and the outer panel would be lost. Although the elastic analysis predicts 16 ksi interlaminar shear stresses in the leading edge, delamination probably would not occur as those shear stresses would be relieved by the crack.

If a material of sufficient impact strength was used in the leading edge, the failure mode of the blade could be altered. The leading edge material must have sufficient strength and ductility to provide 5000 lb/in^2 area under the stress-strain curve as shown in Figure 70. The leading edge spar must extend approximately 1/2 inch chordwise where the bending stress has diminished to 250 ksi to avoid a failure in the B-Al. In addition, the B-Al shear strength must be less than 12 ksi to initiate delamination at the airfoil maximum thickness section. As the bird slice wipes across the blade, at 400 microseconds the delamination will propogate to the airfoil tip and relieve the 300 ksi calculated elastic bending stress. As the bird leaves the blade at 500 microseconds, the delamination must be sufficient to relieve the high trailing edge bending and 140 ksi chordwise bending stress in the airfoil tip. If the delamination does not relieve these stresses, a chordwise crack could initiate at the trailing edge and extend to a radial crack extending from the tip to cause loss of the trailing edge, tip section of the airfoil.

To summarize the dynamic impact analysis, at the leading edge point of impact the tensile and shear stress are greater than the material strength for even the 3 ounce bird, although the high absolute stress values are most likely due to the method of concentrating the bird mass at a single line. The stresses increased with bird size, however, the increase was much less than the increase in mass of the bird slice. Peak radial and chordal tensile stresses (σ_3 and σ_2) and interlaminar shear stresses (τ_{12} and τ_{13}) occurred within 0.2μ seconds of the impact initiation. Peak deflection was the same and occurred at the same time after impact for both cases.

At the cord center at 75% span, the peak radial and chordal tensile stress and interlaminar shear stresses also exceed material strengths. Peak stresses occur as the bird slides to the cord center. Again the stress increase with bird size is less than the increase in bird slice mass. Maximum deflection occurs after the peak stress and is less than that of the leading edge.

At the blade tip and cord center, only the chordal tensile and interlaminar shear stresses exceed material strength. These maximum stresses occur while the bird is moving between the midspan and trailing edge.

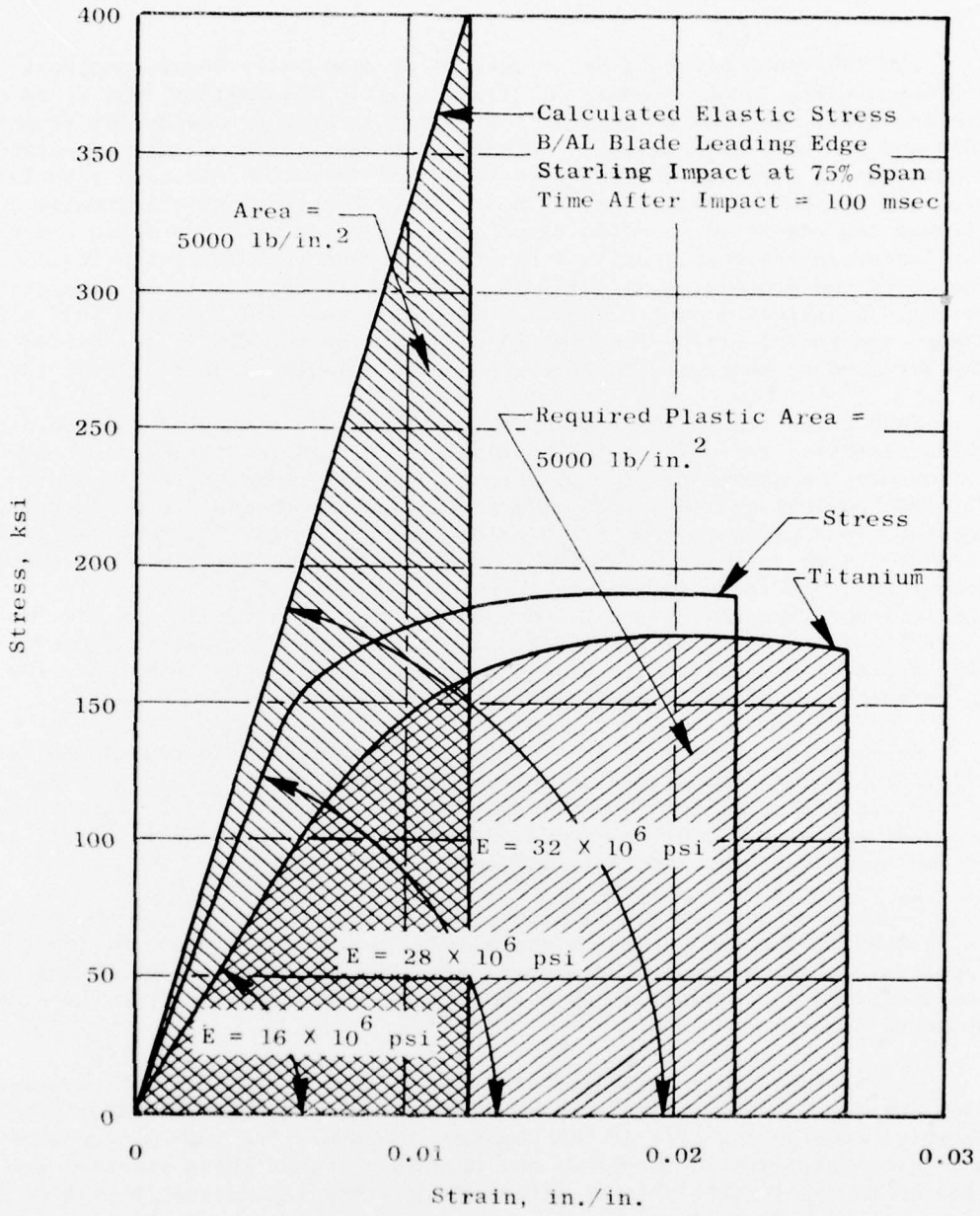

Figure 70. J101 Stage 1 B/Al Blade, Required Strain-Strain Curve from Finite Element Analysis.

SECTION V

SUMMARY AND CONCLUSIONS

The TRW rapid air bonding process which uses fully dense monotapes, a surface preparation to promote localized plastic deformation, and a rapid bonding cycle has been successfully employed to produce composites from 1100, 2024 and 6061 aluminum alloys. Mechanical properties have been comparable to vacuum bonded material and no weakness or contamination has been associated with the air bonded matrix-matrix bond line. The tape surface treatment has allowed the use of low bonding temperatures and appears to provide a mechanism for increasing filament-matrix strength when used in primary fabrication. The cycle and procedures established are directly applicable to blade fabrication. Excellent impact properties were obtained with 46 ft-lb full size Charpy and 65-101 ft-lb^2 for miniature Charpy for the $\pm 15^{\circ}$ 8 mil B-1100 system. The air bonding process also provides an appreciable production cost saving.

Each composite system tested was amenable to air bonding but had distinct characteristics influencing the appropriate fabrication parameters. The 1100 system has the greatest energy absorbing capability through the mechanism filament pullout and shearing. The factors which produce energy absorption reduced those strength properties which depend upon the filament matrix bond strength, such as shear. Fabrication conditions were selected to balance these properties. The 2024 system was almost the oppostite, providing a very strong chemical bond between filament and matrix with high strength and low impact. In this case emphasis in fabrication was placed upon increasing impact. The 6061 system had consistently high strength but the Charpy impact was low. No variation in processing was employed for 6061.

An important aspect of the program was the ability to combine matrix alloys to tailor properties for the desired application. The utility of hybrid materials, selective matrix variation, or a bi-metal construction where the root and tip of a blade are of different alloys could be of great benefit in improving the blade strength and impact performance.

Because boron-aluminum is processing sensitive and because one property is frequently obtained at the expense of another, it is important to define the requirements of the product required. The analysis of the J-101 blade by G.E. was performed in conjunction with fabrication development to provide realistic property goals.

It was found that the calculated design operating condition stresses were high for the 8 mil diameter boron/1100 aluminum materials characterized in the material development part of the program. However, the highly stressed areas are quite localized in the blade and it appears that these stresses can be reduced to significantly lower levels by refining the design in several areas.

The high radial and chordal tensile stresses are surface stresses caused by bending moments induced by the large blade twist angle and a relatively low tm/c. It is anticipated that these local high stresses can be reduced by redefining the blade tm/c.

The three local areas of high shear stress are located at the airfoil root leading and trailing edges. These high stresses are the result of severe geometric transitions into the shank and dovetail. Similar problems have been

encountered in the past and have been reconciled by reducing the severity of the transitions. No major problems are anticipated in reducing these shear stresses substantially.

The stresses calculated for a bird impact were well in excess of boron-aluminum strength. However, the absolute magnitude of these stresses is in doubt because of the bird loading model employed. Of significance was the stress distribution, which correlate with failure observed in whirling arm tests, and the observation that increase in stress was less than the increase in bird slice mass.

REFERENCES

1. "Roll Diffusion Bonding of Metal Matrix Composites," TRW Inc., AFML-TR-74-194, October 1974.

2. "Low Cost Metal Matrix Composite Material," CMC, F33615-74-C-5066.

3. TRW Patent Applied for.

4. "Impact Resistant B/Al Composites for Turbojet Engine Fan Blades," P. Melnyk, I. J. Toth, NASA CR-134770, May 1975.

5. "B/Al Compressor Blades," C. A. Steinhagen, M. W. Stanley, AFML-TR-73-283, October 73.

6. "Impact Resistant Boron/Aluminum Composites for Large Fan Blades," NASA3-19729.

7. "Impact Resistant Boron/Aluminum Large Fan Blades," NAS3-20115.

8. "Fabrication of Boron/Aluminum Fan Blades for SCAR Engines," NAS3-20360.

9. "Boron-Aluminum Fan Blade for SCAR Engine," NAS3-18910.

10. "Characterization of Bird Impacts on a Rigid Plate," J. S. Welbeck, J. P. Barber and H. R. Taylor, AFFDC-TR-75-5.

☆ U. S. GOVERNMENT PRINTING OFFICE: 1977 — 757-001/475